XXXII PhD course in Applied Biology and Experimental Medicine

Department of Chemical, Biological and Pharmaceutical Sciences

University of Messina

THE *IN VIVO* PHARMACOLOGICAL MANIPULATION OF THE NRF2 PATHWAY AND ITS THERAPEUTIC SIGNIFICANCE IN BRAIN DISEASES, WITH A POSSIBILE IMPLICATION IN H_2S-REGULATED LIPIDIC METABOLISM

Dr. Giovanna Casili

Relators:

Prof. Emanuela Esposito

Prof. Salvatore Cuzzocrea

Prof. Csaba Szabo

This work was performed under the supervision of:

Prof. Emanuela Esposito and Prof. Salvatore Cuzzocrea

at the University of Messina, Department of Chemical, Biological and Pharmaceutical Sciences

and

Prof. Csaba Szabo

at the University of Fribourg, Department of Pharmacology

Table of contents

PART I

ABSTRACT

Nuclear factor erythroid 2-related factor 2 (Nrf2), a redox-sensitive transcription factor, plays a critical role in the regulation of cellular defence and contributes to a number of cellular processes. Nrf2 is regulated through an interplay of complex transcriptional and post-translational mechanisms that modulates its activity during cellular perturbations or other biological processes thereby ensuring cellular homeostasis is maintained through the orchestration of adaptive responses. Therefore, an ability to modulate the activity of the Nrf2 pathway holds promise as a therapeutic strategy in certain disease settings.

In this thesis, the role of Nrf2 was evaluated in a mouse model of traumatic brain injury (TBI). TBI is a serious neuropathology that causes secondary injury mechanisms, including dynamic interplay between ischemic, inflammatory and cytotoxic processes. Fumaric acid esters (FAEs) showed beneficial effects in preclinical models of neuroinflammation and toxic oxidative stress, so the aim of the present work was to evaluate the potential beneficial effects of dimethyl fumarate (DMF), the most pharmacologically effective molecules among the FAEs, in a mouse model of TBI induced by controlled cortical impact (CCI). Mice were orally administered with DMF at the doses of 1, 10 and 30 mg/Kg, 1h and 4h after CCI. We performed histological, molecular, and immunohistochemistry analysis on the traumatic penumbral areas of the brain 24 hours after CCI. DMF treatment notably reduced histological damage and behavioral impairments, reducing neurodegeneration as evidenced by assessments of neuronal loss, Fluoro-jade C and TUNEL staining; also, treatment with DMF blocked apoptosis process increasing B-cell lymphoma 2 (Bcl-2) expression in injured cortex. Furthermore, DMF treatment up-regulated antioxidant Kelch- like ECH-associated protein 1/ Nuclear factor erythroid 2- related factor (Keap-1/Nrf2) pathway, inducing activation of manganese superoxide dismutase (Mn-SOD) and heme- oxygenase-1 (HO-1) and reducing 4-hydroxy-2-

nonenal (4-HNE) staining. Also, regulating NF-κB pathway, DMF treatment decreased the severity of inflammation through a modulation of neuronal nitrite oxide synthase (nNOS), interleukin 1 (Il-1β), tumor necrosis factor (TNF-α), cyclooxygenase 2 (COX-2) and myeloperoxidase (MPO) activity, reducing ionized calcium-binding adapter molecule 1 (Iba-1) and glial fibrillary acidic protein (GFAP) expression.

Moreover, the role of Nrf2 pathway, was discusses in a mouse model of nitroglycerin -induced migraine (NTG). Oxidative stress and inflammatory pathways are involved in NTG and endogenous antioxidant defense system has a role in the prevention of hyperalgesia in migraine. In this study, we aimed to evaluate the role of DMF in regulating the hypersensitivity in a mouse model of NTG-induced migraine.

Mice were orally administered with DMF at the doses of 10, 30 and 100 mg/kg, 5 minutes after NTG intraperitoneal injections. We performed histological and molecular analysis on the whole brain and behavioral tests after 4 h by NTG-migraine induction. The expression of nuclear factor kappa-light-chain-enhancer of activated B cells (NF-κB) subunit p65, nuclear factor of kappa light polypeptide gene enhancer in B-cells inhibitor alpha (IκBα), inducible nitrite oxide synthase (iNOS), cyclooxygenase 2 (COX-2), Nrf2, manganese superoxide dismutase (Mn-SOD) and heme-oxygenase-1 (HO-1) were detected by Western blot. Tail flick, hot plate, formalin and photophobia tests were used to evaluate neuropathic pain and migraine-related light sensitivity. DMF treatment notably reduced histological damage as showed by cresyl violet staining; also, regulating both NF-κB and Nrf2 pathway, DMF treatment decreased the severity of inflammation and increased the protective antioxidant action. Moreover, the headache-associated neuropathic pain was significantly reduced.

These results provide the evidence that DMF restores neurological in damaged-brain and it has modulating effect on central sensitization, suggesting a new insight into the potential therapeutical application of DMF on Nrf2 pathway modulation.

1.0 CHAPTER ONE: The role of Nrf2 pathway on oxidative stress regulation

1. 1 Oxidative stress

The origin of the basic principle of stress and stress responses dates back to Selye in 1936 and the concept of oxidative stress has been introduced for research in redox biology and medicine in 1985, in an introductory book entitled 'Oxidative Stress', presenting the knowledge on pro-oxidants and antioxidants and their endogenous and exogenous sources and metabolic sinks [1]. Oxidative stress is considered as an imbalance between production of free radicals and reactive metabolites or reactive oxygen species (ROS) and their elimination by through protective mechanisms, including antioxidants. This imbalance leads to damage of cells and important biomolecules, having a potential adverse impact on the whole organism [2]. Cells are constantly being exposed to oxidative stress, which result from various chemical and oxidative reactions such as those involving environmental toxicants, mutagens and carcinogens. These insults disrupt cellular homeostasis and function and, not surprisingly, have been associated with disease pathogenesis [3].

ROS are a group of molecules and free radicals (atoms or molecules with an unpaired valence electron) derived from oxygen. They can be of exogenous or endogenous origin. The latter is a result of the cell's own metabolism and play important roles in the stimulation of signaling pathways in plant and animal cells in response to changes in intra- and extra-cellular environmental conditions [4]. During endogenous metabolic reactions, aerobic cells produce ROS, such as superoxide anion (O2-), hydrogen peroxide (H_2O_2), hydroxyl radical (OH•), and organic peroxides, as normal products of the biological reduction of molecular oxygen [5].

1.1.2 Pathophysiology of oxidative stress

The terms reactive oxygen species (ROS) and reactive nitrogen species (RNS) referto reactive radical and non-radical derivatives of oxygen and nitrogen, respectively [6]. There are endogenous and exogenous sources of ROS/RNS:

•Endogenous sources of ROS/RNS include: nicotinamide adenine dinucleotide phosphate (NADPH) oxidase, myeloperoxidase (MPO), lipoxygenase, and angiotensin II [7]. NADPH oxidase is the prevalent source of the radical superoxide anion (O2•) which is formed by the one-electron reduction of molecular oxygen, with electrons supplied by NADPH, during cellular respiration. Most of the O_2• is dismutated into the hydrogen peroxide (H_2O_2) by superoxide dismutase (SOD). H_2O_2 is not a free radical because it has no unpaired electrons, but it is able to form the highly reactive ROS hydroxyl ion (OH•) through the Fenton or Haber–Weiss reaction. Hydroxyl radicals are extremely reactive and react especially with phospholipids in cell membranes and proteins. Finally, O_2 may react with NO to form another relatively reactive molecule, peroxynitrite (ONOO−) [8].

•Exogenous sources of ROS/RNS are air and water pollution, tobacco, alcohol, heavy or transition metals, drugs, industrial solvents, cooking (eg, smoked meat, waste oil, and fat) and radiation, which inside the body are metabolized into free radicals [9].

ROS can be divided into two groups: free radicals and non radicals. Molecules containing one or more unpaired electrons and thus giving reactivity to the molecule are called free radicals, while the sharing of unpaired electrons by two free radicals produce non radical forms. Under normal conditions, ROS production and ROS elimination are balanced; while low ROS levels are related with physiological conditions, an increased production of ROS levels is generally associated with pathological conditions; particularly, when ROS levels increase beyond the threshold of this buffering capacity, these reactive species trigger uncontrolled reactions with non-target intracellular compounds, thus oxidizing nucleic acids, proteins, cellular membrane,

and other lipids, given rise to oxidative stress and cellular damage [10]. ROS also affects the expression of several genes by upregulation of redox-sensitive transcription factors and chromatin remodeling, via alteration in histone acetylation/deacetylation. Regulation of redox state is critical for cell viability and organ functions [11].

Oxidative stress plays a role in inflammation, accelerates aging and contributes in variety of degenerative conditions: cardiovascular diseases, atherosclerosis, cancer, cataract, central nervous system disorders, Parkinson's disease, Alzheimer's disease, inflammatory bowel disease, rheumatoid arthritis, diabetes, respiratory diseases, autoimmune diseases, liver diseases, kidney diseases, skin conditions [12].

1.2 The Nrf2-Keap1 pathway

Mammalian cells have evolved complex signaling pathways and defense systems that function synergistically in order to reduce the deleterious effects of such intrinsically and extrinsically generated insults. At the center of the biological response to oxidative stress is the Kelch-like ECH-associated protein 1 (Keap1) - nuclear factor erythroid 2-related factor 2 (Nrf2)-antioxidant response elements (ARE) pathway, which regulates the transcription of many several antioxidant genes, preserving cellular homeostasis and detoxification genes, to avoid cellular damage [13].

Nrf2 is a redox-sensitive transcription factor belonging to the cap'n'collar (CNC) subclass of the basic leucine zipper region containing the protein family. Nrf2 binds to a specific DNA site, the antioxidant response element (ARE), regulating transcription of an array of detoxifying or antioxidant enzymes (gamma-glutamylcysteine synthetase, superoxide dismutase, catalase, glutathione reductase, thioredoxin reductase, peroxiredoxins, and glutathione S-transferase) [14]. This pathway is a redox sensitive transcription factor that induces the expression of a

variety of genes that protect against the deleterious effects of oxidative and chemical stress, thus ensuring normal cellular functions are maintained or restored.

The Keap1–Nrf2 system is a major oxidative stress response pathway [15]. Nrf2 is a basic leucine zipper (bZIP) transcription factor and its heterodimer with small Maf proteins controls the expression of anti-oxidant proteins that protect against oxidative damage triggered by injury and inflammation. Keap1 is an adaptor protein of Cullin-3-based ubiquitin ligase. The mechanism proposed for the Keap1-mediated activation of Nrf2 is the "hinge and latch model", based on the finding that Keap1 homodimer binds to a single Nrf2 molecule through two distinct binding sites (DLG and ETGE motifs), within the Neh2 domain of Nrf2 [16]. The Keap1 forms a homodimer that recognizes ETGE and DLGex motifs of one Nrf2 molecule through the same binding pocket within the DC (double glycine repeat and C-terminal) domain located at the bottom surface of Keap1 and this binding causes Nrf2 ubiquitination [17]. Binding of the high-affinity ETGE motif and low-affinity DLG motif provides a hinge and latch, which facilitate optimal positioning of the lysine residues between the two motifs for ubiquitin conjugation [18].

Under normal conditions, the levels of Nrf2 protein are kept low by the E3 ubiquitin ligase Keap1 (Kelch ECH-associating protein 1), which ubiquitinates Nrf2 in the cytoplasm and targets it for degradation by the 26 S proteasome [19]. This constitutive degradation of Nrf2 allows for only the basal expression of its target stress response genes as part of a housekeeping function. However, under conditions of oxidative stress, or in the presence of electrophilic xenobiotics, the activity of Keap1 decreases and Nrf2 can accumulate in the nucleus where it activates the inducible high expression of its target genes.

In this way, Keap1 functions as a critical sensor of cellular stress and its high redox sensitivity is determined by a number of cysteine residues that are distributed throughout the Keap1 protein and are vulnerable to oxidation or to covalent modification by electrophiles. The Keap1–Nrf2

system protects cellular proteins and DNA from oxidative damage caused by reactive oxygen species and electrophiles, implementing a critical role for cellular detoxification. Consequently, the Keap1–Nrf2 system is an important therapeutic target in cancer and neurodegenerative conditions, as well as many autoimmune and inflammatory diseases [20], [21], [14], [2]. Critical for such intervention strategies is a deep understanding of the structure and function of these proteins. Progress in this respect has relied on the definition of the domain architecture of the Keap1 and Nrf2 proteins and the identification of the specific regions mediating their interactions [22].

1.2.1 Component structures and functions

Nuclear factor erythroid 2-related factor 2 (Nrf2)

The Nrf2 protein in humans is 605 amino acids long and contains seven highly conserved regions known as [Nrf2–ECH (erythroid cell-derived protein with CNC homology)homology] (Neh) domains. Six functional Neh units were identified in Nrf2, each well conserved in the Nrf2 molecules of various species. Neh1 contains the CNC–bZIP domain, which mediates heterodimerization with Maf [23]. The Neh2 domain contains the two degrons that are specifically bound by Keap1, commonly known as the DLG and ETGE motifs after their sequence conservation in the single-letter amino acid code [24]. The Neh3 domain functions as a co-activator that facilitates the transcription of the ARE-dependent genes, while Neh4 and Neh5 domains act together with CBP [CREB cyclic AMP-response element binding protein (CREB) binding protein] and synergistically contribute to the strong transcriptional activation exerted by Nrf2 [25] . Neh6 is the domain that regulates the Keap1-independent regulation of Nrf2 pathway [26]. Neh7 is the domain that facilities retinoid X receptor alpha (RXRα)-mediated Nrf2 repression through a direct interaction between the two proteins [27].

The Nrf2 protein also contains nuclear import/localization signals (NLSs) and nuclear export signals (NESs) which regulate Nrf2 shuttling in and out of the nucleus. Also, human Nrf2 contain six cysteine residues; two of the cysteines (Cys183 and Cys506) and two other key amino acid residues (Ser40 and Tyr568) may also regulate Nrf2 localization and transactivation of target genes through oxidation and phosphorylation, respectively. Nrf2 is truly a master regulator of the antioxidant response [28].

Kelch-like ECH-associated protein 1 (Keap1)

Keap1 is a 69-kDa protein that shares some homology with actin-binding Kelch protein and serves as a negative regulator of Nrf2. The human Keap1 protein sequence contains 627 amino acid residues organized into five domains: i) the N -terminal region (NTR), ii) the Broad complex, Tramtrack, and Bric-a-Brac (BTB), iii) the linker intervening region (IVR), iv) the Kelch domain, and v) the C -terminal region (CTR). BTB domain that attached to act in binding proteins is responsible for homodimerization and interaction with Cullin (Cul3) based ubiquitin E3 ligase complex for Nrf2 ubiquitination. IVR containing cysteine residues, sensitive to oxidation and nuclear export signal (NES) motif. Kelch domain has six kelch repeats (KR1-KR6) and possessing multiple protein contact sites that mediate association of Keap1 with Nrf2 (the Kelch domain interacts with Neh2 domain of Nrf2) and cytoskeleton proteins actin and/or myosin [23].

Human Keap1 contains 27 cysteine residues and seven of them (i.e., Cys151, Cys257, Cys273, Cys288, Cys297, Cys434, and Cys613) are highly reactive towards ROS and electrophiles and probably they are involved in redox sensing [29].

Antioxidant response element (ARE)

The induction of many cytoprotective enzymes in response to reactive oxidative stress is regulated primarily at the transcriptional level. This transcriptional response is mediated by a cis-acting element termed ARE [30], initially found in the promoters of genes encoding the two

major detoxication enzymes, GSTA2 (glutathione S-transferase A2) and NQO1 (NADPH: quinone oxidoreductase 1). ARE possesses structural and biological features that characterize its unique responsiveness to oxidative stress [31], but also it is activated in response to chemical compounds with the capacity to either undergo redox cycling or be metabolically transformed to a reactive or electrophilic intermediate. The alteration of the cellular redox status due to elevated levels of ROS and electrophilic species and/or a reduced antioxidant capacity (e.g. glutathione) appears to be an important signal for triggering the transcriptional response. The consensus sequence of ARE cannot be represented as a single sequence as AREs required for some genes are distinctly different for others. Under oxidative stress conditions, stabilized Nrf2 translocates to the nucleus, forms a heterodimer with Maf, and activates ARE-dependent gene expression. Bach1 (BTB and CNC homology-1) is another negative regulator of certain ARE-dependent genes; it associates with ARE and forms a dimer with Maf protein, preventing Nrf2 from binding to DNA under normal physiological conditions [32].

1.2.2 Mechanisms and regulation of ARE-dependent gene expression

The discovery of the ARE lead to the identification of Nrf2 as the transcription factor capable of both binding to this DNA sequence and inducing the expression of cell defence genes and resulted in a burst of research into this pathway as a potential therapeutic target. The vast number of both natural and synthetic compounds able to induce Nrf2 can be divided into at least 10 groups [33]. Numerous Nrf2 inducers, mostly plant-derived compounds with chemopreventive properties are currently in clinical trials for a variety of diseases. What is evident, however, is that Nrf2 plays a major role in health and disease and it is not surprising that Nrf2 is considered as a potential therapeutic target. The development of a number of Nrf2 inducers as possible pharmacological agents without a complete knowledge of the workings of this pathway and its regulation heightens the need to further our understanding and to determine whether activation of Nrf2 would be beneficial in both the short- and long-term.

1.3 The Nrf2 regulation: Keap1-dependent regulation

1.3.1 Identification of Keap1 as an inhibitor of Nrf2

Several models of Nrf2 regulation have been proposed and can be divided into Keap1-dependent and Keap1–independent regulation of Nrf2. The identification of an inhibitor of Nrf2 derived observing that the deletion of the Neh2 region of the Nrf2 protein resulted in a marked increase in Nrf2 activity in erythroblasts and led to the proposal that this region was responsible for the negative regulation of Nrf2 via an interaction with a repressor protein [34]. Later studies further confirmed this idea by cloning the rat homologue of Keap1 by purifying Nrf2-interacting proteins [35]. Following these discoveries, it was seen that two Keap1 molecules are able to bind to one Nrf2 molecule and that the BTB domain is responsible for the homodimerization of Keap1 and the subsequent inhibition of Nrf2 [36]. When transfected into cells it was observed that Nrf2 would accumulate in the nucleus, however when co-transfected with Keap1 the two would co-localise in the cytoplasm. Moreover, in the presence of both Keap1 and a panel of electrophiles, Nrf2 again localizes in the nucleus, suggesting that Keap1 sequesters Nrf2 in an inactive form in the cytoplasm until faced with an oxidative or electrophilic insult, when Nrf2 is freed and translocates to the nucleus [37]. The thesis that Keap1 is vital in the regulation of the Nrf2 pathway in *in vivo* is highlighted by the observation that Keap1-deficient mice (Keap1−/−) do not survive longer than 3 weeks postnatally due to hyperkeratosis of the digestive system resulting in ulceration of the stomach [38].

It was quickly determined that Keap1 function is not simply binding Nrf2 and sequestering it in the cytosol, thus preventing its translocation to the nucleus, but it also provided a functional role in this pathway.

1.3.2. Ubiquitination and proteasomal degradation of Nrf2

Under basal conditions, Keap1 leads Nrf2 to ubiquitination and proteasomal degradation. In the absence of oxidative stress, Nrf2 is sequestered in the cytosol by the Keap1 homodimer which

acts as a substrate adaptor for the ubiquitination of Nrf2 in a cullin-3 (Cul3) dependentmanner [17]. Keap1 acts as a substrate adaptor for Cul3-dependent E3 ubiquitin ligase complex, thereby bringing together Nrf2 and ROC1/RBX1 (Ring-box protein 1), a ring-box protein which recruits a ubiquitin charged E2 molecule; thus, the ubiquitin molecule is conjugated to one of the lysine residues located on Neh2 domain of Nrf2, facilitating the Nrf2 proteasomal degradation and high turnover of Nrf2 protein [39]. Nrf2 binds the DGR site of each Keap1 subunit via 2 distinct binding motifs in its Neh2 domain, one high affinity, 79ETGE82, and one low affinity, 29DLG31 [16]. When bound at both sites, Nrf2 is perfectly positioned to bear poly-ubiquitination via the Cul3 E3 ligase and is consequently degraded by the 26S proteasome, assuring low basal levels of Nrf2 in the cell.

The changes in Nrf2 half-life associated with oxidative stress and specific electrophiles varies due to the dramatic differences in detectable basal levels of the protein [40]; also, conflicting evidence is on the mechanism by which Nrf2 becomes free in the cell, because some studies suggested that dissociation of the Keap1–Nrf2 complex is caused from electrophiles [41], while others supported the thesis that the electrophiles cause the dissociation of Cul3 from Keap1 thus preventing the proteasomal degradation of Nrf2 [42].

Furthermore, there are those who believe that Nrf2 is primarily a nuclear protein and this nuclear localization is responsible for the basal expression of cell defence genes and that the degradation of Nrf2 via Keap1 is downstream of Nrf2 transcriptional activity [43], whereas this would explain how Nrf2 is capable of regulating the basal expression of genes despite being constantly degraded via Keap1, this idea requires the nucleo-cytoplasmic shuttling of Keap1 [44]. In any case, the concordant thesis is that Keap1 is responsible for the proteasomal degradation of Nrf2 and that the half-life of Nrf2 doesn't depend on the redox state of the cell and that this is at least partially via the interaction with the redox-sensitive Keap1 [45].

Furthermore, following studies showing the involvement of a Keap1-Cul3-Rbx1 complex in directing the proteasome-mediated degradation of Nrf2, demonstrated that, in the presence of several Nrf2 inducers including tBHQ, sulforaphane, eicosapentaenoic acid (EPA) and N-iodoacetyl-Nbiotinylhexylenediamine (IAB), there was a dissociation of Keap1 from Cul3, preventing the ubiquitination and subsequent degradation of Nrf2 [46]. The dissociation of Keap1 and Cul3 was shown to be dependent on the presence of C151 within the BTB domain of Keap1, as C151 is surrounded by four positively charged amino acids (K131, R135 and K150 and H154), theoretically making it highly reactive towards inducers. The modification of C151 by electrophilic Nrf2 inducers may provoke Cul3 dissociation [47].

1.3.3 The cysteines of Keap1 as sensors of oxidative stress

The discovery of Keap1 as a negative regulator of Nrf2 made it possible to test the idea that cysteine residues of Keap1 serve as the sensors for inducers [48]. Several studies have demonstrated the covalent modification of multiple cysteine residues by Nrf2 inducers, which is hypothesized to alter the Keap1 conformation, thus preventing its association with Nrf2, allowing Nrf2 to translocate to the nucleus [49]. As mentioned above, Keap1 is a cysteine-rich protein and the 27 cysteine residues in the human protein are all reactive to varying degrees. The modification of a subset of cysteine residues in Keap1 by Nrf2 inducers with similar structures supports the hypothesis of a “cysteine code” and may underlie the ability of Nrf2 to respond to such a diverse array of compounds [50]. The high frequency of cysteine residues in the Keap1 sequence confers it with a relative high reactivity to electrophilic inducers; particularly, the most reactive Keap1 cysteines residues modified identified are: C257, C273, C288 and C297, within the IVR domain, and a fifth one, C613 in the C-terminal region of murine Keap1 [51].

A later study showed that by modifying the conditions for incubation and sample processing another residue, C151, could be also detected as the most reactive cysteine of the four (C38,

C151, C368 and C489) readily modified cysteine residues in Keap1 by sulforaphane [52]. In oxidative stress conditions or in the presence of electrophiles, it is proposed that subsets of the cysteine residues in Keap1 are modified, contributing to a conformational change in the protein which results in the release of Nrf2 from the low affinity binding site, disturbing the transfer of ubiquitin. In this way, Keap1 molecules become saturated with Nrf2, that is no longer targeted for degradation and newly synthesized, free Nrf2 accumulates in the cytosol.

The modifications of the cysteine residues confer a suppression of Keap1 and a subsequent upregulation of Nrf2, thus providing vital information on the regulation of the Nrf2 pathway. Additionally, although it is plausible that a certain electrophile both modifies a subset of cysteine residues in Keap1 and induces Nrf2, a substantial number of other factors may contribute to this, such as changes in redox state of the cell, changes in transcription and translation and alterations in protein degradation [44].

The precise mechanism through which cysteine modifications in Keap1 lead to Nrf2 activation is not known, but the two prevailing but not mutually exclusive models are (1): the “Hinge and Latch” model, in which Keap1 modifications in thiol residues residing in the IVR of Keap1 disrupt the interaction with Nrf2 causing a misalignment of the lysine residues within Nrf2 that can no longer be polyubiquitinylated and (2) the model in which thiol modification causes dissociation of Cul3 from Keap1 [25]. In both models, the inducer-modified and Nrf2-bound Keap1 is inactivated and, consequently, newly synthesized Nrf2 proteins bypass Keap1 and translocate into the nucleus, bind to the ARE and drive the expression of Nrf2 target genes; also, in addition, proteins such as p21 and p62 can bind to Nrf2 or Keap1 thereby disrupting the interaction between Nrf2 and Keap1[53].

1.3.3.1 Hinge and Latch Model

The ETGE motif within the Neh2 domain of Nrf2 provides a binding site for the beta helix formed by the Kelch repeats of Keap1 and, although a binding occurs in the absence of this

motif, it is insufficient to facilitate the ubiquitination of Nrf2, suggesting the need for a second association to initiate ubiquitination, who sees the involvement of DLG motif [54].

The ETGE and DLG motifs have different affinities for Nrf2 due to different electrostatic interactions. The ETGE motif has 13 electrostatic interactions with Keap1, while DLG has 8 interactions with Keap1; without the binding of both motifs with Keap1, no ubiquitination or degradation of Nrf2 is observed [55].

In the presence of inducers, a conformational change of Keap1 inhibits binding via the DLG motif (the latch) but does not affect binding via the ETGE motif (the hinge) of Nrf2. This prevent the ubiquitination of Nrf2, which is no longer degraded. Keap1 becomes saturated with Nrf2 and newly synthesized Nrf2 proteins are free to accumulate in the nucleus, bind to small Maf proteins and transactivate ARE regulated genes and destabilize Keap1-Nrf2 interaction.

1.3.4 Autophagic degradation of Keap1

The proteasome is the machinery used by the cells to carry out the degradation of specific proteins targeted for destruction for reasons such as misfolding. Autophagy process was generally regarded to be a bulk-degradation pathway for the recycling of a multitude of non-specific cellular organelles and proteins. However, there is growing evidence supporting the notion that the latter pathway is capable of degrading specific targeted proteins [56]. The substrate adaptor Sequestosome1 (p62) acts as a scaffold protein in various signaling pathways targeting specific proteins for degradation via the autophagic pathway [57].

Evidence suggests that p62 has a role in regulating Keap1 degradation via autophagy, altering the ability of the cell to respond to various stresses via this pathway [58]; particularly, it was observed that the ectopic expression of p62 resulted in lower levels of Keap1 protein and increased expression of Nrf2 protein [59]. The suggested model, under conditions of stress, offers a conformational change in Keap1 releases Nrf2 from the low affinity binding site and

p62 takes advantage of this empty site and binds to Keap1 via an STGE motif, a sequence similar to Nrf2s ETGE motif and also to LC3 which is associated with the autophagosome membrane, providing a link between the Keap1–Nrf2 complex and autophagic degradation [60].

1.4 Keap1-independent Regulation of Nrf2

Despite the aforementioned support for the regulation of Nrf2 via Keap1, there is also a mounting evidence showing that Nrf2 can be regulated independently of Keap1. The expression level and function of a protein can be controlled by regulation at various levels, including: transcriptional, post-transcriptional, protein abundance, post-translational modification and subcellular localization. The phosphorylation of Nrf2 by several signal transduction pathways, the involvement of epigenetic factors such as microRNAs or the interaction of Nrf2 with other proteins may also play a role in Nrf2 activation [61].

1.4.1 Transcription regulation and autoregulation

The core DNA sequences, ARE and XRE (xenobiotic-responsive element), are found in the promoter region of many cell defense genes known to be regulated by Nrf2. Nrf2 binds to the ARE to up-regulate gene expression while the XRE is activated by the transcription factor AHR (aryl hydrocarbon receptor). Ligands which activate AHR cause its heterodimerization with ARNT (AHR nuclear translocator) and this complex activates the XRE to promote the activation of the antioxidant pathway via the ARE [62]. XRE and ARE elements are found in proximity within the promoters of several Nrf2 regulated genes as well as Nrf2 itself; the Nrf2 promoter region contains one XRE-like element at position −712 and the Nrf2 mRNA initiation site contains two XRE-like elements at position +755 and +850 [63]. The presence of these DNA binding sites (ARE/XRE) within the promoter region of Nrf2 suggests the ability of Nrf2 to regulate its own transcription.

Since Nrf2 has been implicated in the pathogenesis of various diseases, it is plausible that the Nrf2 gene contains polymorphisms that may predispose individuals to certain health problems. A study by Yamamoto et al. identified the presence of three single nucleotide and one triplet repeat polymorphism in the regulatory region of the Nrf2 gene [64]. In this study, no link was established between the frequency of the polymorphism and the pathogenesis of diseases, but then multiple SNPs in the Nrf2 gene were identified, observing a correlation between the −617 SNP and the susceptibility to acute lung injury (ALI) implicating Nrf2 in the development of this disease [65]. What remains to be determined is what effects these polymorphisms have on the expression levels and activity of Nrf2 and whether this information can be used to tailor drug regimes to individuals and increase drug safety.

1.4.2 Post-transcriptional regulation: microRNAs

MicroRNAs (miRs) are short, single-stranded non-coding RNAs of approximately 21–23 nucleotides in length, transcribed from genetic loci by RNA polymerase II and processed before being exported from the nucleus as short hairpin loops for maturation and cleavage. Upon maturation, these microRNAs form a complex called the RNA-induced silencing complex (RISC) which binds to target mRNAs at the 3′UTR region and exerts its function through mRNA degradation or protein translation inhibition to inhibit protein expression [66]. Recent studies revealed important roles of miRNAs (miRs) in the control of Nrf2 activity through direct targeting of the Nrf2 mRNA and of mRNAs encoding proteins that control the level and activity of Nrf2 [67]. Interestingly, an abnormal expression of miR-144 has been associated with the sickle cell disease (SCD) and this implicates a role for Nrf2 in this disease [68]; recently, the genome-wide miRNA microarray and primary erythroid progenitor data supported a miR-144/NRF2-mediated mechanism of γ-globin gene regulation in SCD [69].

A similar relationship was seen between Nrf2 and miR-28 in breast epithelial cells, where MiR-28 was shown to regulate Nrf2 by binding facilitating the degradation of Nrf2 mRNA as well as promoting the degradation of Nrf2 protein; furthermore, MiR-28 had no effect on either Keap1 protein expression or the Keap1/Nrf2 interaction highlighting a mechanism by which Nrf2 is regulated independently of Keap1 [70]. The actual mechanism by which micro-RNAs regulate Nrf2 and other proteins requires further elucidations.

1.4.3 Post-translational modification: phosphorylation/acetylation

Nrf2 contains many serine, threonine and tyrosine residues, which may provide sites for phosphorylation by different kinases and a number of different pathways have been explored including mitogen-activated protein kinase cascades (MAPK), the phosphatidylinositol 3-kinase (PI3K/AKT) pathway, protein kinase C (PKC), GSK3β and ERK pathways [71]. There have been several studies suggesting that phosphorylation of Nrf2 may contribute to its nuclear exclusion and degradation. The majority of known Nrf2 activators also activate other kinase pathways for example, tBHQ activates the PI3K/Akt pathway while BHA activates the MAP kinases [72]. The identification of GSK3β as a key regulator of Nrf2 stability has provided insight to the activation of Nrf2 by phosphorylation and it may act as a "common downstream effector" for many Nrf2 inducers [71]. The molecular mechanism underlying their roles in the activation of these kinase pathways remains poorly understood as activation of specific pathways is dependent on a number of factors such as the chemical characteristics of the inducing agent, the cell type used, and the sequence of the ARE, ultimately adding to the complexity of the regulation of Nrf2 by the previously described signaling pathways.

1.4.4 Nrf2 cysteine modifications

Although much attention has been focused on the modification of reactive cysteine residues in Keap1, the modification of cysteines in Nrf2 is another possible mechanism for its regulation. Under the conditions of oxidative stress or in the presence of electrophiles, it is possible that

modification at Cys-183 prevents the binding of exportin Crm1 to Neh5 domain resulting in nuclear accumulation Nrf2 [73]. Mutations at Cys119, Cys235, and Cys506 reduced the binding of Nrf2 to endogenous ARE demonstrating multiple and critical roles of Nrf2 cysteine residues for inducer-sensing and Keap1-independent ubiquitination/degradation of Nrf2 as well as transactivation by Nrf2 [74].

1.4.5 Cross-talk between Nrf2 and other pathways

A further Nrf2 independent regulation is through its interaction with other proteins. This could be as a result of direct binding with Nrf2 or through competing with its negative regulator Keap1. Many proteins compete with Keap1 including fetal Alz-50 clone, prothymosin and caveolin-1 (Cav-1). Cav-1 is a scaffold protein functions in signal transduction and uptake of lipophilic compounds and the knockdown of Cav-1 using siRNA resulted in Nrf2-Keap1 dissociation; further analysis showed that the Nrf2-Keap1 association was increased following mutation of the Cav-1 binding motif on Nrf2 [75].

NF-κB, another transcription factor important in regulating cellular homeostasis, has been shown to cross-talk with Nrf2, negatively regulating its activity. The p65 subunit of NF-κB binds to Keap1 to enhance ubiquitination of Nrf2, thus affecting the ability of Nrf2 to regulate the expression of downstream ARE-dependent genes [76].

1.5 The role of Nrf2 in diseases

Nrf2 is referred to as the "master regulator" of the antioxidant response, modulating the expression of hundreds of genes that control different processes such as immune and inflammatory responses, tissue remodeling and fibrosis, carcinogenesis and metastasis, and even cognitive dysfunction and addictive behavior [77]. Thus, the dysregulation of Nrf2-regulated genes provides a logical explanation for the connections, both direct and indirect, between oxidative stress and at least 200 human diseases involving these various physiological

processes. Harnessing the beneficial effects of pharmacological activation of Nrf2 remains an important aspect of Nrf2-based chemoprevention and of intervention in other chronic diseases, such as neurodegeneration, diabetes, cardiovascular disease, and chronic kidney and liver disease [78]. However, studies have increasingly revealed that Nrf2 is already high in certain cancer and disease stages, indicating that pharmacological agents designed to mitigate the potentially harmful or transformative effects associated with prolonged activation of Nrf2 should also be considered.

1.5.1 Nrf2 in cardiovascular disease

Cardiovascular disease (CVD) is the main cause of death worldwide and it covers a wide array of disorders. Several risk profiles are involved in CVD where ROS is a central mediator and it can cause apoptosis, increasing adhesion molecules and cytokines that enhance monocyte adhesion [79]. Oxidative stress is involved in mitochondrial dysfunction, which is related to bioenergetic defects and an alteration in mitochondrial dynamics. This provokes transcription impairment and cell damage. Blockage of the mitochondrial electron transfer in complex III leads to the release of electrons which reduce molecular oxygen to superoxide (O2•) and increases intracellular ROS production [80]. A series of studies reported that interventions against endoplasmic reticulum (ER) stress and Nrf2 activation reduce myocardial infarct size and cardiac hypertrophy in animals exposed to I/R injury and pressure overload [81]. Oxidative stress is strongly implicated in the development of cardiac dysfunction and myocardial apoptosis contributes to the pathogenesis of heart failure; furthermore, Nrf2 activation in ischemia and I/R injury is being considered protective towards cardiomyocytes [82]. Nrf2 has been reported to operate downstream of NADPH oxidase-4, regulating GSH redox process in cardiomyocytes and to protect the heart in chronic hypertension [84].

1.5.2 Nrf2 in liver disease

Early studies noted that Nrf2 KO mice were more susceptible to acetaminophen-induced liver injury [83]. Studies have shown the induction of Nrf2 and regulated genes by acetaminophen and its reactive metabolite within the non-toxic and toxic dose ranges. Other compounds have also been associated with enhanced hepatotoxicity in Nrf2 KO animals [84]. Other small molecule inducers of Nrf2 have been shown to protect against the oxidative and electrophilic stress associated with various drug-induced liver injuries [85]. Again, a previous study found that Nrf2 activation prevents alcohol-induced oxidative stress and accumulation of free fatty acids in liver by increasing genes involved in antioxidant defense and by decreasing genes involved in lipogenesis [86]. These findings together suggest the possibility of using Nrf2-inducing agents as an adjuvant/co-treatment to prevent drug toxicities in the liver.

1.5.3 Nrf2 in kidney disease

Kidney disease affects ~ 10% of the population worldwide and oxidative stress is a major driver of various kidney problems, promoting the progression from acute to chronic injury [87]. Yoh et al., demonstrated that aged female Nrf2 KO mice developed lupus-like autoimmune nephritis, suggesting that Nrf2 regulates homeostasis in the aging kidney [90]; in addition, Nrf2 KO mice exposed to streptozotocin showed enhanced susceptibility to hyperglycemia-induced diabetic nephropathy [88]. The role of Nrf2 in conferring protection against kidney injury has been highlighted in animal models of renal ischaemic-reperfusion and the pre-induction of Nrf2 in these models ameliorated the deleterious effects of the nephrotoxins [89]. These studies together highlighted an important role for Nrf2 in the kidney and identify the transcription factor as a promising target for treating numerous renal diseases. Recently, Nrf2 was identified as a key molecule involved in protection against renal damage associated with hemolysis, opening novel therapeutic approaches to prevent renal damage in patients with severe hemolytic crisis [89].

1.5.4 Nrf2 in diabetes

Dysregulations of Nrf2 have also been demonstrated in type I and II diabetes. Increased oxidative stress is a typical feature of diabetes that leads to cellular dysfunction and metabolic changes in many tissues [90]. In diabetes, oxidative stress impairs glucose uptake in muscles and fats and decreases insulin secretion from pancreatic cells; numerous evidences have recently elucidated the role of Keap1-Nrf2 system in metabolic and energy-balance regulation [91]. Recently, Qin et al. showed the properties of antioxidant Ginsenoside Rg1 (GS Rg1) administration to reduce inflammation state in streptozotocin (STZ)-induced diabetic rats. The underlying mechanisms may be involved in AMPK/Nrf2/HO-1 pathway [92].

1.5.5 Nrf2 in cancer

There is an increasing body of evidence pointing toward the role of Nrf2 in cancer initiation and progression; in normal and premalignant tissues, Nrf2 holds an important role in cytoprotection and cancer prevention. Comprehensive genomic analyses have found somatic mutations and other alterations in the Keap1 or Nrf2 genes and in well-known tumor suppressor genes or oncogenes, in various types of cancer [93]. Several studies have shown that Nrf2-Keap1 pathway protects against oxidative stress, chemotherapeutic agents and radiotherapy in cancer [94]. However, Jeong et al. [95] found that Keap1/Nrf2 mutations increase radio resistance and predict local tumor recurrence in patients undergoing radiotherapy. The discovery of the dual role of Nrf2-Keap1 pathway enabled scientists to understand Nrf2 signaling in cancer and to develop pharmacological compounds targeting Nrf2 for the prevention and treatment of cancer.

1.5.6 Nrf2 in neurodegenerative disease

The role of Nrf2 in neurodegenerative diseases is complex. During neurodegeneration, Nrf2 can be activated or suppressed depending on the affected cell type and stage of disease. The target genes of Nrf2 have been involved in the regulation of glutathione (GSH), antioxidant

proteins/enzymes, drug-metabolising enzymes or drug transporters, proteasome subunits, pentose phosphate pathway enzymes and enzymes involved in nucleotide synthesis [96]. The pathological processes generate ROS, which in turn, cause oxidative stress and damage to lipids, proteins and DNA. These pathophysiological events encompass a wide variety of neurodegenerative diseases, including Alzheimer's disease (AD), Parkinson's disease (PD), Huntington's disease, ischaemia and stroke.

Alzheimer's disease (AD) is a progressive neurodegenerative disease characterised by loss of neuronal integrity, memory impairment and cognitive decline. Studies have shown that the expression of Nrf2 target genes were increased in AD patients [97]. One study provided a strong evidence that direct Keap1-Nrf2 disruptors can specifically target the defects in Nrf2 activity observed in AD, showing a link between Nrf2 and AD-mediated cognitive decline [98]. The neuroprotective role of Nrf2 in AD had been mainly proposed through GSK-3β in the regulation of the Nrf2 pathway [99].

Parkinson's disease (PD) is a type of movement disorder and it occurs when neurons in the brain do not produce enough dopamine. A link has been revealed between the transcription factor Nrf2 and PD at genetic level, showing that a functional haplotype in the human NFE2L2 gene promoter of Nfr2, with slightly increased transcriptional activity, is associated with decreased risk and delayed age of onset of PD [100]. Furthermore, the localization of Nrf2 was founded in PD brain in addition to cytoplasm, observed in neurons, collectively suggesting that the Nrf2–ARE signal has been activated in PD [101].

2.0 CHAPTER TWO: Dimethyl fumarate (DMF) on Nrf2-pathway regulation

2.1 Fumaric acid esters

Fumaric acid esters (FAE), also known as fumarates, are ester derivatives of fumaric acid, an intermediate in the citric acid cycle, which is a basic cellular process that generates energy in the mitochondria substances, exerting various activities on cutaneous cells and cytokine networks. FAE have been used individually in patients with psoriasis since the late 1950s, but in the 1990s, a mixture of dimethylfumarate (DMF) and three salts of monoethylfumarate (MEF), Fumaderm®, gained approval for the oral treatment of moderate-to-severe plaque-type psoriasis in Germany. FAEs are used to treat adults with moderate to severe psoriasis and also have been reported in treating some patients with systemic lupus and severe disseminated granuloma annulare [102].

The mechanisms of action by which FAE improve psoriasis are not yet completely understood. FAE are thought to elicit their effects through multiple immunomodulating effects [103]. Recent experimental studies have described various immunomodulatory, anti-inflammatory, and anti-oxidative properties of FAE. Given the broad range of FAE's effects, FAE are now being applied for diseases other than psoriasis [104]. Favorable effects of off-label use of FAE have been reported for several inflammatory and granulomatous skin diseases, including sarcoidosis, cheilitis granulomatosa, granuloma annulare, necrobiosis lipoidica, and lupus erythematosus [105]. In addition, FAE have been proven to be effective in multiple sclerosis and FAE became approved as treatment for multiple sclerosis by the FDA and the European Medicines Agency in 2013 [106]. Furthermore, FAE are being evaluated for various other diseases, including Huntington disease, myocardial infarction, and asthma.

2.1.1 Different FAE-formulations

Today there are several different FAE-formulations in use. The only licensed FAE-formulation for psoriasis treatment to date is Fumaderm, which is approved for use in Germany. Fumaderm

is a mixture of DMF and the calcium-, magnesium- and zinc-salt of MEF. Two strengths of tablets are available: Fumaderm initial 105 mg tablets containing 30 mg of DMF and 75 mg of MEF-salts; and Fumaderm 215 mg tablets, which contain 120 mg DMF and 95 mg of MEF-salts. DMF is thought to be the active FAE component in Fumaderm treatment. A double-blind study comparing DMF monotherapy with combination therapy of DMF and MEF salts showed no statistically significant differences in efficacy between the two FAE formulations [107].

A FAE-formulation with delayed-release DMF (BG-12, also known as Tecfidera, Biogen Idec, Cambridge, MA, USA) was approved for the treatment of relapsing multiple sclerosis in 2013 by the FDA following two successful Phase III studies [108].

2.1.2 Pharmacokinetics and pharmacodynamics of FAE

FAE seem to deplete glutathione in circulating immune cells, which induces the expression of the anti-inflammatory protein heme oxygenase 1 (HO-1); in turn, this results in inhibition of pro-inflammatory cytokine production of TNF-α, interleukin (IL)-12, and IL-23, which could explain the beneficial response by FAE in psoriasis treatment [109]. The mechanisms of action of FAE have also been ascribed to other immunomodulating effects, including inhibiting the maturation of dendritic cells, inducing T-cell apoptosis, differentiation of T-helper 2 and T-helper 17 cells and interfering with leukocyte extravasation by reduction of endothelial adhesion molecule expression [110]. Moreover, FAE are capable of inhibiting keratinocyte proliferation and inhibiting angiogenesis by reducing vascular endothelial growth factor receptor-2 expression [111].

2.2 Dimethyl fumarate (DMF)

Dimethyl fumarate (DMF) is derived from the simple organic acid fumaric acid which is named after the earth smoke plant (*Fumaria officinalis*). Dimethyl fumarate (DMF) was licensed in 2013 as an oral first-line therapy for relapsing-remitting (RR) multiple sclerosis patients. It has a strong efficacy with neuroprotective and immunomodulatory effects and a favourable benefit-

risk profile. Following oral administration, DMF undergoes rapid enzymatic hydrolysis in the alkaline milieu of the small intestine, where abundant esterases rapidly metabolize orally-ingested DMF into its primary, active metabolite monomethyl fumarate (MMF). Although DMF does not show any binding affinity to serum proteins, MMF is 50% bound to plasma proteins [112]. Systemic MMF concentrations in the circulation peak between 2–2.5 hours after ingestion, while, in clinical practice, systemic MMF peaks may be delayed for several hours if DMF is ingested with high calorific, fat-rich meals. Importantly, orally ingested DMF is not readily found in the systemic circulation and less than 0.1% of its initial dosage can be detected in the urine ; also, there was no evidence of accumulation after multiple doses (e.g. 240 mg delayed-release DMF three times daily for 2 days) with MMF concentrations below detectable limits at the end of treatment day [113].

For optimized pharmacokinetics with predominant release in the small intestine, DMF was formulated as an oral delayed release preparation which was initially named BG12 as the study compound. Given its pharmacokinetic profile, the compounds needs application every 12 hours (i.e. twice daily) with a dosage of 2 × 240 mg used in clinical practice. Lower dosages and application frequencies were initially tested, but did not yield sufficient effects [114].

2.2.1 Tolerability and safety of DMF

Supportive evidence for the safety profile of DMF was provided by a number of other studies with FAE preparations (including DMF/MEF). The major adverse effects that patients treated with DMF can develop are diarrhoea, abdominal pain and flushing, most of them were mild in severity. Gastritis, erosive gastritis, gastric ulcer and gastroduodenitis are most likely to occur during the first few weeks of therapy [115]. Treatment with FAEs, including dimethyl fumarate, may decrease lymphocyte and leukocyte counts, becoming a risk for progressive multifocal leukoencephalopathy (PML) [116].

2.2.2 Dosage and administration of DMF

The recommended starting dosage of DMF is 120 mg orally twice a day for 7 days. The dosage is then increased to the recommended maintenance dosage of 240 mg orally twice a day. DMF can be taken with or without food, however, administration with food may reduce the incidence of flushing [108].

2.2.3 Mechanism of action

Numerous scientific studies are still underway aimed at clarifying the ultimate mechanism of DMF action. Like other first-line immunomodulators, DMF may not only exert a single mechanism of action but is rather characterized by pleiotropic biological effects. The first in vitro studies with high concentrations of FAEs pointed at proapoptotic effects on T-cells, with a dose-dependent ability to promote so called T-helper cell type 2 (Th2) immune responses characterized by the production of interleukin-(IL) 4, or IL-5 [117]. More recent in vivo and in vitro studies further elaborated on the effect of DMF on dendritic cells, showing a prevailing effect on Th2-cell-promoting, so called type II, dendritic cells, these studies provided further insights on the cascades of cellular events that may follow exposure to DMF. Beyond its effects on T-cells and dendritic cells, DMF may also target several other immunologically active cell types: neutrophils, macrophages, monocytes, endothelial cells or keratinocytes [118]. In human studies with lower numbers of MS patients, recent analyses focused on immunophenotyping of peripheral blood mononuclear cells under DMF therapy and proved prevailing effects on CD8-positive T-cells and also regulatory T-cells independent from lymphopenia.

Although, the exact mechanism of action of DMF is unknown, the drug and its metabolite are thought to work by activation of Nrf2-pathway, which is involved in the cellular response to oxidative stress. Protection of the neuron from oxidative metabolic stress may be provided by increased levels of antioxidant proteins. In addition, DMF may have anti-inflammatory effects because of its blockade of nuclear factor kappa-B and its ability to prevent release of

proinflammatory cytokines, lymphocyte activation, and differentiation of antigen-presenting cells [119]. Other experiments suggest that hydroxycarboxylic acid receptor 2 (HCAR2) activation, rather than Nrf2 activation, may be partially responsible for the beneficial action of DMF in PD and MS models [120]. HCAR2 is a G protein–coupled receptor whose ligands are hydroxyl-carboxylic acids produced from energy metabolism in order to sense cellular metabolic status; also, HCAR2 is expressed in immune cells and other cell types. HCAR2 is a major therapeutic target of DMF in neurodegenerative disorders [121].

2.3 Aim of the thesis PART I

On the basis that:

- The Nrf2 pathway plays a critical role in maintaining homeostasis under conditions of cellular stress
- The Nrf2 pathway is involved in brain health and disease, with implication of cerebral inflammation
- The Nrf2 regulation DMF-mediated could be a useful therapeutic tool to counteract brain diseases

The key aim of this thesis was to better define the chemical and molecular mechanisms that are required for the pharmacological manipulation of Nrf2 and the likely therapeutic significance of modulating the activity of this important pathway. In this first part, this thesis examined the responsiveness of the Nrf2 pathway to DMF treatment on two mouse models, respectively of traumatic brain injury (TBI) and nitroglycerin (NTG) induced-migraine, in order to understand the translational relevance of the *in vivo* findings.

3.0 CHAPTER THREE: Dimethyl Fumarate attenuates neuroinflammation and neurobehavioral deficits induced by experimental traumatic brain injury.

3.1 Introduction

Traumatic brain injury (TBI) is the third cause of mortality and disability [122], clinically considered a “silent epidemic” because the derived problems are not immediately visible and the common underestimation of the actual incidence of this pathology causes that society is unaware of the impact of TBI [123]. In past decades, the research of TBI made great progress in clarifying the pathophysiological mechanisms, so now it is known that TBI is a heterogeneous disorder with several shades [124]. These consist of a primary insult resulting from the direct biomechanical forces and a secondary insult that plays an important role in the brain damage and death following TBI. Instead, the secondary injury is caused by an incompletely understood and complex cascade of physiologic and biochemical factors continuing for hours to days post-injury, leading to catabolic intracellular processes that involve overproduction of free radicals, activation of cell death signaling pathways and up- regulation of inflammatory mediators [125]. The role of secondary brain injury is decisive in determining outcome from severe head injury [126]. Large lines of evidences demonstrate that oxidative stress plays a sensitive role in secondary injury after TBI [127]. For this reason, the oxidative stress was extensively investigated as major contributors to the pathophysiology of secondary TBI damage [128]. The most common free radical generated almost immediately following TBI is superoxide anion (O _.), which promotes the formation of other reactive oxygen species/reactive nitrogen species (ROS/RNS) leading to lipid peroxidation. In post- TBI pathophysiologic context, a remarkable importance is attributed to peroxynitrite, produced by coupling NO with superoxide [129, 130]. Recent studies have suggested that Nrf2, a pleiotropic transcription factor, is a master regulator of anti-oxidative defense responses for protecting cells from cytotoxic/oxidative damage in neuronal environment [131]. Furthermore, the role of Nrf-

2 in protection against TBI-induced secondary brain injury, inducing antioxidant and detoxifying enzymes and by regulating inflammatory cytokines, is subject of great scientific interest [132].

Moreover, TBI triggers a series of inflammatory processes that, via nuclear factor kappa- light-chain-enhancer of activated B cells (NF-κB), contribute to neuronal damage and failure of functional recovery, through a complex cascade of post traumatic events that can be divided into a hemodynamic, metabolic, neuroendocrine and immune responses leading to a multifocal pathophysiologic process [133]. This vicious cycle of inflammation- damage-inflammation is driven by infiltrating inflammatory cells like activated microglia, neutrophils and macrophages that produce multiple pro-inflammatory mediators, such as cytokines, chemokines, neuronal nitric oxide synthase (nNOS) and cyclooxygenase (COX)-2 and can be additional sources of O2_. [134]. The understanding of oxidative stress mechanisms and the development of anti-inflammatory strategies are of primary interest to optimize TBI treatment and may provide useful therapeutic strategies for neurodegenerative diseases. Concerning this aspect, in the last few years, in vitro and in vivo studies have explored the therapeutic potential of a class of molecules, fumaric acid esters (FAEs), for the treatment of inflammatory and oxidative diseases. Dimethyl fumarate (DMF), the most pharmacologically effective molecule among the FAEs, is an oral therapeutic agent for the treatment of relapsing-remitting Multiple Sclerosis (MS) patients [114]. More importantly, DMF was discovered to impact the anti-oxidative stress cell machinery promoting the transcription of genes downstream to the activation of Nrf-2. Furthermore, it was ascertained that DMF can alleviate early brain injury and secondary cognitive deficits after experimental subarachnoid hemorrhage modulating Nrf-2 pathway [135]. Previously, it has been suggested that the anti- inflammatory activities of DMF consists of the NF-κB inhibition and reduction of pro-inflammatory responses [136]. Effective TBI treatments remain a major unmet clinical need to limit secondary injury and enhance neural

repair [137]. Given that pathological processes involved in secondary brain injury are complex and interrelated, is desirable to find a possible target which can interrupt multi- pathological mechanisms modulating Nrf-2 pathway, thus providing a valid clinical support therapy.

3.2 Materials and Methods

3.2.1 Animals

Male CD1 mice (25 to 30 g, Envigo, Italy), aged between 10 and 12 weeks, were used for all studies. Mice were housed in individual cages (five per cage) and maintained under a 12:12 hour light/dark cycle at 21 ± 1°C and 50 ± 5% humidity. Standard laboratory diet and tap water were available ad libitum. The University of Messina Review Board for the care of animals approved the study. Animal care was in compliance with Italian regulations on protection of animals used for experimental and other scientific purposes (Ministerial Decree 16192) as well as with the Council Regulation (EEC) (Official Journal of the European Union L 358/1 12/18/1986).

3.2.2 Controlled cortical impact (CCI) experimental TBI

TBI was induced in mice by a controlled cortical impact (CCI) by using the controlled impactor device Impact OneTM Stereotaxic impactor for CCI (Leica, Milan, Italy) as previously described [138]. A craniotomy was induced in the right hemisphere, with a Micro motor hand piece and drill (UGO Basile SRL, Comerio Varese, Italy), among the sagittal suture and the coronal ridge. The bone flap wasremoved and the craniotomy enlarged additionally with cranial rongeurs (New Adalat Garh, Roras Road, Pakistan). A cortical contusion was made on the exposed cortex using the controlled impactor device Impact OneTM Stereotaxic impactor for CCI (Leica, Milan, Italy). Concisely, the impacting shaft was extended and the impact tip was lowered over the craniotomy site until it touched the dura mater. Subsequently, the rod was retracted and the impact tip was advanced to produce a brain injury of moderate severity for mice (tip diameter: 4 mm; cortical contusion depth: 3 mm; impact velocity: 1.5 m/sec).

Immediately after injury, the skin incision was secure with nylon sutures, spreading 2% lidocaine jelly to the lesion site to reduce pain. Sham mice underwent the same surgical procedure including anesthesia and craniotomy but were not injured.

3.2.3 Experimental groups

Mice were randomly allocated into the following groups:

Sham group: mice were subjected to identical surgical procedures except for CCI and were kept under anesthesia for the duration of the experiment (n=20).

Sham + vehicle group: mice were subjected to identical surgical procedures except for CCI, plus vehicle used for DMF, carboxymethyl cellulose (CMC), orally administrated 1h and 4h after craniotomy (n=20).

Sham + DMF (1 mg/kg) group: mice were subjected to identical surgical procedures except for TBI shock plus DMF (1 mg/kg in 10 % CMC) oral administration 1h and 4h after craniotomy (n=20).

Sham + DMF (10 mg/kg) group: mice were subjected to identical surgical procedures except for TBI shock plus DMF (10 mg/kg in 10 % CMC) oral administration 1h and 4h after craniotomy (n=20).

Sham + DMF (30 mg/kg) group: mice were subjected to identical surgical procedures except for TBI shock plus DMF (30 mg/kg in 10 % CMC) oral administration 1h and 4h after craniotomy (n=20).

TBI group: mice were subjected to CCI (n=20) and were kept under anesthesia for the duration of the experiment (n=20).

TBI + vehicle group: mice were subjected to CCI, plus vehicle used for DMF (CMC) orally administrated 1h and 4h after craniotomy (n=20).

TBI + DMF (1 mg/kg) group: the mice were subjected to CCI plus administration of DMF (1 mg/kg in 10 % CMC) oral administration 1h and 4h after craniotomy (n=20).

TBI + DMF (10 mg/kg) group: the mice were subjected to CCI plus administration of DMF (10 mg/kg in 10 % CMC) oral administration 1h and 4h after craniotomy (n=20).

TBI + DMF (30 mg/kg) group: the mice were subjected to CCI plus administration of DMF (30 mg/kg in 10 % CMC) oral administration 1h and 4h after craniotomy (n=20).

The doses (1, 10 and 30 mg/kg) and the administration route (orally) of DMF used in this study was based on previous in *in vivo* studies on colitis and neuroinflammation studies on spinal cord injury and Parkinson's disease experiments [139-141], dose response and time- course studies by our laboratory. The timing of orally DMF administration at 1h and 4h after TBI, between the primary and secondary injury, has the potential to either prevent or to reduce the final neurological deficit. Also, several recent studies illustrated the importance of initiating therapeutic interventions as soon as possible following TBI, preferably within 4h post-injury, to achieve the best possible neuroprotective effect 24.

Furthermore, experimental data regarding the animals from Sham, TBI and Sham+DMF groups were not showed because vehicle and DMF administration did not demonstrate toxicity or any other effect in comparison to sham control animals. Moreover, TBI+DMF (1 and 10 mg/kg) groups were only subjected to histological analysis because these groups didn't demonstrate any improvement of TBI injury, so we decided to continue to analyze only DMF 30 mg/kg treatment.

Mice were sacrificed 24h after TBI, the brains removed and then dissected in order to evaluate the following parameters: histology analysis, Western blot analysis and Immunohistochemical analysis. In a separate set of experiments, a cohort of 10 animals from each group were observed after TBI, receiving DMF daily until the sacrifice, in order to evaluate the behavioral testing.

3.2.4 Tissue processing and histology

Sagittal sections of 7-μm thickness were processed from the perilesional brain area of each animal and were evaluated by an experienced histopathologist. Sections were then

deparaffinized with xylene, and then stained with hematoxylin and eosin. All sections were studied using an Axiovision Zeiss microscope (Milan, Italy). Histopathologic changes of the grey matter were scored on a five-point scale [142, 143]: 0, no lesion observed; 1, grey matter contained one to five eosinophilic neurons; 2, grey matter contained five to 10 eosinophilic neurons; 3, grey matter contained more than 10 eosinophilic neurons; 4, small infarction (less than one third of the grey matter area); 5, large infarction (more than half of the grey matter area). The scores from all the sections of each brain were averaged to give a final score for individual mice. All the histological studies were performed in a blinded fashion.

3.2.5 Stereological assessments of lesion volume and neuronal loss: Crystal violet

Cresyl violet-stained 60-μm coronal sections were used for neuronal loss analysis. For TBI-induced cortex neuronal cell loss, the optical fractionator method of stereology was employed as previously described [144]. Briefly, every fourth 60-μm section between −1.22 mm and −2.54 mm from bregma was analyzed beginning from a random start point (i.e. the section where different hippocampal sub-regions were distinctly visible). A total of 5 sections were analyzed. The sampled region for each cortex sub-region was demarcated in the injured hemisphere and cresyl-violet neuronal cell bodies were counted using Stereoinvestigator software (MBF Biosciences, Williston, VT). The number of surviving neurons in each cortex sub-region was divided by the volume of the region of interest to obtain the cellular density expressed in counts/mm^3.

3.2.6 Fluoro-Jade C (FJC) staining

To detect degeneration of cortical neurons, sections of cortical penumbra area of injured brain were stained with Fluoro-Jade C (Millipore, Billerica, MA, USA) as previous described [145]. Briefly, slides were immersed in 80% Ethanol with 1% NaOH for 5 min, followed by 2 min in 70% Ethanol, 2 min in distilled water, and incubated in 0.06% potassium permanganate solution for 10 min. Slides were subsequently rinsed in water, transferred to a 0.001% solution of Fluoro-

Jade C in 0.1% acetic acid. The slides were then rinsed in distilled water, air dried and cleared in xylene and then cover-slipped with DAPI as above. Green Fluoro-Jade C staining was quantified using Image J.

3.2.7 TUNEL staining

To determine the extent of intracerebral neuronal cell death, TUNEL was performed using a "Fluorescein In Situ Cell Death Detection Kit" (Roche Diagnostics GmbH, Mannheim, Germany), according to the manufacturer's instructions, as previously described [146]. Briefly, sagittal sections of 7-µm thickness were processed from the cortical perilesional brain area of each animal and were dried for 30 min followed by fixation in 10% formalin solution at RT. After washing in PBS (three times for 3 min), sections were incubated in ice-cold ethanol-acetic acid solution (2:1) for 5 min at -20°C. Thereafter, they were washed in PBS and incubated in a permeabilization solution with 3% Triton X-100 in PBS for 60 min at RT, then incubated with the TdT enzyme in a reaction buffer containing fluorescein-dUTP for 90 min at 37°C. Negative control was performed using only the reaction buffer without TdT enzyme. Positive controls were performed by digesting equal brain sections with DNase grade I solution (500 U/ml; Roche) for 20 min at RT and always kept separate from the other samples thereafter. After labelling, the sections were washed again in PBS and to visualize the unstained (TUNEL-negative) cells, the sections were covered with Vectashield® mounting medium for fluorescence with DAPI (Vector). All samples were evaluated immediately after staining using an Axioskop 40 fluorescence microscope (Zeiss, Germany) at 460 nm for DAPI and 520 nm for TUNEL fluorescence and analyzed by Alpha digi doc 1201 software (Alpha Innotech, San Leandro, CA, USA).

3.2.8 Behavioral testing

In another set of experiment, all animals were subjected to behavioral tests every day, for 10 or 5 days post-CCI. All behavioral testing was conducted during the light cycle phase and in

enclosed behavior rooms (50–55 dB ambient noise) within the housing room. The mice were placed in behavior rooms 5 min for 2 days for acclimation prior to the onset of behavioral testing. The behavioral tests were conducted by three different reliable expert observers blinded to the injury status of the animals. Tests are described below:

Elevated pluz-maze (EPM)

The EPM test was used to measure anxiety-like behavior, as described previously [147]. The EPM apparatus (Panlab, S.L.- Harvard Apparatus, Spain) consisted in two open arms (30 x 5 x 0.25 cm) and two enclosed arms (30 x 5 x 15 cm) extended from a common central platform (5 x 5 cm) and the entire apparatus was elevated by a single central support to a height of 60 cm above floor level. The behavioral model was based on rodents' aversion of open spaces that leads to thigmotaxis. The mouse was placed on the central platform facing an open arm and behavior was videotaped with a camera fixed above the EPM. The percentage of time spent on the open arms was scored by a researcher blind of the animal treatment. Anxiety was indicated by an increase in the proportion of time spent in the closed arms and a decrease in the proportion of entries into the open arms. The total numbers of arm entries and number of closed-arm entries were used as measures of general activity.

Rotarod test

The rotarod treadmill (Accuscan, Inc., Columbus, OH, USA) provided a motor balance and coordination assessment. This test was performed as previously described [148]. Each animal was placed in a neutral position on a cylinder (1 cm diameter for mice), then the rod was rotated with the speed accelerated linearly from 0 to 24 rpm within 60 s, and the time spent on the rotarod was recorded automatically. The maximum score given to an animal was fixed to 60. For testing, animals were given three trials and the average score was used as the individual rotarod score.

Short-term sensorimotor deficit analysis

Beam balance and beam walking tasks were assessed in mice at day 0 (before surgery) and at 1-5 days post TBI to evaluate short term sensorimotor deficit as previous described [149]. Gross vestibulomotor function was evaluated on a beam balance task in which the time the animal stained on an elevated, 1.5 cm wide wooden beam was recorded up to a maximum of 60 s. Three trials were performed per mouse every day. Training/pre- assessment was completed on the day before surgery/injury. Spinning on the beam was counted as a fall (a cushioned pad was used to prevent injury). On the day before injury, mice were trained to escape a bright light and loud white noise, by traversing a narrow wooden beam (2.5 × 100 cm) and entering a darkened goal box at the opposite end. The noise and light were terminated when the mouse entered the goal box. Four pegs (3 mm diameter and 4 cm high) were equally spaced along the center of the beam to increase the difficulty of the task. The mice remained in the goal box for 30 sec between trials. If the mice did not cross the beam in 60 sec or fell off, the light and noise were stopped and the mice was placed in the goal box. Performance was assessed by measuring the latency to traverse the beam. The mice were also given a beam-walking score to denote progression along the beam during the beam walk test. Animals successfully reaching the goal box were assigned 5 points. Mice not reaching the goal box were assigned lesser scores, depending on either their final spot on the beam when 60 s had elapsed, or the spot at which they fell off. The final daily beam walking score was the mean score of the three beam-walking trials.

Elevated Biased Swing Test

The EBST provided a motor asymmetry parameter and involved handling the animal by its tail and recording the direction of the biased body swings. The EBST consisted of 20 trials with the number of swings ipsilateral and contralateral to the injured hemisphere recorded and expressed in percentage to determine the biased swing activity. This analysis was performed as previous described [150].

Tail Suspension test (TST)

The TST has been employed as a measure of depression-like behavior. It was performed with each mouse 24 h post-TBI. Briefly, according to methods described previously [151]. Mice were suspended by the tail with a piece of adhesive tape (1 cm from the tip, 17 cm long) 55 cm above the desk. A camera recorded the movement of the mouse for 6 min. Mice were considered immobile when they hung passively and motionless. The immobility time was calculated by subtracting the total amount of mobility time from the 360 s of test time.

3.2.9 Western blot analysis

Western blot analysis was performed on tissues harvested 24 h post-TBI, in the traumatic penumbra area from the ipsilateral injured brain and, in a similar area, from the sham control tissues using antibodies as described earlier. Cytosolic and nuclear extracts were prepared as described previously [152]. The expression of nuclear factor of kappa light polypeptide gene enhancer in B-cells inhibitor alpha (IκB-α), Kelch-like ECH-associated protein 1 (Keap-1), manganese superoxide dismutase (Mn-SOD), hemeoxygenase 1 (HO-1), neuronal nitric oxide synthase (nNOS), cyclooxygenase 2 (COX-2), interleukin 1 (Il-1β), tumor necrosis factor (TNF-α), B-cell lymphoma 2 (Bcl-2) and ionized calcium-binding adapter molecule 1 (Iba-1) was quantified in cytosolic fraction. Nuclear factor kappa-light- chain-enhancer of activated B cells (NF-κB) and nuclear factor erythroid 2- related factor 2 (Nrf-2) expressions were quantified in nuclear fraction. The filters were probed with specific Abs: anti- NF-κB (1:500; Santa Cruz Biotechnology) or anti-Nrf-2 (1:500; Santa Cruz Biotechnology, SC-722) or IκB-α (1:500; Santa Cruz Biotechnology), anti-Keap 1 (1:500; Abcam), anti-MnSOD (1:500; Millipore) or anti-HO-1 (1:500; Santa Cruz Biotechnology) or anti-iNOS (1:500; Cell Signaling) or anti-COX-2 (1:500; Cayman) or anti-Il-1β (1:500 Santa Cruz Biotechnology), or anti-TNF- α (1:1000; Abcam) or anti-Bcl-2 (1:500; Santa Cruz Biotechnology) or anti-Iba-1 (1:500; Abcam) in 1 × PBS, 5% w/v non fat dried milk, 0.1% Tween-20 at 4 °C, overnight. To

ascertain that blots were loaded with equal amounts of proteins they were also incubated in the presence of the antibody against β-actin protein (cytosolic fraction 1:500; Santa Cruz Biotechnology) or lamin A/C (nuclear fraction 1:500 Sigma–Aldrich Corp.). Signals were detected with enhanced chemiluminescence (ECL) detection system reagent according to the manufacturer's instructions (Thermo, USA). The relative expression of the protein bands was quantified by densitometry with BIORAD ChemiDoc TMXRS+software and standardized to β-actin and lamin A/C levels. Images of blot signals (8 bit/600 dpi resolution) were imported to analysis software (Image Quant TL, v2003).

3.2.10 Immunohistochemical analysis

For 4-HNE detection, the sagittal sections of 7-μm thickness were processed from the perilesional brain area of each animal and pre-treated with 0.1M $NaBH_4$ in 0.1M MOPS (pH= 8.0) for 10 min and rinsed off with 0.2 M PBS for three times. The sections were then incubated in 0.3% H_2O_2 for 30 min and rinsed three times with 0.2M phosphate-buffered saline (PBS). Following that, the sections were blocked with a blocking solution (5% goat serum, 0.25% Triton X-100, 1% dry milk, 0.2 M PBS) for 2 h at room temperature and then incubated in the primary anti-HNE antibody (rabbit anti-HNE Michael Adducts, Calbiochem) diluted 1:500 in the same blocking solution overnight at room temperature. The sections were then rinsed with 0.2M PBS five times and then incubated in secondary goat anti-rabbit antibody (Vectastain ABC-AP kit) for 1at room temperature. The sections were then rinsed with 0.1M Tris-HCl and incubated in Vector blue (Vector blue alkaline phosphatase substrate kit III). They were then rinsed with tap water four times and mounted onto gelatinized slides. For immunohistochemical localization of ionized calcium-binding adapter molecule 1 (Iba-1), glial fibrillary acid protein (GFAP) and myeloperoxidase (MPO), the sagittal sections of 7-μm thickness were processed from the perilesional brain area of each animal were incubated overnight with one of the following primary antibodies (all dilutions in PBS): monoclonal anti Iba-1 antibody (1:100,

Santa Cruz Biotechnology), polyclonal anti-GFAP polyclonal antibody (1:100, Santa Cruz Biotechnology), polyclonal anti-MPO (1:100, Merck- Millipore) as previously described 35. Photomicrographs were assessed by densitometric analysis using Imaging Densitometer (AxioVision, Zeiss, Milan, Italy).

3.2.11 Myeloperoxidase activity (MPO)

Myeloperoxidase activity (MPO) was determined as previously described [153]. Ipsilateral injured brain and also similar area from the control and/or contralateral tissues collected at the specified time, were homogenized in a solution containing 0.5% hexa-decyl- trimethyl-ammonium bromide dissolved in 10 mm potassium phosphate buffer (pH 7) and centrifuged for 30 min at 20 000 g at 4°C. An aliquot of the supernatant was then allowed to react with a solution of tetra-methyl-benzidine (1.6 mm) and 0.1 mm H_2O_2. The rate of change in absorbance was measured spectrophotometrically at 650 nm. MPO activity was expressed in units/mg protein.

3.2.12 Materials

DMF was obtained by Sigma-Aldrich (97%, 242926 Sigma-Aldrich). Unless otherwise stated, all compounds were obtained from Sigma-Aldrich. All other chemicals were of the highest commercial grade available. All stock solutions were made in non-pyrogenic saline (0.9% NaCl, Baxter, Milan, Italy) or 10% dimethyl sulfoxide.

3.2.13 Statistical analysis

All values in the figures and text are expressed as mean ± standard error of the mean (SEM) of N observations. For the *in vivo* studies N represents the number of animals studied. In the experiments involving histology, the figures shown are representative of at least three experiments performed on different experimental days. Statistical analysis was performed with GraphPad Prism 7 (GraphPad Software; USA). Differences were analyzed by t-test or by one-way analysis of variance (ANOVA) followed by Bonferroni post-hoc test for multiple

comparisons. Values obtained from the same subjects at different time points were analyzed with repeated-measure ANOVA and Bonferroni post-hoc. A p-value of less than 0.05 was considered significant ($p<0.05$). Each P value was adjusted to account for multiple comparisons.

3.3 Results

3.3.1 DMF treatment reduced the severity of brain trauma and the infarct outcome

The histological analysis of brain sections at the level of the perilesional area revealed a relevant damage in TBI-injured mice, observed through tissue disorganization, white matter alteration and inflammation in the brain parenchyma (Figure 1B, see densitometry analysis 1F) (F value= 36.63; df= 4) compared to sham animals (Figure 1A, see densitometry analysis 1F) (F value= 36.63; df= 4). DMF treatment, at the dose of 1 mg/kg and 10 mg/kg, didn't show any improvement in injured brains at 24 hours after TBI (Figures respectively 1C and 1D, see densitometry analysis 1F) (F value= 36.63; df= 4). Instead, DMF treatment, at the dose of 30 mg/kg, significantly reduced the brain tissue damage at 24 hours after TBI (Figure 1E, see densitometry analysis 1F) (F value= 36.63; df= 4).

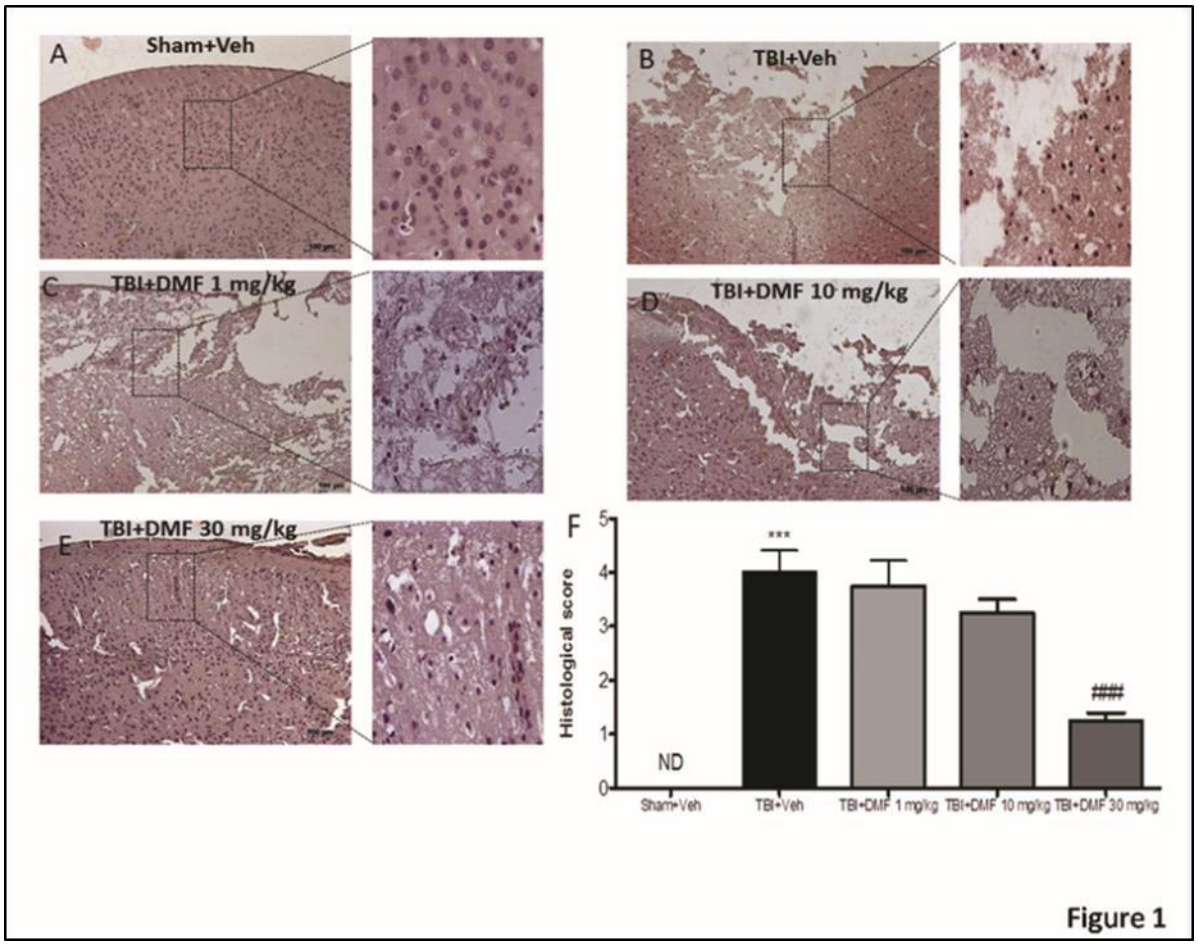

Figure 3.1: Effects of DMF treatment on histological alterations after TBI

A histological examination of brain sections at the levels of the perilesional area, stained 24 hours after TBI, showed tissue disorganization and inflammation in TBI injured mice (panel B, TBI+Veh condition, see histological score F) respect to intact tissue structure observed in control mice (panel A, Sham+Veh condition, see histological score F). A significant protection from the TBI was apparent in DMF 30 mg/kg treated mice (panel E, TBI+DMF 30 mg/kg condition, see histological score F) respect to minor protection with low doses of treatment (panel C and D, respectively TBI+DMF 1 mg/kg and 10 mg/kg). The figures are representative of at least three experiments performed on different experimental days. Sham control tissue was used for comparison. Data are means ± SEM of 10 mice for each group. (F value= 36.63; df= 4). One-Way ANOVA test ($p< 0.0001$) followed by Bonferroni post-hoc test for multiple comparisons. ***$p< 0.001$ vs. Sham; ###$p< 0.001$ vs. TBI. ND, not detectable.

3.3.2 Protective effects of DMF treatment to reduce acute neural injury and degeneration and to modulate apoptosis-induced cell death through Bcl-2

In a separate study we assessed TBI-induced neurodegeneration by cresyl violet stained coronal sections from mice brain 24 h post-injury. Stereological analysis revealed significant reduced cell density in lesion size at 24 h post TBI (Figure 2A, panel TBI+Veh) when compared to control mice (Figure 2A, panel Sham+Veh). The neuron cell density significantly augmented

by DMF treatment 1 and 4 h after TBI (Figure 2A, panel TBI+DMF 30 mg/kg) (F value= 178.5; df= 2). Furthermore, to determine the effects of DMF treatment on degeneration of cortical neurons after TBI, we performed Fluoro-Jade C (FJC) staining. Nearly none FJC positive cells were found in control mice (Figure 2B, panel FJC Sham+Veh) compared to DAPI positive cells (Figure 2B, panel DAPI Sham+Veh), while a significant increase of FJC staining in TBI-injured mice (Figure 2B, panel FJC TBI+Veh). Interestingly, DMF treated mice 24 h after TBI presented significantly less FJC-positive neurons in the brain cortex (Figure 2B, panel FJC TBI+DMF 30 mg/kg) (F value= 240.3; df= 2). Moreover, to determine the extent of intracerebral neuronal cell death, TUNEL staining was performed. Few TUNEL-positive apoptotic cells were found in control mice (Figure 2C, panel TUNEL Sham+Veh). As is shown in Figure 2C, panel TUNEL and Merged TBI+Veh, brain injury caused cortical neurodegeneration, with a significant increase in TUNEL positive cells at 24 h after brain damage. Interestingly, DMF treated mice 24 h after TBI presented significantly less TUNEL-positive neurons in the brain cortex compared with TBI+Veh animals (Figure 2C, panel TBI+DMF 30 mg/kg) (F value= 29.40; df= 2).

Recent findings showed that changes in intracellular expression of Bcl-2 are correlated to the pathology of neuronal injury, because the neurodegeneration following TBI is an active process and proteins associated with cell death participate in this cascade [154]. Thus, to test the role of DMF treatment on apoptosis process, brain homogenates, taken 24 h after TBI, were processed for Western Blot analysis for Bcl-2 expression. Brain sections from sham-operated mice showed a basal Bcl-2 expression (Figure 2D), that was notably reduced in brain homogenates from TBI group (Figure 2D). DMF treatment significantly up-regulated Bcl-2 expression (Figure 2D) (F value= 29.04; df= 2).

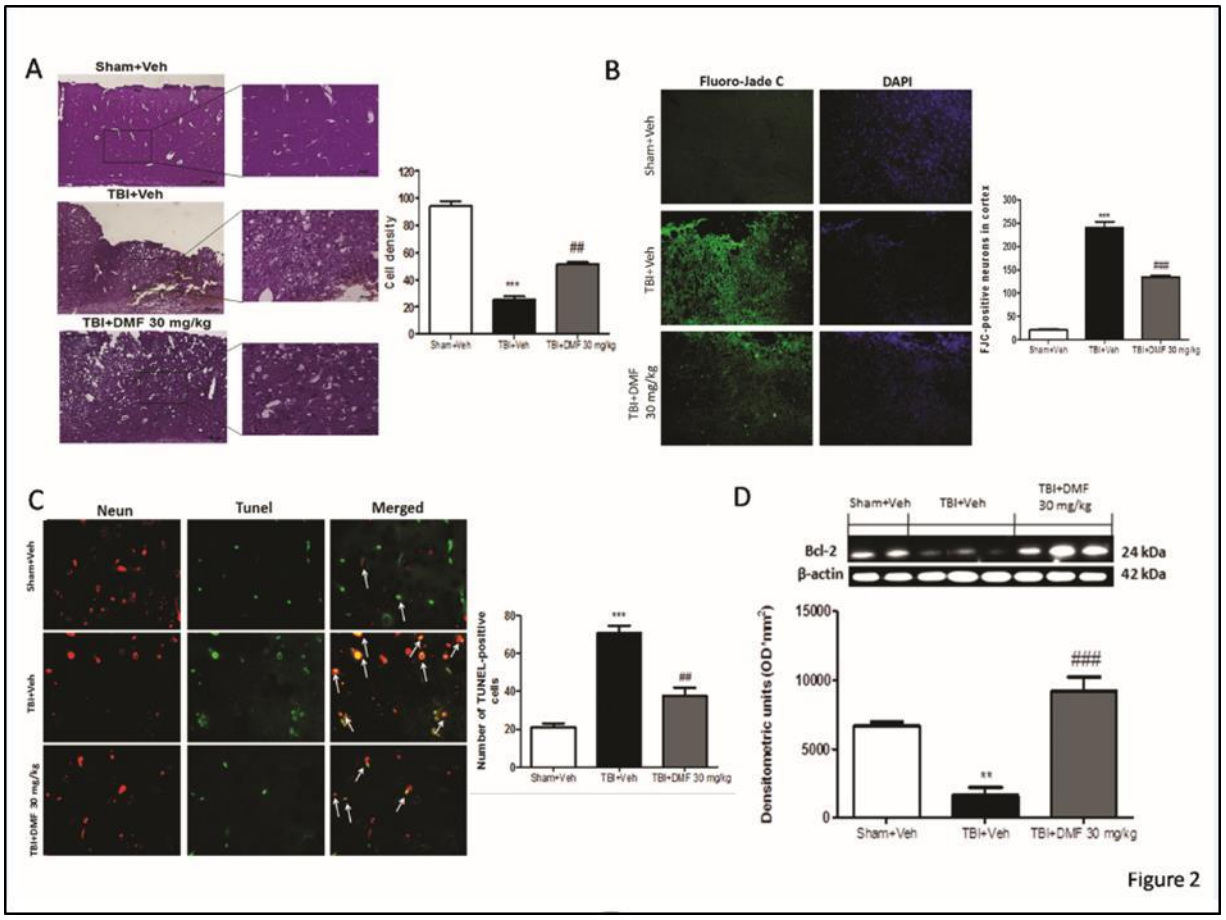

Figure 3.2: Effects of DMF treatment on infarct area and volumes following TBI Stereological analysis of brain sections (A). (F value= 178.5; df= 2). One-Way ANOVA test (p< 0.0001) followed by Bonferroni post-hoc test for multiple comparisons. FJC staining in brain sections (B). All sections were taken from mice sacrificed 24 h post-TBI. Green is FJC and blue is DAPI, a control for equal numbers of cell nuclei. DMF treatment significantly reduced FJC positive staining, reporting to control levels (B). (F value= 240.3; df= 2). One- Way ANOVA test (p< 0.0001) followed by Bonferroni post-hoc test for multiple comparisons. TUNEL staining of lesion area in brain slides (C). The number of TUNEL positive cells in CCI injured mice was significantly higher than control mice (C), while DMF treatment significantly reduced the apoptotic damage (C). (F value= 29.40; df= 2). One- Way ANOVA test (p< 0.0008) followed by Bonferroni post-hoc test for multiple comparisons. The Bcl-2 expression was significantly reduced in CCI-injured mice, at 24 h after TBI (D). DMF treatment significantly attenuated the apoptotic process induced by trauma (D) (F value= 29.04; df= 2). One-Way ANOVA test (p< 0.0008) followed by Bonferroni post-hoc test for multiple comparisons. Sham control tissue was used for comparison. Western blot analysis was performed on tissues harvested 24 h post-TBI. A representative blot of lysates obtained from each group is shown and densitometry analysis of all animals is reported (n = 10 mice from each group). Each data are expressed as mean ± SEM from n = 10 male CD mice for each group. One-Way ANOVA test. **p< 0.01 vs. Sham; ##p< 0.01 and ###p<0.001 vs. TBI.

3.3.3 Effects of DMF treatment on recovery and improvement in behavioral function

To investigate the relationship between neurological deficits in the setting TBI we used motor and neurological behavioral tests. In the first, to assess motor function mice were subjected 24 h after TBI to rotarod test, considered the most sensitive vestibulomotor measure. TBI- injured mice displayed a range of impairments in locomotor tasks (Figure 3A). DMF treatment at the

dose of 30 mg/kg gradually but significantly improved latency compared to TBI group (Figure 3A) (P interaction<0.0002; F interaction= 31,45; df= 2).

Furthermore, as the motor asymmetry a clinical hallmark post injury symptom in a mouse model of TBI, it was appropriate consider this aspect assessing the Elevated biased swing test (EBST). TBI-damaged mice showed significant impairments in motor deficits as revealed by significantly higher biased swing activity compared to control group, while DMF treatment, 24 h after TBI, significantly reduced the percentage of biased swing activity (Figure 3B) (P interaction<0.0001; F interaction= 88,35; df= 2). Also, since anxiety is considered a critical component of behavioral change after brain injury, TBI-injured mice were subjected to the EPM at 24h after TBI (Figure 3C) (F value=36.70; df= 2). Again, at different times: 1, 2, 3, 6 and 10 day (Figure 3E) (F value=44.02; df= 2). Animals were treated with DMF 30 mg/kg every day. The daily treatment of DMF significantly improved latency compared to TBI damaged group (Figure 3D), (F value= 36.86; df= 2), as observed by a decreased permanence in closed arms and by an increment in the number of entries in open arm (Figures 3D and 3C). Furthermore, to test sensorimotor functions, beam balance test, beam walk test and beam walk score were determined at days 0-5 post TBI.

Sham mice exhibited transient and small fluctuations in the beam balance time (Figure 3F), beam walking score (Figure 3H) and beam walking latency (Figure 3G) during days 1-5 after surgery. Instead, TBI-injured mice showed significant deficits in motor functions, reflected by the reduced beam balance time (Figure 3F) and beam walking score (Figure 3H), with a beam balance time partially recovered, but not statistically significant different from post- TBI day 1 (Figure 3G). Interestingly, DMF treated animals exhibited a faster neurological recovery trend after TBI as shown in Figure 3F (F value= 11.12; df= 2, ANOVA for repeated measures (p=0.0029); in Figure 3G (P interaction= 0.0045; F interaction= 9,715; df= 2) and in Figure 3H (P interaction=0.004; F interaction= 18,80; df= 2). Furthermore, because the most common

psychiatric complaint in patients with mild TBI is depression, the tail suspension test (TST) has been employed as a measure of depression-like behavior.

Likewise, different studies on TBI model in mice also found that the severe brain injuries were associated with significant increases in immobility time in TST. We too observed that TBI significantly increases immobility time in TST, but DMF treatment significantly reduced the immobility time (s) already 24 h after TBI as shown in Figure 3J, highlighting the acute antidepressant activity of DMF. (Figure 3J) (F value= 66.28; df= 2).

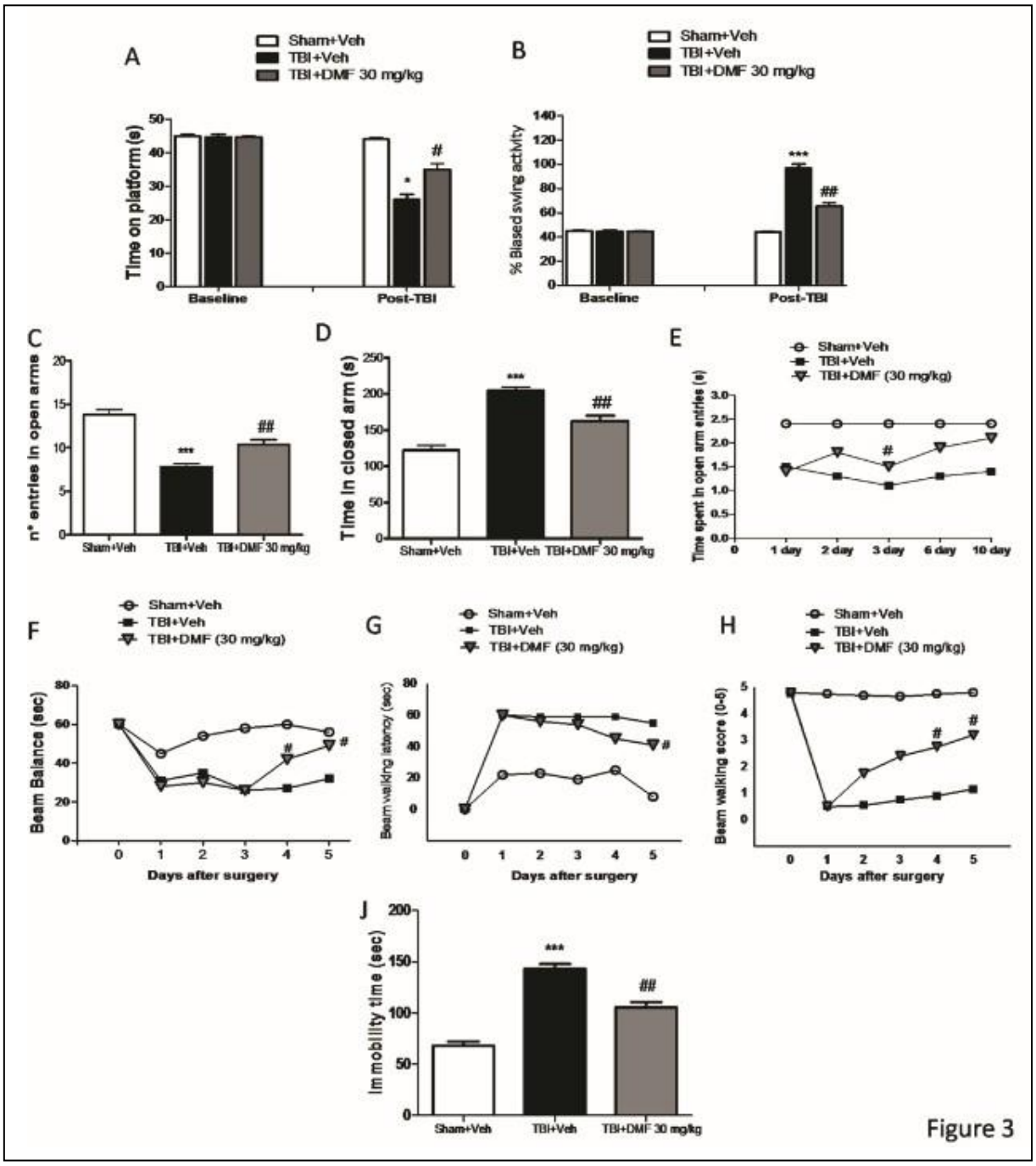

Figure 3

Figure 3.3: Effects of DMF treatment on behavioral and neurological function

TBI-injured mice showed significant impairments in motor deficits as revealed by shortened time to stay on rotarod (A) (P interaction<0.0002; F interaction= 31.45; df=2). Two-Way ANOVA test followed by Bonferroni post-test, and augmented biased swing activity (B) (P interaction<0.0001; F interaction=88.35; df=2), Two-Way ANOVA test followed by Bonferroni post-test. On the contrary treatment with DMF 1h and 4h post-TBI significantly improved motor function (A and B). Moreover, DMF treatment was able to improve cognitive function as evaluated by Elevated Plus Maze test at 0 days (C) (F value= 36.70; df= 2), One-Way ANOVA test (p< 0.0001) followed by Bonferroni post-hoc test for multiple comparisons. and (D) (F value= 36.86; df= 2), One-Way ANOVA test (p< 0.0001) followed by Bonferroni post-hoc test for multiple comparisons. Also, at 1, 2, 3, 6 and 10 days after TBI E) (F value= 44.02; df= 2), ANOVA for repeated measures followed by Bonferroni posttest (p< 0.0001). Furthermore, DMF treatment ameliorated sensorimotor activity as evaluated by beam balance test (F) (F

value= 11.12; df= 2), ANOVA for repeated measures followed by Bonferroni post- test (p= 0.0029), beam walking latency test (G) (P interaction= 0.0045; F interaction= 9.715; df=2), Two-Way ANOVA test followed by Bonferroni post test, beam walking score (H) (P interaction= 0.004; F interaction= 18.80; df=2), Two-Way ANOVA test followed by Bonferroni post-test, and tail suspension test (J) (F value= 66.28; df= 2), One-Way ANOVA test (p< 0.0001) followed by Bonferroni post-hoc test for multiple comparisons and Two-Way ANOVA test. Each data are expressed as mean ± SEM from n = 10 male CD mice for each group. *p < 0.05 and ***p < 0.001 vs Sham; #p < 0.05 and ##p< 0.01 vs. TBI.

3.3.4 Effects of DMF treatment on antioxidant response activation

Oxidative stress plays a key role in determining neuronal cell damage. Nrf-2 is a transcription factor with strong antioxidant effects, which protects neurons from ROS- induced damage. We evaluated the effect of DMF on Keap-1/Nrf-2 pathway and related proteins by Western blot analysis. Respectively, cytosolic Keap-1 and nuclear Nrf-2 expression showed a tendency to decrease following TBI as compared to control mice (Figure 4A and Figure 4B), while DMF administration 24 h after TBI up-regulated the activities of Keap1 and Nrf-2 (Figure 4A) (F value= 20.20; df= 3) (Figure 4B) (F value= 14.35; df= 3) (p=0.0052). Interestingly, DMF treatment alone, administered in control mice, didn't increase Nrf-2 expression (Figure 4A). Moreover, in TBI-injured mice, there was an important decrement in Mn-SOD expression (Figure 4C) (F value= 21.62; df= 3) (p=0.0018), while the levels of HO-1 were decreased only slightly following damage (Figure 4D) (F value= 13.23; df= 3) (p=0.0063). Interestingly, treatment with DMF 30 mg/kg up-regulated Mn-SOD and HO-1 expression (Figure 4C and 4D respectively). Furthermore, as 4-HNE a major end product from lipid peroxidation of omega-6 polyunsaturated fatty acids (PUFA) induced by oxidative stress, in this study, we examined the role Nrf-2 mediated of DMF in regulating the 4-HNE induced gene expression of antioxidant and detoxifying enzymes. 4-HNE staining was performed 24h after TBI by immunohistochemical analysis, observing a remarkable higher positive staining for TBI brain sections (Figure 4E, panel TBI+Veh) compared to sham control slide (Figure 4E, panel Sham+Veh), while DMF treatment significantly modulate the positive staining for 4-HNE (Figure 4E, panel TBI+DMF 30 mg/kg) (F value= 57.00; df= 2), (p=0.0001).

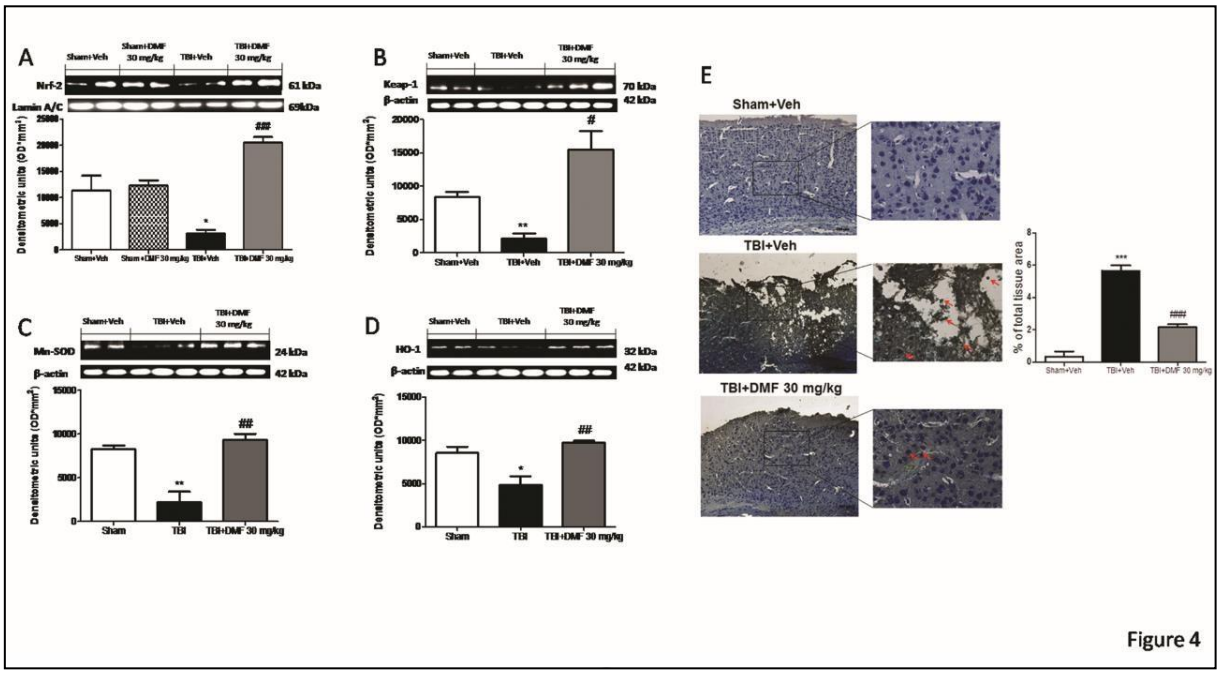

Figure 3.4: Effects of DMF treatment on antioxidant response activation

The expression of Nrf-2 and Keap-1 levels showed a tendency to decrease following trauma as compared to control mice (A) (F value= 20.20; df= 3), One-Way ANOVA test (p=0.0004) followed by Bonferroni post-test and (B) (F value= 14.35; df= 3). One-Way ANOVA test (p=0.0052) followed by Bonferroni post-test. DMF treatment caused an up- regulation of Nrf2 levels and Keap-1 (A and B). In terms of antioxidant enzyme expression in TBI-injured mice, there was a greater decrease in HO-1 and Mn-SOD levels (D and C). Treatment with 30 mg/kg DMF significantly increased Mn-SOD and HO-1 expression (C) (F value= 21.62; df= 3), One-Way ANOVA test (p=0.0018) followed by Bonferroni post-test and (D) (F value= 13.23; df= 3), One-Way ANOVA test (p=0.0063) followed by Bonferroni post-test. Furthermore, 4-HNE immunohistochemical analysis 24 h after TBI, confirmed that DMF treatment significantly modulated 4-HNE-oxidative stress induced by TBI (E) (F value= 57.00; df= 2), One-Way ANOVA test (p=0.0001) followed by Bonferroni post-test. Sham control tissue was used for comparison. Western blot analysis was performed on tissues harvested 24 h post-TBI. A representative blot of lysates obtained from each group is shown and densitometry analysis of all animals is reported (n = 10 mice from each group). Data are means ± SEM of 10 mice for each group. One-Way ANOVA test. *p< 0.05, **p< 0.01 and ***p< 0.001 vs. Sham; #p< 0.05, ##p< 0.01 and ###p< 0.01 vs. TBI.

3.3.5 The anti-inflammatory effects of DMF treatment following TBI

To evaluate the anti-neuroinflammatory effect by which DMF treatment may regulate cytokines expression and nitric oxide (NO) role during brain trauma, we assessed the expression of NF-κB, IκB-α, nNOS, COX-2, Il-1β and TNF-α by Western blot analysis in perilesional area of brain homogenates 24h after CCI. We observed that TBI damage caused respectively a significant NF-κB nuclear translocation and IκB-α cytosolic phosphorylation, almost completely inhibited by DMF 30 mg/kg treatment, as observed in: Figure 5A, (F value= 52.13; df= 2) (p=0.0004) followed by Bonferroni post-test and in Figure 5B, (F value= 82.54; df= 2)

(p=0.0001). A significant increase in nNOS expression was observed in the brain from mice subjected to TBI (Figure 5C), while DMF treatment significantly reduced trauma-induced nNOS expression (Figure 5C) (F value= 42.10; df= 2) (p=0.0064). Moreover, COX-2 expression was significantly elevated in CCI-injured mice in comparison to controls (Fig. 5D, F value 21.04). The rise in COX-2 expression induced by trauma was considerably blocked by treatment with DMF 30 mg/kg (Figure 5D) (F value= 21.04; df= 2) (p=0.0019). Also, DMF plays an important role in the regulation of pro-inflammatory processes, shifting the balance between pro-inflammatory cytokines such as Il-1β and TNF-α. Western blot analysis showed a marked increasing in both Il-1β and TNF-α following TBI compared to sham mice (Figure 5E) (F value= 398.4; df= 2) (p<0.0001) and (Figure 5F) (F value= 843.8; df= 2) (p<0.0001). DMF treatment, at the dose of 30 mg/kg, showed a significant reduction in both cytokines (Figure 5E and 5F).

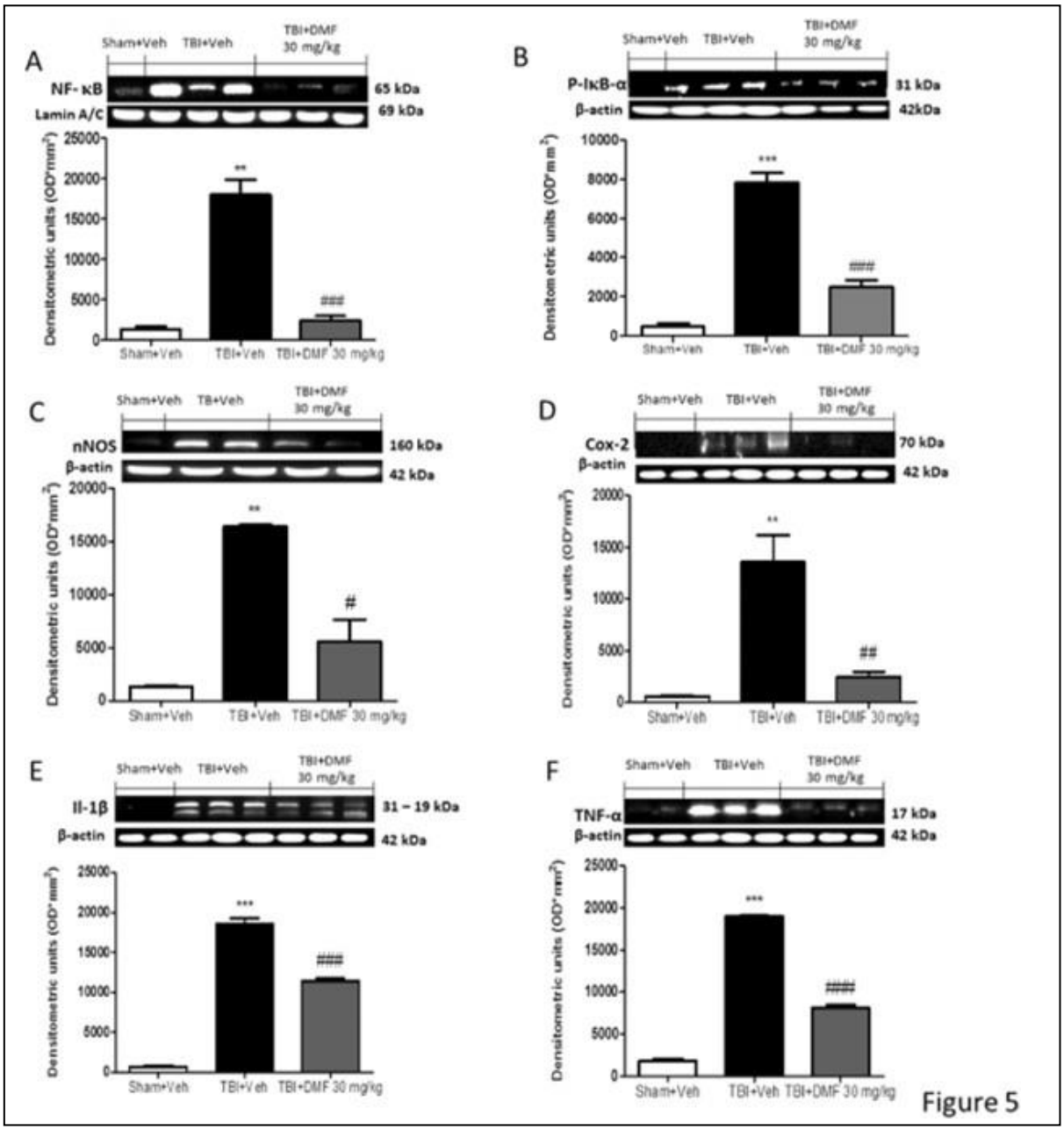

Figure 3.5: Effects DMF treatment on inflammatory pathway

By Western Blot analysis, we observed an evident NF-κB nuclear translocation and IκB-α phosphorylation following TBI, notably reduced by DMF treatment respectively (A) (F value= 52.13; df= 2), One-Way ANOVA test (p=0.0004) followed by Bonferroni post-test and (B) (F value= 82.54; df= 2), One-Way ANOVA test (p=0.0001) followed by Bonferroni post-test. A significant increase of nNOS levels was observed in the brain from mice subjected to trauma (C), while, on the contrary, DMF treatment reduced TBI-induced nNOS expression (C) (F value= 42.10; df= 2), One-Way ANOVA test (p=0.0064) followed by Bonferroni post-test. Further, COX-2 expression was significantly higher TBI-injured mice as compared to controls (D) and this effect was partially blocked by DMF 30 mg/kg (D) (F value= 21.04; df= 2), One-Way ANOVA test (p=0.0019) followed by Bonferroni post-test. Moreover, there was a significant expression of Il-1β and TNF-α in CCI-injured mice, respectively (E) (F value= 398.4; df= 2), One-Way ANOVA test (p<0.0001) followed by Bonferroni post-test and
(F) (F value= 843.8; df= 2), One-Way ANOVA test (p<0.0001) followed by Bonferroni post-test., robustly reduced by DMF treatment (E and F respectively). Sham control tissue was used as control. Western blot analysis was performed on tissues harvested 24h post-TBI.
A representative blot of lysates obtained from A representative blot of lysates obtained from each group isshown and densitometry analysis of all animals is reported (n = 10 mice from each group). Each data are expressed as

mean ± SEM from n = 10 male CD mice for each group. One-Way ANOVA test. **p< 0.01 and ***p< 0.001 vs. Sham; #p< 0.05, ##p< 0.01 and ###p< 0.001-

3.3.6 The role of DMF treatment on myeloperoxidase (MPO)-mediated oxidative stress, microglia and astrocytes activation.

Acute inflammation is a normal response to brain injury and the inflammatory process following TBI is correlated with neutrophil accumulation and microglia activation in the brain [155]. Therefore, we analyzed the effects of DMF treatment on neutrophilic infiltration by measuring brain MPO activity and positive staining by immunohistochemical analysis. As indicated by MPO activity, TBI produced a robust neutrophilic infiltration into the affected striatum of mice at 24 h after trauma compared with sham mice (Figure 6A). Treatment with DMF 30 mg/kg attenuated neutrophils accumulation into the brain at 24 h after injury (Figure 6A) (F value= 133.2; df= 2) (p<0.0001). The protective role of DMF treatment against MPO-mediated stress was confirmed by immunohistochemical analysis, observing a reduced positive staining in brain sections from DMF treated mice compared to brain sections from TBI-damaged animals (Figure 6B, panel TBI+Veh) (t value= 7,071; F value= 1.0004; df= 4), (p=0.0021). Moreover, also considering that MPO-mediated oxidative stress plays important roles in microglia activation, Iba-1 expression was evaluated by Western Blot and immunohistochemical analysis. We observed a significant increase in Iba-1 expression and positive staining in the brains 24 h after TBI, as shown respectively in Figure 6C (F value= 33.75; df= 2) (p=0.0092) and in Figure 6D, panel TBI+Veh (F value= 64.33; df= 2) (p<0.001); while the treatment with DMF 30 mg/kg significantly reduced microglia activation, returning it at control values (respectively Figure 6C and 6D, panel TBI+DMF 30 mg/kg). Also, to better evaluate the broad effects of TBI-induced neuroinflammatory response and DMF effects on astrocytes, GFAP staining was performed 24 h after TBI, observing a significant positive staining in sections from TBI-injured mice, easily reduced by DMF treatment (Figure 6E, panel TBI+DMF 30 mg/kg) (F value= 88.33; df= 2) (p<0.0001).

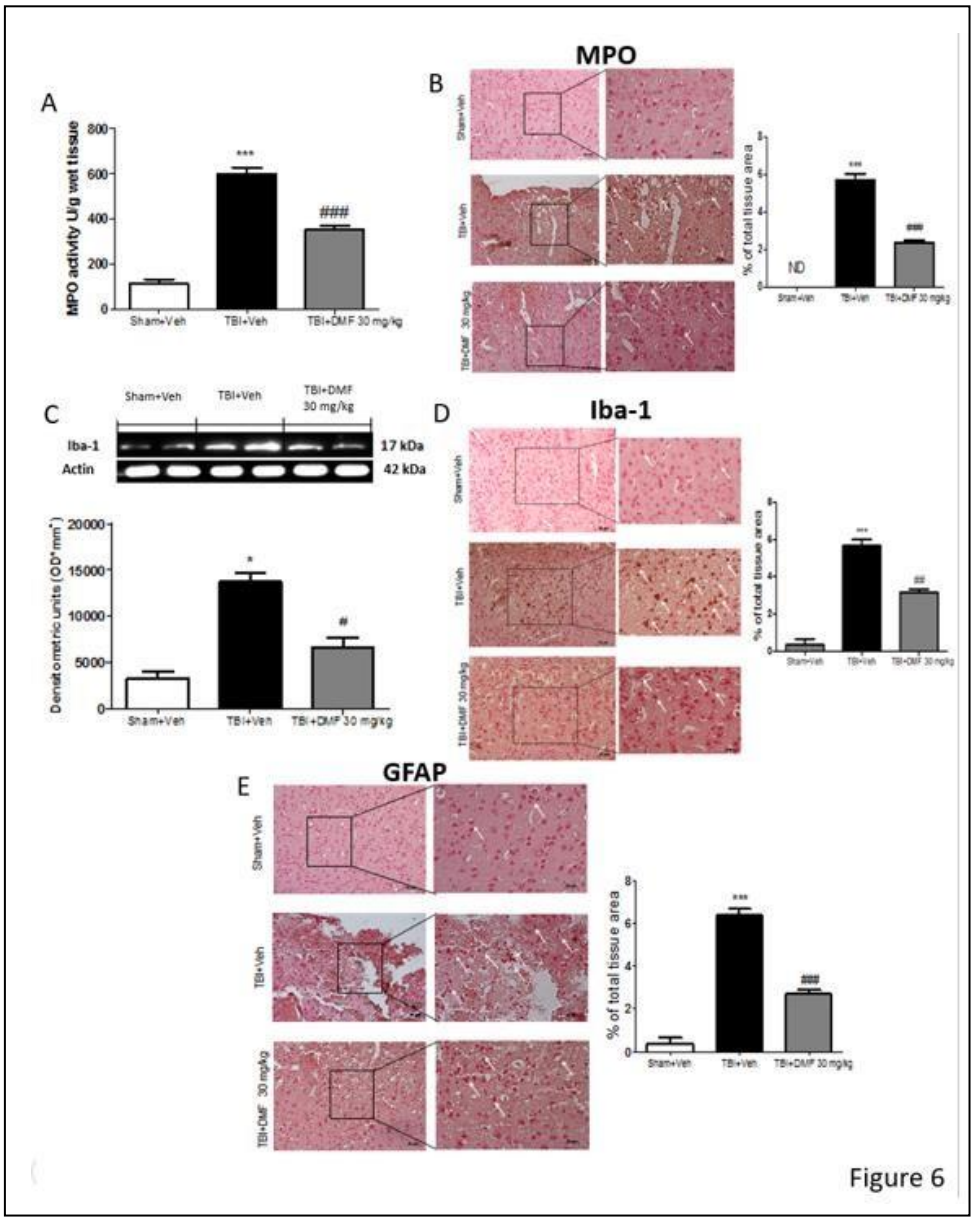

Figure 3.6: Effects of DMF treatment on neutrophil accumulation and microglia activation

MPO activity was significantly increased in the brain from TBI-induced mice (A and B) in comparison with sham animals (A and B). DMF treatment significantly reduced the TBI induced increase in neutrophil accumulation (A) (F value= 133.2; df= 2), One-Way ANOVA test ($p<0.0001$) followed by Bonferroni post-test, and (B) (t value= 7.071; F value= 1.0004; df= 4), T test ($p=0.0021$). Moreover, a remarkable increment in microglia and astrocytes activation was observed by Iba-1 and GFAP expression in TBI-injured animals (C, D and E), notably reduced by DMF treatment at 24h after trauma (C) (F value= 33.75; df= 2), One- Way ANOVA test ($p=0.0092$) followed by Bonferroni post-test, (D) (F value= 64.33; df= 2), One- Way ANOVA test ($p<0.001$) followed by Bonferroni post-test and (E) (F value= 88.33; df= 2), One-Way ANOVA test ($p<0.0001$) followed by Bonferroni post-test. Sham control tissue was used as control. Western blot analysis was performed on tissues harvested 24 h post-TBI. Each data are expressed as mean ± SEM from n = 10 male CD mice for each group. One-Way ANOVA test and T test. *p< 0.05 and ***p< 0.001 vs. Sham; #p< 0.05, ##p< 0.01 and ###p< 0.001 vs. TBI. ND, not detectable.

3.4 Discussion

Traumatic brain injury (TBI) is a complex injury with a broad spectrum of symptoms and disabilities, possibly caused by an external mechanical force and leading to permanent or temporary impairment of cognitive, physical and psychosocial functions, with an associated diminished or altered state of consciousness [122] [123]. Despite the prevalence and cost of TBI-related disabilities, there is a paucity of literature reviewing modern approaches to pharmacotherapy [156]. Among the factors leading to TBI outcome, there are biochemical mechanisms generating oxidative stress. The role of Nrf-2 in protection against TBI-induced secondary brain injury is particularly interesting, because Nrf-2 signaling cascade modulates both inflammation and oxidative stress. There are many drugs, already used clinically, that activate Nrf-2 system, including fumaric acid ester DMF [157]. DMF is known to impact the anti-oxidative stress cell machinery promoting the transcription of genes downstream to Nrf-2 activation. Mice are the mainstay of in vivo immunological experimentation and they respect human biology remarkably well. This conservation of function is reflected in recent reports on the sequencing of both the human and mice genomes, which reveal that to date only 300 or so genes appear to be unique to one species or the other [158]. DMF formulation therapy reduces inflammation and immune activation in numerous cell lineages *in vitro*, particularly cells of the immune system. Indeed, several studies on Nrf-2 knockout mice demonstrated that deletion of Nrf-2 exacerbates brain injury after TBI in mice, increasing severity of neurological deficit, apoptosis and brain, suggesting that, through Nrf-2, DMF may play an important role in protecting brain injury after TBI, possibly by modulating oxidative stress. Furthermore, DMF combines safety and efficacy and has potential that goes beyond the anti-inflammatory effects, protecting glial cells, oligodendrocytes and neurons [159]. Since it is warranted to identify and design novel approaches capable of improving motor, sensory and cognitive outcome in order to enhance the quality of life of the TBI patients, in light of recently discoveries, the aim of this

study was to evaluate the protective role of DMF on a mouse secondary head injury from TBI-induced neurotoxicity and neuroinflammation, modulating Nrf-2 pathway. In addition, our intent was to give a new molecule that could support and improve the current therapies.

CCI model reproduces many of the features of brain injuries, including motor deficits, memory and neuron loss [160]. However, since by histological study, DMF 1 and 10 mg/kg treatments didn't show any effective amelioration, we continued this experimental study using only the dose of 30 mg/kg. The present study demonstrated, for the first time, that DMF treatment, at the dose of 30 mg/kg, significantly alleviated brain injury. Also, TBI is known to result in behavioral function impairment and numerous neurological deficits and the altered motor coordination is associated to a major depression, considered a common sequel in TBI survivors [161]. Several studies have shown that Nrf-2, a major redox-sensitive transcription factor involved in the cellular defense against oxidative stress, increases susceptibility to depressive-like behavior [162]. The tail suspension test has been employed as a measure of depression-like behavior and it is based on the assumption that the emotional state of an animal will influence their efforts to escape an aversive situation and that the internal states relates to the duration of the escape response [162]. Through the tail suspension test, the reduced immobility time highlights the potential anti-depressant and/or neuroprotective properties of DMF treatment. Also, the neuromotor evaluation was performed in acute phase, with Rotarod test and EBS test, revealing that DMF improved latency and percentage of biased swing activity compared to TBI animals.

Moreover, in chronic phase, with EPM test, we showed that TBI-damaged mice spent more time in closed arms, sign of anxiety-like behavior, but this alteration was partially reversed in mice by DMF administration at the dose of 30 mg/kg. Furthermore, beam balance test, beam walking latency and beam walking score were performed underling a faster neurological recovery at day 5 post TBI in treated mice. The alteration of neuromotor coordination is related

to the fact that TBI, as brain insults, causes rapid cell death and a disruption of functional circuits, in the affected regions. The damage is due partly to neuronal death in the infarcted tissue but also to cell dysfunction in the areas surrounding the infarct that encompass the part of the under perfused penumbra that survives the insult, the non-ischemic peri-infarct tissue, and remote brain areas that are connected to the area of tissue damage 48. Recent studies highlighted the protective effect of DMF on brain damage [163]. In our study, we confirmed that DMF treatment, at the dose of 30 mg/kg, ameliorated the lesion area, partially reducing post traumatic neuronal loss, as shown by stereology analysis. Again, in a traumatic event as TBI, free radicals can damage neurons and other major cell types by enhancing DNA damage, which results in endothelial injury and blood-brain barrier breakdown by initiating apoptotic cascades. In this study, we shown that DMF treatment significantly reduced TUNEL and FJC positive neuronal cells, significantly blocking apoptotic process TBI-induced. Also, the regional alterations in the cellular levels of Bcl-2 family of apoptosis-associated genes following brain injury are associated with traumatic cell death [164]. Raghupathi et al., [154] postulated that the vulnerability of neurons to TBI could be related their endogenous levels of Bcl-2, observing an acute loss of Bcl-2 immunoreactivity in the injured brain regions following brain injury. This decreased expression of Bcl-2 suggested that neuronal survival might be compromised due the "apostat" mechanism of cell death, which suggests a shift in the cellular ratio of cell death activator proteins and suppressor proteins, which regulates the fate of a cell. We demonstrated that DMF treatment did not only bring Bcl-2 to control values, but also up- regulated this anti-apoptotic protein, thus preserving neuronal survival.

A vast amount of circumstantial evidence implicates high energy oxidants and oxidative stress as mediators of secondary damage associated with TBI [165]; Nrf-2 is a pleiotropic transcription factor and a key genomic homeostatic regulator that, through antioxidant response elements (ARE) within the regulatory region of many target genes, coordinates anti-oxidative

and detoxification processes, allowing all types of cells in the neurovascular unit to adapt to detrimental conditions caused by intracellular or extracellular stress and it can regulate multiple mechanisms of secondary brain injury [166]. The properties of fumarate, combined with our data suggest that DMF up-regulated the Nrf-2 transcriptional system, inducing the expression of phase II detoxifying enzymes [167], such as HO-1 and Mn- SOD, that work together to contest oxidative stress and inflammation. DMF treatment, via the Nrf-2 pathway, inhibiting cerebral oxidative stress by inducing antioxidant and detoxifying enzymes, up-regulates Keap-1, Mn-SOD and HO-1 expression, conferring resistance against neurodegenerative damage. The brain is highly sensitive to oxidative stress because consumes about 20–30% of inspired oxygen and contains high levels of both polyunsaturated fatty acids and redox transition metals, making it an ideal target for a free radical attack. Free radical acting on polyunsaturated fatty acids leads to the formation of highly reactive electrophilic aldehydes, including 4-hydroxy-2-nonenal (4- HNE), the most abundant lipid peroxidation product, expression of oxidative stress condition in experimental models of TBI [168]. In this study, we demonstrate that DMF treatment reduced 4-HNE positive staining, underlying that the induction of protective enzymes by 4-HNE appears to be an adaptive response to enhance elimination of 4-HNE and reduce its toxicity.

Oxidative stress injury aggravates neuronal damage stimulating the expression of cytokine and promoting inflammatory reactions [169]. In fact, the identification of NF-κB binding cites in the promoter region of the Nrf-2 gene suggests cross talk between these two regulators of inflammatory processes [170]. In this study, we observed that DMF treatment, mostly at the dose of 30 mg/kg, inhibiting the nuclear translocation of NF-κB, represents a functional system to regulate neuroinflammation in response to oxidative stress. Also, nuclear upregulation of NF-κB and cytosol IκB-α phosphorylation is a hallmark of inflammatory brain diseases [171], but DMF treatment significantly reduced IκB-α phosphorylation. Indeed, as immediate

consequence to the trauma, a robust inflammatory response is elicited in the injured brain, involving a cellular component, comprising the activation of resident glial cells, microglia and astrocytes and secreting inflammatory mediators like Il-1β and TNF-α. In this study, we demonstrated that DMF treatment significantly reduced Il-1β and TNF-α levels, significantly enhanced and prolonged following brain damage. Considering that Il-1β results in the activation of COX-2 isoform [172] and that, under pathologic conditions, COX-2 activity increases ROS levels and toxic prostaglandin metabolites that can exacerbate brain injury [173], we evaluated the role of DMF treatment on COX-2 expression. The slowed DMF-mediated COX-2 activity strengthened the therapeutic potential of DMF thanks to its involvement in COX-2- dependent anti-inflammation and antioxidant Nrf2/ARE signaling.

However, oxidative stress is intimately linked as well not only to inflammation, but also to other components of the neurodegenerative process, such as nitrosative stress [174]. Various isoforms of the nitric oxide (NO) producing enzyme nitric oxide synthase (NOS) are elevated in brain injury [175], thus indicating that disruption to NO signaling is part of a common pathophysiological pathway that leads to oxidative exacerbations and blood brain barrier leakage [176]. In sight of this, different observations indicated that targeting the NO modulating system is an attractive approach for developing TBI therapy [177]. In our study, we demonstrated that DMF treatment notably reduced nNOS expression, suggesting nitric oxide-mediated adaptive responses in damaged brain via translocation and activation of Nrf-2 pathway.

Furthermore, in this study, we demonstrated that DMF treatment significantly reduced the robust infiltration of neutrophils typically generated following TBI [178]. Again, it is known that MPO-dependent oxidative stress plays an important role in microglia activation after TBI [179]. In our work, we demonstrated that DMF treatment reduced microglia and astrocytes

activation, suggesting a critical role of DMF in the neuroinflammation decrement and in neurons survival enhancement.

Therefore, prior to applying DMF as an adjunctive treatment to conventional therapy, further studies about DMF treatment should be done. For example, because antioxidant genes are, in part, under the control of sex hormones, and sex specific differences in treatment effects may depend on redox biology [180]. Future work should be focused on biological sex with DMF treatment and its differential impact on oxidative stress and inflammation. In addition, age effects with DMF and immunoscenence should also be considered.

Furthermore, this could make it clear, in TBI clinical trials, on the different shooting in male and female athletes' brains following concussion injury and recovery. Moreover, the chronic oxidative stress that appears with age affects all nervous cells [181] as soon as the treatment with DMF increased the risk of developing lymphopenia with increasing age [182]; accordingly, being aging and immunosenescence a risk factor for DMF induced progressive multifocal leukoencephalopathy (PML), further studies could be made on DMF treatment in relation to age. Furthermore, a promising direction for clinical diagnosis and prognosis is the use of fluid biomarkers, with preference for serum biomarkers. Serum biomarkers would provide a potentially very low-cost and time-efficient method for detection, evaluation and prognosis of TBI. Also, the selection of appropriate biomarkers to gauge potential treatment response could be indicative to optimize DMF treatment dose [183].

3.5 Conclusions

In summary, these results indicate that NF-κB/Nrf-2 pathway greatly contribute to the therapeutic effect of DMF treatment, although additional studies will be needed to can affirm that without this pathway there isn't further effect of DMF. Then, given its excellent pharmacokinetic profile, further studies with DMF as a potential neuroprotective supportive therapy in TBI could be explored. These findings look to enhance the therapeutic efficacy of

DMF, at the dose of 30 mg/kg, in brain damage, showing noticeably greater effects in restoring neurological deficits, reducing inflammation, apoptosis and oxidative stress. Therefore, DMF therapy could be proposed as reinforcement to currently conventional therapies, designed to counteract neurobehavioral deficits, promoting an anti-oxidative and anti-inflammatory state.

4.0 CHAPTER FOUR: Dimethyl fumarate alleviates the nitroglycerin (NTG)-induced migraine in mice

4.1 Introduction

Migraine is the third most common disease worldwide, with a global prevalence estimated at 14.7% in both genders and for heavy impact on patients daily life represents a major cause of disability [184]. Although the main cause of migraine is unknown, various factors such as genetics and environmental factors, are involved in the onset of migraine attacks [185]. Recommended medications for the acute treatment of migraine encompass triptans, nonsteroidal anti-inflammatory drugs (NSAIDs) and analgesics; particularly, the-counter analgesics and nonsteroidal anti-inflammatory drugs for acute mild migraine and specific prescription drugs (triptans and ergot alkaloids) for acute severe migraine [186]. While it is true that triptans have been the first successful mechanism-driven treatment in the field, recently, new targets involved in migraine pathogenesis have emerged and new drug classes have been studied for migraine attack therapy [187]. Recently, calcitonin gene-related peptide (CGRP) antagonists are occupying a position of redress in the treatment of migraine [188]; the discovery that the levels of the CGRP peptide increase during a migraine attack and the infusion of CGRP can provoke a migraine attack claimed the development of small molecule antagonists, designed to block CGRP receptor action by preventing binding of the CGRP peptide [189]. Encouraged by the efficacy of blocking CGRP for the treatment of migraine, monoclonal antibodies able to block either CGRP or its receptor were developed and tested in several preclinical modalities and the field has been very active, with one antibody drug approved and three antibody drugs in phase III clinical trial [190]. Several studies have been conducted to test the efficacy and safety of these drugs. In general, blocking CGRP in migraine patients is seemingly both efficient and well tolerated, however, blocking CGRP may pose a risk in

subjects with comorbidities such as cardiovascular diseases, besides the fact that long-term effects are still unknown and that are often accompanied by high prices [191].

Migraine sufferers still have no effective and widely applicable drug treatment methods, thus the developing of more effective and safe anti-migraine agents is still a pressing task. Further studies are needed to investigate the possibility of combining different drug classes to optimize the clinical response and the potential role of the novel drugs in medication-overuse headache [187].

Though migraine causes aren't understood, demonstrated that oxidative stress is an universal migraine trigger. High levels of oxidative stress are associated with a four-fold increase in migraine risk and a recent study found that nearly all documented migraine triggers are associated with oxidative stress [192]. Also, migraine is a result of the interaction between multiple genes with environmental factors and triggers. The discovery of genes involved in this disease may lead to new insights into the molecular pathways in the pathogenesis of migraine because the discussed polymorphisms may influence the phenotypic features of migraine patients [193, 194]. Particularly, oxidative stress, has been implicated in various headache disorders because arises an imbalance between the production of reactive oxygen species (ROS) and elimination by antioxidant defense mechanisms, consequently with endogenous ROS that can cause oxidative damage to DNA, lipids, and proteins [195].

The master regulator of cellular cytoprotective responses to oxidative stress is Nrf2 [196]. DMF, the most pharmacologically effective molecule among the FAEs and an oral therapeutic agent for the treatment of relapsing-remitting Multiple Sclerosis (MS) patients [197], was discovered to impact the anti-oxidative stress cell machinery promoting the transcription of genes downstream to the activation of Nrf2 [159]. In fact, it has been found that the Nrf2/ARE pathway is the most important endogenous antioxidant defense system, and plays a critical role in regulating cellular oxidation, cell defense, and protection; moreover, increasing data points

out the protective role of Nrf2/ARE pathway activation in the brain [198]. A recent study demonstrated that activation of the Nrf2/ARE pathway inhibited the activation of trigemino vascular system (TGVS) and prevented the induction of hyperalgesia, however without specifying the underlying mechanisms of migraine [199].

Thus, the aim of this study was to investigate the role of DMF, as an activator of Nrf2/ARE pathway, in NTG-induced hyperalgesia and its underlying mechanisms. In fact, it has been demonstrated that NTG administration produces attacks phenotypically similar to spontaneous migraine attacks and sensitizes trigeminal and cortical structures that underlie migraine allodynia [200].

Furthermore, it has been shown that the combination of paracetamol and caffeine is a serious candidate for the first line treatment of acute episodic of migraine [201]. Paracetamol exerts its analgesic activity through a direct effect on the central nervous system, at least in part mediated by the serotonergic system [202]. Recently, evidence from clinical trials indicated that the combination of caffeine with analgesics medications is useful in some forms of primary or secondary headache [203]; also, it was demonstrated adjuvant analgesia, as well as some intrinsic analgesia, in the treatment of headache conditions, showing the superiority of the combinations containing caffeine over the association of aspirin and paracetamol alone [204]. Moreover, a clinical trial showed that the simple combination of paracetamol 1,000 mg + caffeine 130 mg seems to be as efficient and safe as sumatriptan 50 mg by mouth and this could be an important indication for patients suffering from migraine who cannot assume triptans [205]. In this study, we used TACHICAF, a combined drug of caffeine and paracetamol, as positive control; by doing so, we expect to consider DMF as an effective therapeutic approach to treat migraine pathology, reducing the side effects of traditional migraine treatments.

4.2 Materials and methods

4.2.1 Animals

CD1 mice (male 25 to 30g, Envigo, Italy), aged between 10 and 12 weeks, were used for all studies. Mice were housed five per cages (five per cage) and maintained under a 12:12 h light/dark cycle at 21 ± 1◦C and 50 ± 5% humidity. Standard laboratory diet and tap water were available *ad libitum*. The University of Messina Review Board for the care of animals approved the study. Animal care was in compliance with Italian regulations on protection of animals used for experimental and other scientific purposes (Ministerial Decree16192) as well as with the Council Regulation (EEC) (Official Journal of the European Union L 358/112/18/1986).

4.2.2 Migraine induction and DMF administration

Nitroglycerin (NTG) was prepared from a stock solution of 5.0 mg/ml nitroglycerin in 30% alcohol, 30% propylene glycol, and water (American Regent). NTG was freshly diluted in 0.9% saline to a dose of 10 mg/kg. The vehicle control used in these experiments was 0.9% saline. All injections were administered as a 10 mg/kg volume. Animals were treated orally with DMF at the dose of 30 mg/kg and 100 mg/kg, 5 min following NTG injection. Mice were sacrificed 4 hours following NTG injection, the whole brain with rostral spinal cord was removed and then dissected in order to evaluate the following parameters: histology analysis and Western blot analysis. In a separate set of experiments, a cohort of 10 animals from each group were observed after NTG injection, receiving DMF until the sacrifice, in order to evaluate the behavioral testing.

4.2.3 Experimental groups

Animals were divided into six groups:

1) Sham *group*: mice received saline (n=20).

2) NTG *group*: mice received NTG (10 mg/kg) intraperitoneally (n=20);

3) NTG+TACHICAF *group*: mice received TACHICAF orally (100 mg/kg) 5 min after NTG (10 mg/kg) intraperitoneally (n=20);

4) NTG+DMF (10 mg/kg) *group*: mice received orally DMF at the dose of 10 mg/kg 5 min after NTG injection (n=20);

5) NTG+DMF (30 mg/kg) *group*: mice received orally DMF at the dose of 30 mg/kg 5 min after NTG injection (n=20);

6) NTG+DMF (100 mg/kg) *group*: mice received orally DMF at the dose of 100 mg/kg 5 min after NTG injection (n=20).

7) DMF alone *group*: mice received orally DMF (100 mg/kg) (n=20)

Experimental data regarding groups 7 are not showed, as DMF administration didn't result in either toxicity or improvement in comparison to sham controls.

4.2.4 Behavioral testing

Tail flick test

Warm- and cold-water tail flick tests were conducted to assess thermal allodynia. Water temperature was maintained at 46 °C+/− 0.1 °C using a hot plate or at 15 °C +/− 0.1 °C using crushed ice. For testing, each mice were gently wrapped in a terry cloth towel and its tail submerged 5 cm. Latency to flick or curl the tail was recorded with a 40-s cut-off [206].

Formalin test

The formalin test was performed according to the method of Tjolsen et al. [207]. A sub-dermal injection of 1% formalin (formaldehyde diluted in 0.9% saline) is made into the midplantar region of the right hindpaw of a mouse. This elicits a distinct behavioral response to the formalin injection characterized by the mouse licking the affected paw. Immediately following the injection, the mouse intensely licks the paw for approximately 1-5 min (Phase 1). This initial behavior is considered the acute phase and is thought to be mediated primarily by the response of the damaged local tissue. The acute phase is followed by a more prolonged inflammatory

phase (about 15to 60 min, Phase 2) period of licking then ensues, which are primarily mediated by inflammatory mechanisms. Thus, animals are monitored for any effects of the investigational compound on both phases of persistent pain. DMF administration is performed 5 min before NTG treatment [208].

Hot plate test

The hot plate test was carried out to assess the effects of agents on the thermal nociceptive threshold. Mice were placed on 52-58 °C hot plate. The response latency to either a hind-paw lick or jump was recorded. In the absence of a response, the animals were removed from the hot plate at 60 s to avoid tissue injury, and a 60 s latency was assigned as the response. The latency time to pain reaction was measured at 30, 60, 90, 120 and 240 min post NTG-induction [209].

Light/dark test

An apparatus was made to create a light/dark box used to quantify the ICHD-3 criteria of photophobia and reduced activity associated with migraine. Clear lids of the black and center gray chambers were covered with heavy black construction paper (inside ≤ 5 lux); the white chamber with clear lids served as the light portion (inside ≥635 lux). On test day, mice were placed into the center chamber for a 1 min acclimation period after which the guillotine-style doors were opened to allow access to the entire apparatus. Time in the light chamber and total number of photobeam breaks during a 5 min test session were recorded [210].

Elevated Plus Maze test

Anxiety is one of the common behavioral conditions in migraine, so anxiety deficits were evaluated using Elevated Plus Maze (EPM) system, as previously described [147]. EPM consisting of two open arms and two enclosed arms, animals were placed on the centre of the maze facing an open arm and following measures scored: time spent in enclosed arms (sec) and number of entrance into open arms.

Tissue processing and histology

Following 4 hours NTG injection, animals were evaluated by an experienced histophatologist. Longitudinal sections of 7 µm thickness were processed from the brainstem at the trigeminal nucleus SpV. Sections were then deparaffinized with xylene and then stained with cresyl violet. For cresyl violet staining the slides were fixed as described by [211]. All sections were studied using an Axiovision Zeiss microscope (Milan, Italy). Histopathologic changes of the grey matter were scored on a five-point scale: 0, no lesion observed; 1, grey matter contained one to five eosinophilic neurons: 2 grey matter contained five to 10 eosinophilics neurons; 3, grey matter contained more than 10 eosinophilics neurons; 4, small infarction (less than one third of the grey matter area); 5, large infarction (more than half of the grey matter area). The scores from all the sections of each brain were averaged to give a final score for individual mice. All the histological studies were performed in a blinded fashion [212].

Western blot analysis

Western blot analysis was performed on whole brain with rostral spinal cord tissues harvested 4 hours after NTG injection. Cytosolic and nuclear extracts were prepared as described previously [213]. The expression of nuclear factor of kappa light polypeptide gene enhancer in B-cells inhibitor alpha (IκB-α), inducible nitric oxide synthase (iNOS), cyclooxygenase 2 (COX-2), manganese superoxide dismutase (Mn-SOD), hemeoxygenase 1 (HO-1) was quantified in cytosolic fraction. Nuclear factor kappa-light-chain-enhancer of activated B cells (NF-κB) and nuclear factor erythroid 2- related factor 2 (Nrf2) expressions were quantified in nuclear fraction. The filters were probed with specific Abs: anti- NF-κB (1:500; Santa Cruz Biotechnology) or anti-Nrf2 (1:500; Santa Cruz Biotechnology, SC-722) or IκB-α (1:500; Santa Cruz Biotechnology), anti-MnSOD (1:500; Millipore) or anti-HO-1 (1:500; Santa Cruz Biotechnology), anti-COX-2 (1:500; Cayman) or iNOS (1:500, Santa Cruz) in 1 × PBS, 5% w/v non fat dried milk, 0.1% Tween-20 at 4 °C, overnight. To ascertain that blots were loaded

with equal amounts of proteins they were also incubated in the presence of the antibody against β-actin protein (cytosolic fraction 1:500; Santa Cruz Biotechnology) or lamin A/C (nuclear fraction 1:500 Sigma–Aldrich Corp.) as described [212].

4.2.5 Statistical analysis

All data are expressed as the mean ± SD. Statistical analyses were performed using PRISM 5 version 5.0 (SPSS Inc., Chicago, IL, USA). Data at different time points were analyzed using a two-way analysis of variance (ANOVA) followed by Bonferroni post-hoc-test. Other data were analyzed using one-way ANOVA followed by Bonferroni post-hoc-test. P value < 0.05 was considered as statistically significant.

4.3 Results

4.3.1 DMF treatment restored the NTG-induced damage in trigeminal nucleus

The symptoms that appear before the onset of migraine are related to abnormal neuronal activity in cortical and brainstem structures; particularly it is widely accepted that trigeminal sensory information can reach the hypothalamus via multisynaptic pathways through the brainstem [214]. Central processes of sensory afferents enter the brainstem via the trigeminal tract and pass caudally while giving off collaterals that terminate mainly in lamina V of the spinal trigeminal nucleus (SpV), modulating the perception of trigeminal pain [215]. Thus, to define the NTG-induced alterations of SpVC area, whole brain with the rostral cervical spinal cord sections were stained with cresyl violet, observing a significant neuronal damage in NTG-injured mice (Figure 1B, see histological score Figure 1F) respect to control and control + TACHICAF group (Figure 1A and 1C, see histological analysis 1F). On the contrary, the treatment with DMF, mainly at the dose of 100 mg/kg, significantly ameliorated the cyto architecture of SpVC area, restoring a large number of trigeminal neurons (Figure 1E, see histological score Figure 1F).

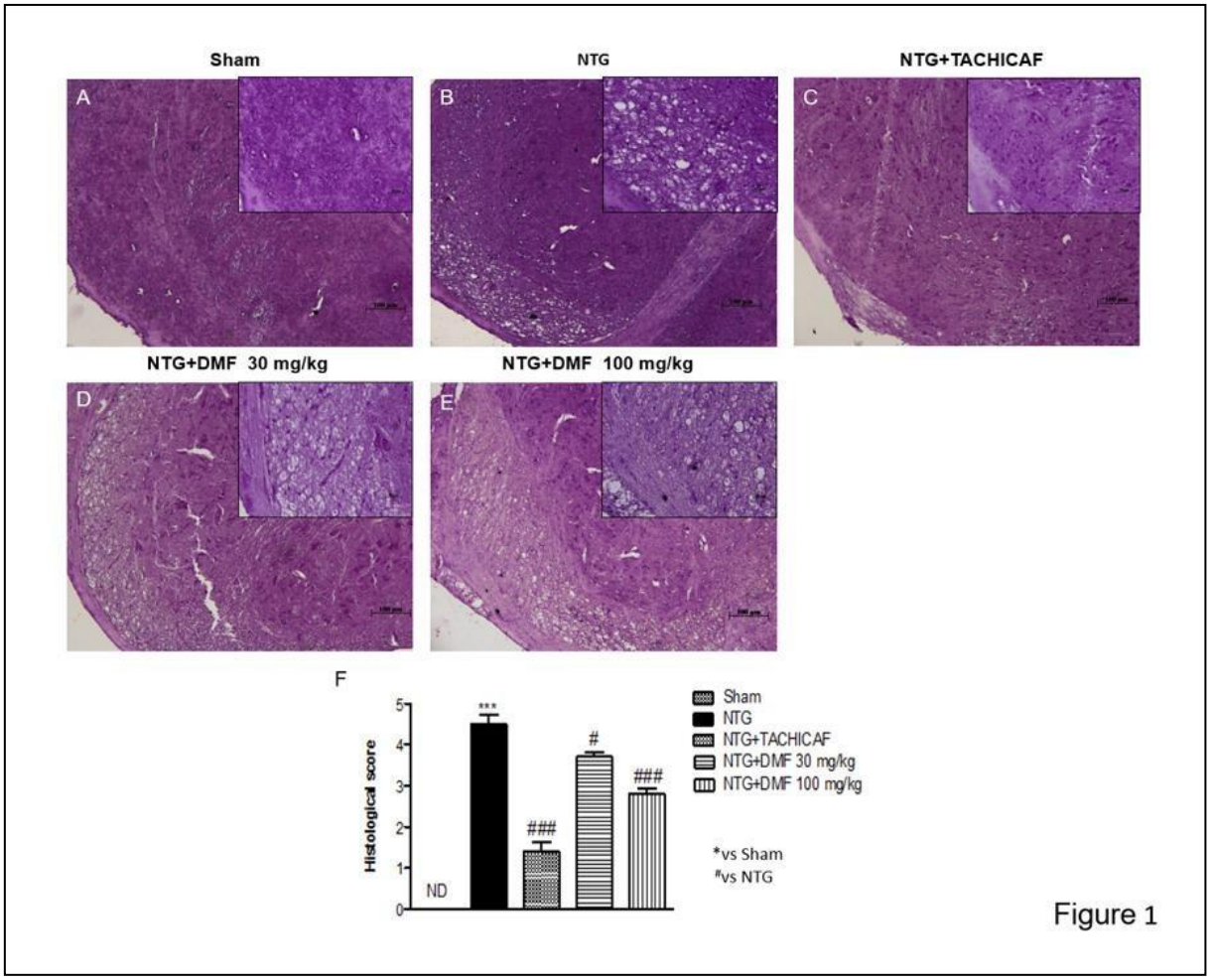

Figure 4.1: Effects of DMF treatment on NTG-induced damage

The neuronal damage in Sp5C area was observed in NTG-injured mice (B, B1 and F, F1) respect to control and control + TACHICAF group (respectively A, A1; C, C1 and F, F1). The treatment with DMF, mainly at the dose of 100 mg/kg, significantly restored a large number of trigeminal neurons in Sp5C area (E, E1). Data are means ± SEM of 10 mice for each group. One-Way ANOVA followed by Bonferroni post- test. ND, not detectable. ***p< 0.001vs. Sham; #p< 0.05 and ###p< 0.001vs. NTG.

4.3.2 The protective effects of DMF to reduce NTG-induced hyperalgesia

NTG-evoked hyperalgesia in mice has been developed as a model for sensory hypersensitivity associated with migraine [216]. The tail flick test is a thermal hyperalgesia test in which the tail of the animal is subjected to a heat source, removing spontaneously the tail ("tail flick") when the fell situation become uncomfortable. In this study, DMF treatment administered after NTG caused a significant increase in tail flick latency, suggesting a DMF-mediated antinociceptive

effect (Figure 2A). Moreover, injection of NTG elicits thermal hypersensitivity in a time-dependent manner, thus, in this study, we evaluated the effect of DMF treatment on NTG-induced thermal hypersensitivity using the Hot plate test. The result highlighted that DMF treatment, at both doses of 30 and 100 mg/kg, significantly increased the latency time to pain reaction related to the increase in time up to 240 min after NTG injection. Indeed, the pathophysiological mechanisms involved with migraine are suggestive of an increased and prolonged hyperexcitability to stimuli, especially within the trigeminal distribution. In the formalin test, the total number of flinches/shakes evoked by formalin injection was counted in phases 1 (Figure 2C) and 2 (Figure 2D) of the formalin test. In the control and TACHICAF group, the injection of formalin resulted in a highly reliable, typical, biphasic pattern of flinches/shakes of the injected paw, being characterized by an initial acute phase of nociception within the first 5 min, followed by a prolonged tonic response from 15 to 60 min after formalin injection. DMF administration, at both doses of 30 and 100 mg/kg, significantly reduced the nociceptive behavior in both phases of the formalin test (Figure 2C and 2D). NTG administration significantly increased the total number of flinches/shakes in phase II of formalin test, while DMF treatment significantly alleviated the nociceptive behavior induced by NTG administration during phase I and II of the test (Figure 2C and 2D).

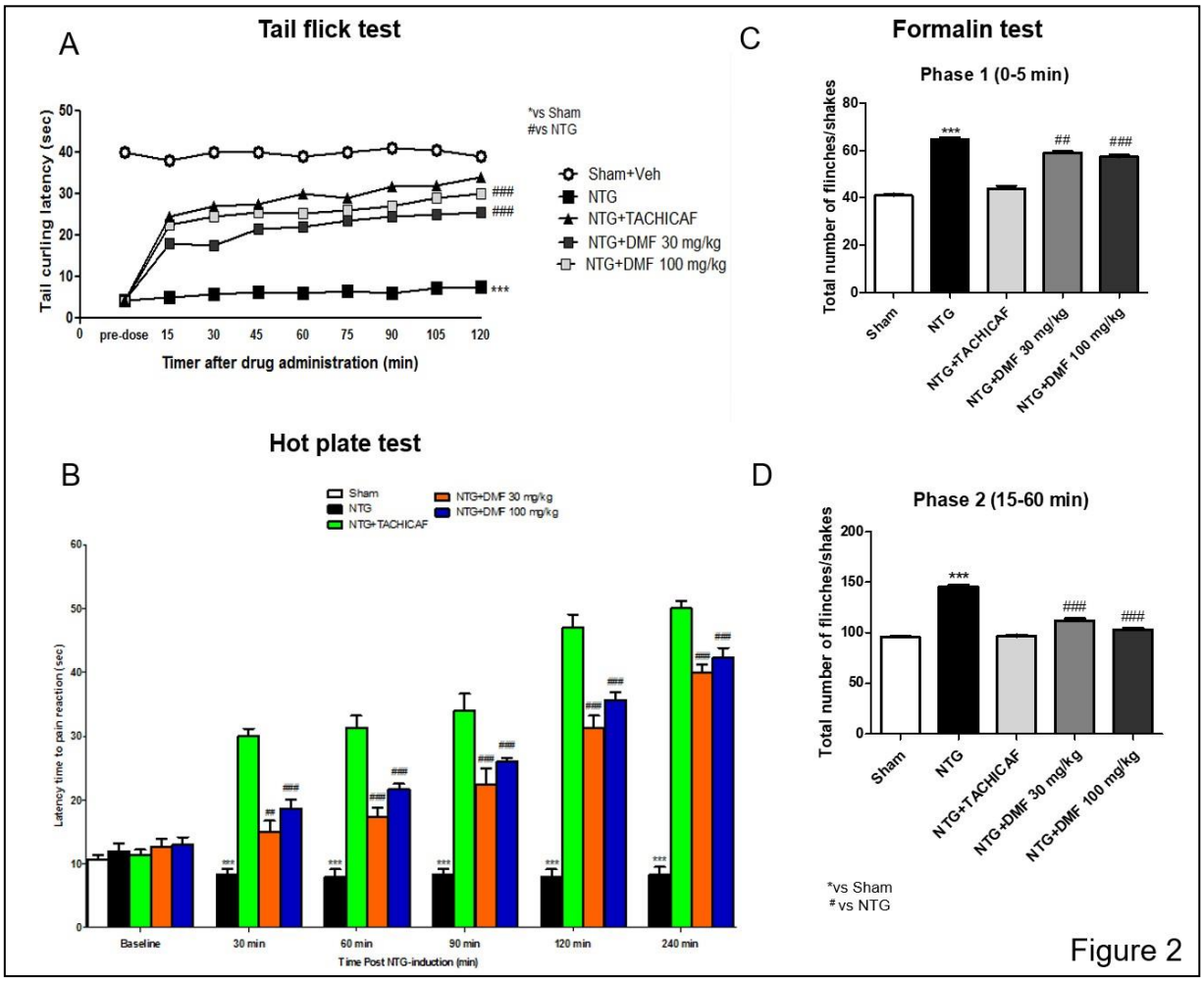

Figure 4.2: Effects of DMF treatment on NTG-induced hyperalgesia

In tail flick test, DMF treatment at 30 and 100 mg/kg administered after NTG vehicle, caused a significant increase in tail curling latency (A) respect to NTG group (A). In Hot plate test, i.p. injection of NTG increased thermal hypersensitivity in a time-dependent manner (B), while DMF treatment, at both doses of 30 and 100 mg/kg, significantly increased the latency time to pain reaction related to the increase in time up to 240 min after NTG injection (B). In formalin test, NTG administration significantly increased the total number of flinches/shakes in phase I and II respect to control groups (C and D), while DMF treatment at 30 and 100 mg/kg significantly alleviated the nociceptive behavior induced by NTG administration during phase I and II of the test (C and D). Data are means ± SEM of 10 mice for each group. One-Way ANOVA and Two-Way ANOVA followed by Bonferroni post- test. ***p< 0.001vs. Sham; ##p< 0.01 and ###p< 0.001vs. NTG.

4.3.3 The role of DMF in the comorbidity between migraine and anxiety

Anxiety and mood disorders have been shown to be the most relevant psychiatric comorbidities associated with migraine, influencing disease prevalence and clinical outcomes [217]. Studies reported that mood and anxiety disorders are two to ten times more common in migraineurs than in the general population [218]. In this study, the time in closed arm and number of closed arm entries on the EPM test were used to evaluate anxiety. NTG-injected mice showed anxiety

and fear to explore and they stationed in closed arm (Figure 3A), while DMF-treated mice were encouraged and started to spend more time in open arm (Figure 3A). In the same way, in migraine-affected mice, the number of entries in closed arm significantly increased (Figure 3B) respect to control and TACHICAF groups (Figure 3B); DMF treatment, mainly at 100 mg/kg, reduced the number of entries in closed arm and augmented the permanence time in open arm (Figure 3B). Indeed, a common and debilitating symptom often present in headache disorders is photophobia, related to pain caused by the trigeminal system alteration [219]. In this study, mice with migraine displayed a strong tendency to stay longer in the dark zone respect to control mice and TACHICAF-treated mice (Figure 3C). Conversely, NTG-injected mice, treated with DMF at both doses of 30 and 100 mg/kg, started to leave the dark area and stayed more in the light zone (Figure 3C).

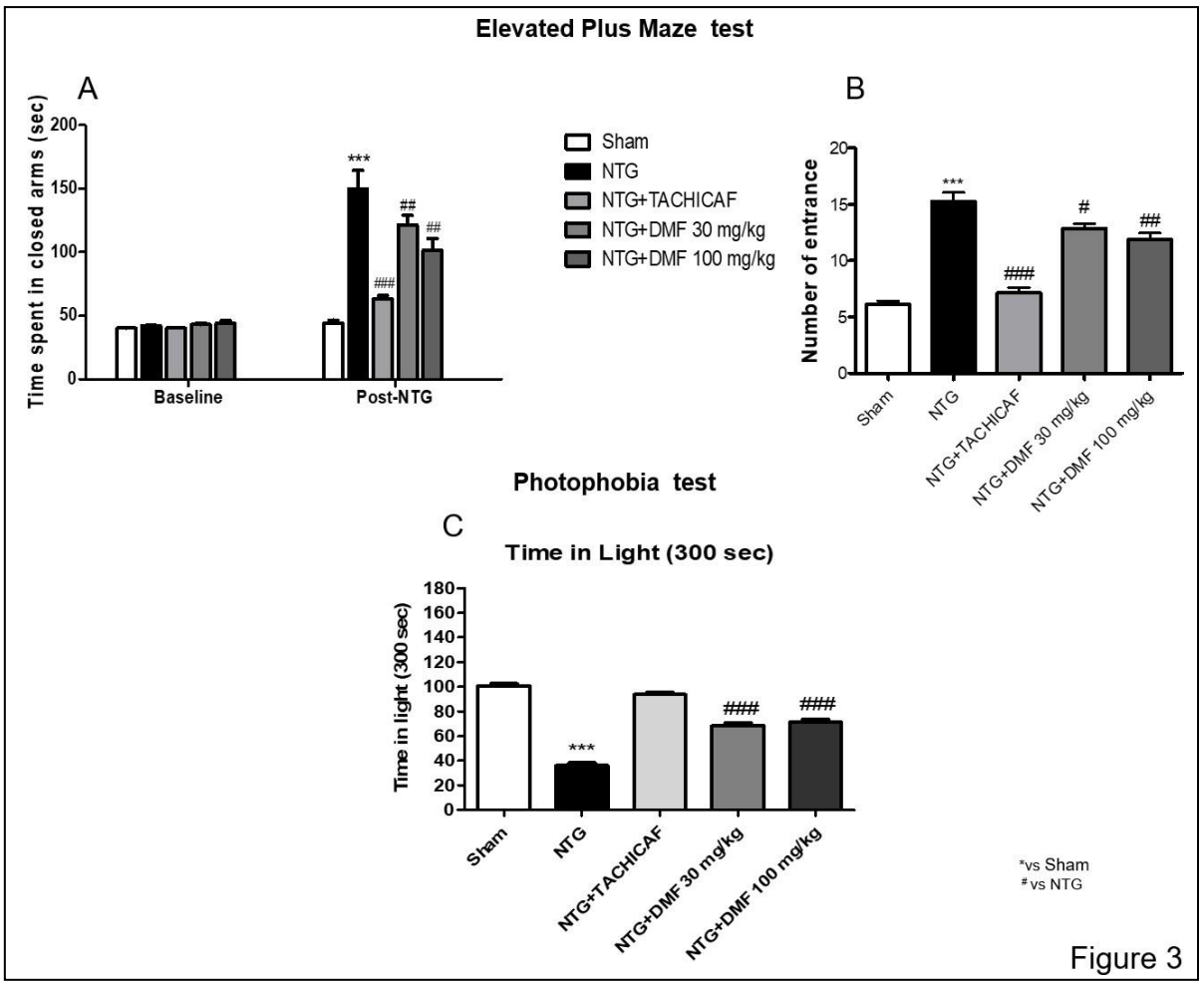

Figure 3

Figure 4.3. Effects of DMF treatment on NTG-induced anxiety and photophobia

EPM test was used to evaluate anxiety. NTG-injected mice showed anxiety stopping in closed arm (A), while DMF-treated mice spent more time in open arm (A). In the same way, in NTG-injectd mice, the number of entries in closed arm increased (B), while DMF treatment significantly augmented the residence time in open arm (B). In photophobia test, mice with migraine displayed a strong tendency to stay longer in the dark zone respect to control mice (C), while NTG-injected mice, treated with DMF stayed more in the light zone (C). Data are means ± SEM of 10 mice for each group. One-Way ANOVA followed by Bonferroni post- test. ND, not detectable. ***p< 0.001vs. Sham; #p< 0.05, ##p< 0.01 and ###p< 0.001vs. NTG.

4.3.4 The role of DMF on antioxidant system in NTG-induced migraine

Oxidative stress is also believed to play a role in the pathogenesis of migraine [220]. Nrf2 is a transcription factor with strong antioxidant effects, which protects neurons from ROS-induced damage. We evaluated the effects of DMF on Nrf2 pathway and related proteins, in whole brain with the rostral cervical spinal cord samples, by Western blot analysis. Respectively, nuclear Nrf2 expression showed a tendency to increase following NTG-injection as compared to sham and TACHICAF groups (Figure 4A, see densitometric analysis Figure 4A1); DMF administration, at both doses of 30 and 100 mg/kg, after migraine induction, up-regulated the activities of Nrf2 (Figure 4A, see densitometric analysis Figure 4A1). Moreover, DMF treatment, at both doses of 30 and 100 mg/kg, after NTG injections, up-regulated the activity of Mn-SOD (Figure 4B, see densitometric analysis Figure 4B1), respect the basal expression in controls groups (Figure 4B, see densitometric analysis Figure 4B1). Indeed, the levels of HO-1 were increased following NTG-damage compared to control and TACHICAF groups (Figure 4C, see densitometric analysis Figure 4C1). Interestingly, treatment with DMF 30 and 100mg/kg significantly up-regulated, in the same way at both doses, HO-1 expression (Figure 4C, see densitometric analysis Figure 4C1).

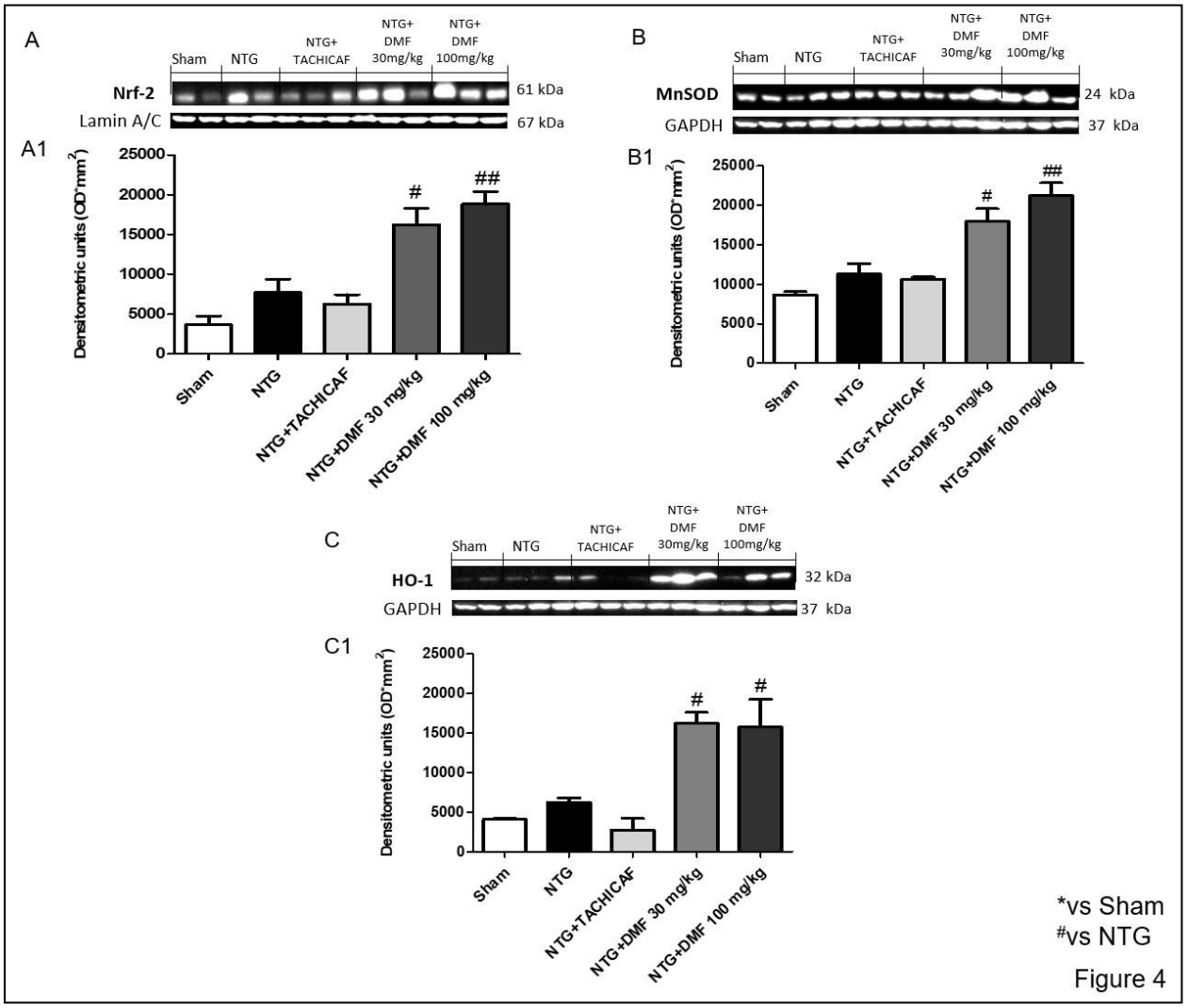

Figure 4.4: Effects of DMF on antioxidant system in NTG-induced migraine

The expression of Nrf2, Mn-SOD and HO-1was observed by Western Blot analysis in whole brain with the rostral cervical spinal cord samples of mice, 4h after NTG-injections. Respectively, nuclear Nrf2 expression increased following NTG-injection as compared to sham and TACHICAF groups (A), while DMF administration, at 30 and 100 mg/kg, up-regulated Nrf2 activity (A). The same result was obtained for Mn-SOD expression (B). The levels of HO-1 were notably increased following NTG-damage compared to control groups (C), while DMF treatment, at 30 and 100mg/kg, significantly up-regulated Mn-SOD and HO-1 expression (B and C). Data are means ± SEM of 10 mice for each group. A representative blot of lysates obtained from each group is shown and densitometry analysis of all animals is reported (n = 10 mice from each group). One-Way ANOVA followed by Bonferroni post-test. #p< 0.05 and ##p< 0.01 vs. NTG.

4.3.5 The effects of DMF on NF-κB inflammatory pathway in NTG-induced migraine

Oxidative stress-induced acute inflammatory responses may play an important role in the pathogenesis of acute pain arising from migraine [195]. To evaluate the anti-neuro

inflammatory effect by which DMF treatment may regulate cytokines expression during headache attack, we assessed the expression of NF-κB, IκB-α, iNOS, and COX-2, in whole brain with the rostral cervical spinal cord samples by Western blot analysis. We observed that NTG-injections caused a significant NF-κB nuclear translocation, almost completely inhibited by DMF 30 and 100mg/kg treatments, as observed in Figure 5A and 5A1. Also, DMF treatment, only at the dose of 100 mg/kg, significantly reduced IκB-α cytosolic degradation respect to NTG-injected mice (Figure 5B, see densitometric analysis Figure 5B1); still, the treatment with TACHICAF significantly reduced the cytosolic degradation of IκB-α (Figure 5B, see densitometric analysis Figure 5B1). In control group, the levels of IκB-α were significantly high respect to NTG group (Figure 5B, see densitometric analysis (Figure 5B1).

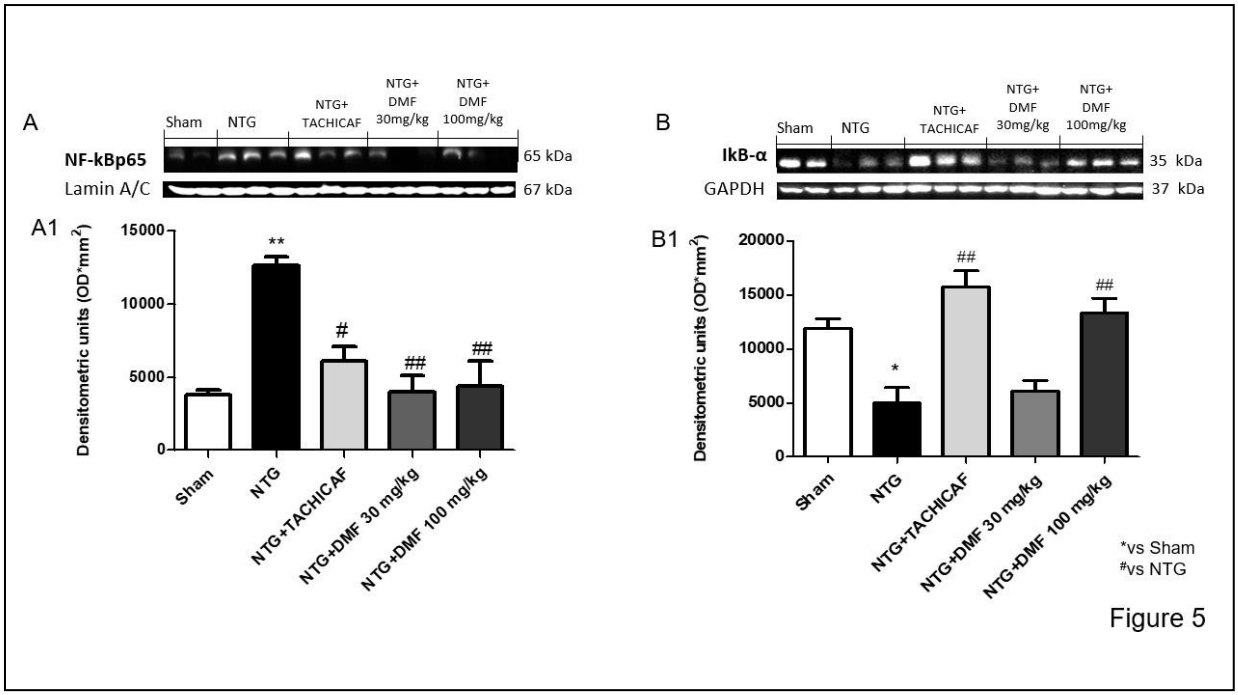

Figure 4.5: Effects of DMF on NF-κB inflammatory pathway in NTG-induced migraine

The expression of NF-κB and IκB-α was observed by Western blot analysis, in whole brain with the rostral cervical spinal cord samples of mice, 4h after NTG-injections. We observed that NTG-injections caused a significant NF-κB nuclear translocation, almost completely inhibited by DMF 30 and 100 mg/kg treatment (A). Also, DMF treatment, only at the dose of 100 mg/kg, significantly reduced IκB-α cytosolic phosphorylation (B), while in NTG-injected mice the levels of IκB-α cytosolic phosphorylated were significantly increased respect to

control groups (B). Data are means ± SEM of 10 mice for each group. A representative blot of lysates obtained from each group is shown and densitometry analysis of all animals is reported (n = 10 mice from each group). One-Way ANOVA followed by Bonferroni post- test. *p< 0.05 and **p< 0.01 vs. Sham; #p< 0.05 and ##p< 0.01 vs. NTG.

Indeed, a significant increase in iNOS expression was observed in the whole brain with the rostral cervical spinal cord samples from mice injected with NTG (Figure 6A, see densitometric analysis Figure 6A1), while DMF treatment significantly reduced iNOS expression at 30 and 100 mg/kg (Figure 6A, see densitometric analysis Figure 6A1) such as TACHICAF administration (Figure 6A, see densitometric analysis Figure 6A1). COX-2 expression was significantly elevated in NTG-injected mice in comparison to control and TACHICAF groups (Figure 6B, see densitometric analysis Figure 6B1). The rise in COX-2 expression induced by NTG was considerably blocked by treatment with DMF 30 and 100 mg/kg (Figure 6B, see densitometric analysis Figure 6B1).

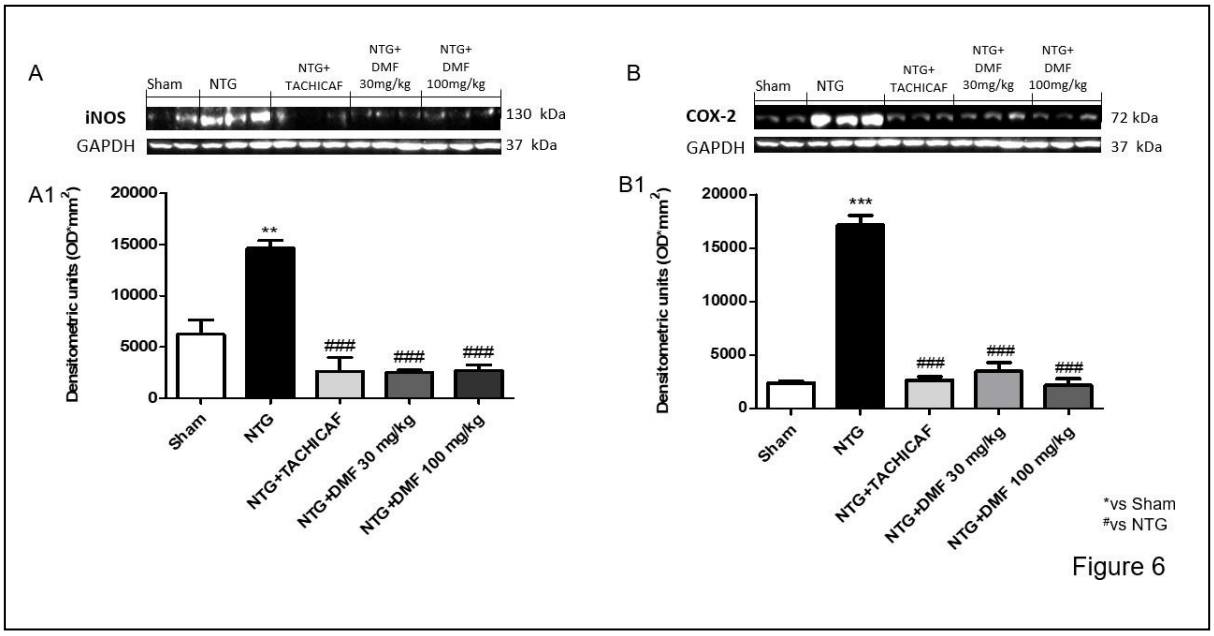

Figure 6

Figure 4.6. Effects of DMF on iNOS and COX-2 expression in NTG-induced migraine

The expression of iNOS and COX-2 was observed by Western blot analysis, in whole brain with the rostral cervical spinal cord samples of mice, 4h after NTG-injections. A significant increase in iNOS expression was observed in NTG group (A), while DMF treatment significantly reduced iNOS expression at 30 and 100 mg/kg (A). Alike, COX-2 expression was significantly elevated in NTG-injected mice in comparison to controls (B). The rise in COX-2 expression induced by NTG was considerably blocked by treatment with DMF 30 and 100 mg/kg (B). Data are means ± SEM of 10 mice for each group. A representative blot of lysates obtained from each group is shown and densitometry analysis of all animals is reported (n = 10 mice from each group). One-Way ANOVA followed by Bonferroni post- test. **p< 0.01 and ***p< 0.001 vs. Sham; ###p< 0.001 vs. NTG.

4.4 Discussion

Migraine represents one of the most disabling disorders [221]; therefore, medical approach should be individualized for adequate treatment of the migraine and other vascular risk factors. Several studies have shown that oxidative stress plays a role in central sensitization [222]. There are many factors that lead to the generation of oxidants in migraine; these could be explained by the metabolic changes in the cerebral cortex associated with intracellular calcium overload during cortical spreading depression (CSD) that bring at an increasing oxygen necessity which could induce oxidative stress [223, 224]. Local changes of cerebral blood flow may enhance the generation and release of free radicals, thus causing increased accumulation of lipid peroxidation by-products in blood [225, 226]. However, there are some conflicting data on the significance of oxidative stress in migraine [227, 228]. The activity of antioxidant defense system is difficult to explain, therefore, a depth study of oxidative stress pathways may provide the desired information on the role of oxidative stress in migraine.

It has been found that Nrf2/ARE pathway is the most important endogenous antioxidant defense system and plays a critical role in regulating cellular oxidation, cell defense, and protection [229]. Nrf2 signaling cascade modulates both inflammation and oxidative stress. There are many drugs, already used clinically, that activate Nrf2 system, including fumaric acid ester DMF [157]. DMF is an orally administered fumarate ester, approved as first-line monotherapy in early stage of multiple sclerosis. Because DMF is rapidly and completely hydrolyzed by esterase, before reaching the systemic circulation, the pharmacologic activity of DMF is due to

its active metabolite MMF. Although nowadays the precise mechanism of action of DMF is not completely characterized, is thought to exert neuroprotective effects by activating Nrf2 transcriptional pathway [198]. DMF was discovered to impact the anti-oxidative stress cell machinery promoting the transcription of genes downstream to the activation of Nrf2, which besides immune regulatory effects. Furthermore, DMF combines safety and efficacy and has potential that goes beyond the anti-inflammatory effects, protecting glial cells, oligodendrocytes and neurons [159].

Recently studies demonstrated that DMF is highly active to counteract oxidative stress and inflammation by activating the Nrf2 genetic program to promote axonal regeneration and neurological recovery in MS as well as in other neurodegenerative diseases [230] , demonstrating that DMF can alleviate early brain injury and secondary cognitive deficits in experimental subarachnoid hemorrhage [231].

Moreover, the role of Nrf2 pathway was recently observed in *in vivo* model of headache demonstrating that the modulation of the Nrf2/ARE pathway inhibited the activation of trigemino vascular system (TGVS) and prevented the induction of hyperalgesia [199] . In support of this finding, we investigated the neuroprotective effect of DMF in NTG-induced hyperalgesia through the modulation of Nrf2/ARE pathway and its underlying mechanism.

The effect of DMF on analgesia was observed by the hot plate test, tail flick and formalin test, which are standard behavioral models for the assessment of analgesia [232]. Our result showed the analgesic role of DMF thought a significantly reduction of mechanical allodynia caused by NTG administrations, relieving stimulus-evoked spontaneous nociception. Moreover, in acute and chronic hyperalgesia conditions, DMF was able to counteract peripherally pain, as evaluated by the reduction of total number of flinches/shakes in formalin test.

The primary headache, particularly migraine, has a bidirectional relationship with depression and anxiety. Patients with depression have a more than three-fold relative risk of developing

migraine compared with non-depressed patients. Similarly, migraineurs have a more than three-fold relative risk of developing depression compared with patients without migraine[233] . The EPM test, used in this study, quantified the anxiety-like behavior associated with repeated migraine attacks demonstrating the importance of DMF treatment to reduce the rates of anxiety and depression.

Furthermore, the perception of migraine headache is intensified during exposure to light [234]; in fact, the migraine photophobia is experienced by nearly 90% of migraineurs with normal eyesight and depends on photic signals from the eye that converge on trigemino vascular neurons somewhere along its path. In this study, we showed that NTG injection caused light aversion in mice that was attenuated by DMF treatment, in a dose dependent manner.

The most common migraine-associated symptoms (nausea, throbbing pain, photophobia) originate from activation of nociceptors innervating pial, arachnoid and dural blood vessels. Central processes of meningeal sensory afferents enter the brainstem via the trigeminal tract and pass caudally while giving off collaterals that terminate in the spinal trigeminal nucleus (SpVC) and upper cervical spinal cord. Anatomical and electrophysiological studies have shown that the nociceptive innervation consists of unmyelinated (C-fibers) and thinly myelinated (Aδ fibers) axons containing vasoactive neuropeptides such as substance P (SP) and calcitonin gene-related peptide (CGRP), that originate in the trigeminal ganglion [235]. A large number of endogenous inflammatory mediators believed to be released during migraine are capable of activating and sensitizing peripheral and central trigeminovascular neurons, particularly the sensitization of second-order neurons in the SpVC mediates cephalic allodynia as well as muscle tenderness [236]. The majority of Aδ and C nociceptive primary afferents terminate in lamina V of the SpVC. These meningeal nociceptors converge on trigemino vascular SpVC neurons that receive additional input from the adjacent skin and muscles [237]. Pardutz et al., have demonstrated that NTG, as nitric oxide donor, is thus able to differentially

influence Aδ and C nociceptive primary afferent fibres in the superficial laminae of rat spinal trigeminal nucleus caudalis [238]. In this study, we observed that DMF significantly reduced the SpVC degeneration induced by NTG-administration, resulting in a reduction in referred pain perception caused by the resultant convergence of intracranial (visceral) and extracranial (somatic) primary afferents onto SpVC neurons.

Central sensitization associated with activation of NF-κB in the trigemino cervical complex (TNC) is reported to be involved in the pathogenesis of migraine [199] . NF-κB is believed to be implicated in multiple signaling pathways in variable headache settings and, particularly, Li et al. showed that the impairments due to NTG-induced migraine are caused by the activation of NF-κB signal transduction pathway [239]. Also, the activation of NF-κB transcriptional activity in brain nuclei that are relevant for pain transmission observed in an animal model of migraine suggested a potential new avenue for the development of anti-migraine drugs [240]. In the past, it was demonstrated that targeting the inflammatory response by selectively inhibiting NF-κB, offers a promising therapeutic approach for the treatment of headache [241]. Recently, in a study on the upregulation of inflammatory gene transcripts in chronic migraineurs, it has been discovered that 3 of the 4 genes that are abnormally expressed in chronic migraine patients - the NF-κBIA, the TNFAIP3 and the ILR2 - are tightly related to the NF-κB family pathway, suggesting that suppression of NF-κB activation is critical in resolving the inflammation and consequently in reducing the pain involved in the pathophysiology of the studied chronic migraine patients [242]. Collectively, the findings point to a dual mechanism in headache: the first is activation of proinflammatory pathways and the second is suppression of pathways involved in resolving the inflammation. Particularly, in headache, neurogenic inflammation is responsible of the characteristic symtomps as pain and sensitization, because mast cells that reside close to primary nociceptive neurons are capable of triggering local inflammation [243].

Recently, it has been demonstrated that DMF induced Nrf2 expression suppresses the NF-κB mediated inflammatory pathway [244]. Moreover, the identification of NF-κB binding cites in the promoter region of the Nrf2 gene suggests cross talk between these two regulators of inflammatory processes [141] . In this study, we demonstrated that DMF treatment inhibited the nuclear translocation of NF-κB, representing a functional system to regulate neuroinflammation in response to migraine. NF-κB activation is correlated with an up regulation of pro-inflammatory mediators such as TNF-α, interleukins and prostaglandins as well as nitrosative stress. In this study DMF treatment significantly reduced iNOS and COX-2 expressions. In response to inflammatory and oxidative stimuli, up regulation of Nrf2 signaling inhibits the overproduction of pro-inflammatory cytokines and chemokines as well as limiting the activation of NF-κB [245]. In normal conditions, Nrf2 is located in the cytosol, under oxidative stressors Nrf2 translocate to the nucleus activating anti-oxidative genes [246]. Inthis study, we observed that NTG administration significantly increased nuclear Nrf2 expression in mice as well as the expression Nrf2-regulated phase II enzymes, Mn-SOD and HO-1 [247] . DMF treatments markedly upregulated the antioxidant enzymes demonstrating its important role in the reduction of oxidative stress related to migraine.

45 Conclusions

Thus, in this study we demonstrated for the first time the key role of DMF in migraine relieve, modulating the inflammatory state and strengthening the antioxidant Nrf2 transcriptional pathway. Also, considering that anxiety plays an important fact in migraine risk, detecting anxiety symptoms and implementing pharmacological and not treatments targeting Nrf2/NF-κB pathway, could improve headache control and patient's quality of life. In conclusion, DMF could be considered as promising therapeutic approach in counteract the oxidative stress associated to migraine.

PART II

ABSTRACT

Hydrogen sulfide (H_2S) is generated in the adipose tissue from L-cysteine by cystathionine γ-lyase (CSE) or cystathionine β-synthase (CBS) and from 3-mercaptopyruvate by 3-mercaptopyruvate sulfurtransferase (3-MST). These enzymes occur widely in mammalian cells and tissues and produce H_2S, which plays multiple roles, including regulation of insulin resistance and glucose homeostasis. H_2S-synthesis occurs in adipocytes and therefore the question arises as to whether endogenous or exogenous H_2S may modulate adipocyte maturation and the associated lipid accumulation. H_2S interacts with Nrf2 pathway by enhancing Nrf2 nuclear translocation and stimulating expression of Nrf2-targeted downstream proteins and mRNA levels. In this part of the thesis, the effects of slow-releasing (GYY4137) H_2S donors and the 3-MST inhibitor 2-[(4-hydroxy-6-methylpyrimidin-2-yl)sulfanyl]-1-(naphthalen-1-yl)ethan-1-one (HMPSNE) on 3T3L1 adipocyte cells, to assess the modulation of adipogenesis by H_2S *in vitro*. Confluent 3T3L1 cells, a fibroblast-like mouse preadipocyte cell line, were differentiated into mature adipocytes in presence or absence of GYY4137 and HMPSNE. Additionally, we established 3-MST knockdown 3T3L1 cells were treated with GYY4137. To evaluate the effect of H_2S on lipid accumulation during the adipogenesis process. Red Oil O staining, cell viability and toxicity, H_2S detection, western blot analysis and arrays on antioxidant transcription factors were performed.

Differentiation of the adipocytes was associated with a time-dependent increase in lipid accumulation, as assessed by Red Oil O staining. A further upregulation of lipid accumulation was observed in cells treated with 3-MST inhibitor HMPSNE. In contrast, treatment with H_2S donors significantly reduced lipid accumulation into the maturing adipocytes.

Taken together, this study shows that H_2S plays an important role in the regulation of adipogenesis, and/or adipocyte lipid uptake and/or lipid metabolism. We hypothesize that an

inhibition of endogenous H_2S-synthesis may contribute to an impairment of lipid homeostasis during various obesity/metabolic syndromes. Moreover, a further investigation on 3-MST knockdown cells, could shed light on possible interactions between 3-MST-and Nrf2 pathway. On-going work focuses on the molecular mechanisms through which H_2S modulates the process of adipogenesis.

5.0 CHAPTER FIVE: The role of H_2S on adipogenesis

5.1 Hydrogen sulfide

Hydrogen sulfide (H_2S) is one of three gasotransmitters together with nitric oxide (NO) and carbon monoxide (CO), historically perceived as a highly toxic gas with the distinctive smell of rotten eggs. It is an endogenous signal transmitter via protein sulfhydration, and, at low intracellular concentrations (0.01 to 1 μM) donates electrons to complex II of the mitochondrial electron transport chain, thereby stimulating ATP production, but at about 3–30-fold higher concentrations, H_2S becomes toxic by binding to and inhibiting cytochrome C oxidase in complex IV of the electron transport chain, the last complex in the chain prior to ATP synthesis by complex V [248]; cyanide, which also inhibits cytochrome C oxidase, increases mitochondrial generation of superoxide and induces oxidative stress in cells.

Another mechanism that may be involved in H_2S toxicity includes hydrogen peroxide production and oxygen depletion during H_2S oxidation by oxy- and methemoglobin ($O_2 + H_2S = S° + H_2O_2$), also slightly inhibiting erythrocyte superoxide dismutase (SOD) and inhibited catalase, which suggests that cellular damage could be due to increased levels of reactive oxygen species [249].

As a signaling molecule, H_2S plays an important role in physiology and shows great potential in pharmaceutical applications [250]. Recently, this pungent gas was discovered to be synthesized enzymatically in mammalian and human tissues, which positively transformed the apparent image of H_2S into a promising therapeutic compound [251]. Literature evidences suggest that H_2S may be involved in anti-inflammatory and anti-tumorigenic processes [252] [253], in ion channels regulation [254], cardiovascular protection [255] and antioxidant response [256]. However, the exact role that H_2S plays depends on the specific circumstance, its concentration and the interplays with other signaling molecules, especially NO and CO.

5.1.1 Physical and chemical properties of H_2S

Under ambient temperature and pressure, H_2S is a colorless gas, flammable and poisonous in high concentrations. H_2S is water soluble, with a solubility range from ~80 mM at 37 °C [19], up to ~117 mM (condition unspecified) [257]. These differences are apparently due to the experimental conditions including pressure, temperature and the composition of the solution. H_2S equilibrates between the gas phase and the aqueous phase and its properties of gas–aqueous distribution including Henry's Law coefficient have been studied. H_2S is lipophilic and can diffuse through membranes without facilitation of membrane channels [258].

H_2S is a weak acid, with a pKa_1 values varied from 6.97 to 7.06 at 25 °C, and pKa_2 from 12.35 to 15 [259].

5.1.2 Endogenous production of H_2S

In mammalian cells H_2S is generated via both enzymatic and nonenzymatic pathways, although the nonenzymatic pathway only accounts for a small portion of H_2S production. Among the enzymes involved in the production of H_2S, cystathionine β-synthase (CBS) and cystathionine γ-lyase (CSE) have been investigated most extensively. CBS and CSE are pyridoxal-5′-phosphate (PLP)-dependent enzymes, which means that they generate H_2S by using pyridoxal 5'-phosphate (vitamin B6). CBS converts homocysteine into cystathionine, which is then converted to L-cysteine by CSE; both enzymes transform L-cysteine to H_2S. H_2S is also synthesized from D-cysteine by tandem enzymes cysteine aminotransferase (CAT) and 3-mercaptopyruvate sulfurtransferase (3-MST) [260], as shown in Figure 5.1.

CBS is expressed predominantly in the central nervous system (CNS), with high concentrations in astrocytes. The normal cellular function of CBS is in the trans-sulfuration pathway, catalyzing the condensation of homocysteine with serine to form cystathionine. In contrast, CSE is mainly responsible for the production of H_2S outside the CNS [261].

Chemically, CBS activity is confined to chemical transformations at the β-position, while CSE is proficient at catalyzing reactions at the β- and γ-carbons of substrates [262]. Furthermore, because homocysteine appears to be unable to bind to the site at which the external aldimine with PLP is formed in CBS, the contribution from CSE to the H_2S production is increased under conditions of moderate and severe hyperhomocysteinemia [263] .

3-MST, a PLP-independent enzyme, is localized in the neurons along with cysteine aminotransferase (CAT); 3-MST and CAT are also found in the vascular endothelium. CAT catalyzes the reaction of L-cysteine with *α*-ketoglutarate to form 3-mercaptopyruvate (3MP), which is further catalyzed by 3-MST to generate H_2S in the presence of thiol and reducing agents [264]. The PLP-dependent trans-sulfuration pathway, which contains both CBS and CSE for H_2S production, takes place in the cytosol, while H_2S synthesis *via* CAT and 3-MST also occurs in mitochondria.

All H_2S-synthesizing enzymes are expressed in the vascular wall including endothelial cells, smooth muscle cells, and perivascular adipose tissue [265].

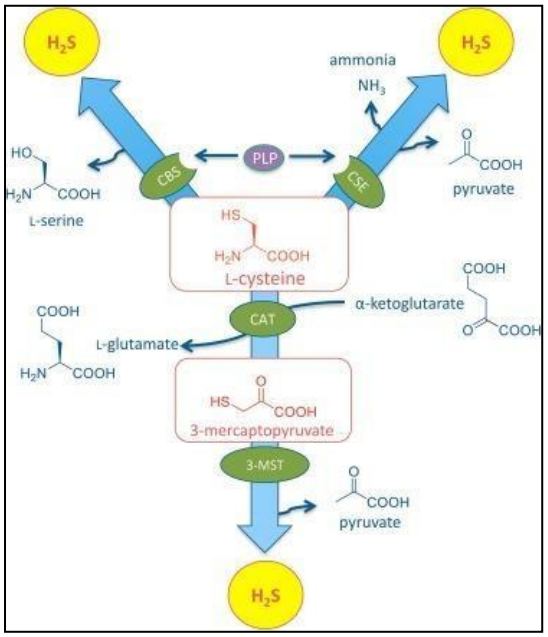

Figure 5.1: Overview of endogenous H_2S synthesis in mammalian cells

Adapted from Chadwick R. Powell, Kearsley M. Dillon, John B. Matson, A review of hydrogen sulfide (H_2S) donors: Chemistry and potential therapeutic applications, Biochemical Pharmacology, Volume 149, 2018, Pages 110-123.

5.1.4 Exogenous production of H_2S

The vast majority of studies that have examined the potential role of H_2S in health and disease utilized commercially available sulfide salts such as sodium sulfide (Na_2S) and sodium hydrosulfide (NaSH) [266]. Over time, it has been understood that these sodium salts have disadvantages, such as the rapid peak in H_2S levels and short half-life when dissolved or injected. Recently, H_2S donors, with a regulated release, have been developed; with these slow-release H_2S donor molecules, it is possible to expose animals, tissue and cells to H_2S generated in a more physiological manner [267]. Of course, there is not a single ideal donor and that depends on the situations, sometimes a fast donor may be required, other times slow release is best. The more common donors are: the naproxen-based H_2S donor ATB-346, which exhibits anti-inflammatory effects [268], GIC-1001, an orally administered trimebutine maleate salt H_2S donor used as an alternative to sedatives in colonoscopies [269] and GYY4137, a water-soluble derivative of Lawesson's reagent (LR), which also releases H_2S via hydrolysis [267]. In a direct amperometric comparison of H_2S release rates from GYY4137 and NaSH, GYY4137 released H_2S with a peaking time of $\sim$10 min versus $\sim$10 s for NaSH in phosphate buffer pH 7.4, however, the peaking concentration for GYY4137 was $\sim$40-fold lower than for NaSH even at a 10-fold higher concentration of GYY4137 used in this study [267].

5.1.5 H_2S metabolism

H_2S is the only inorganic substrate enzymatically oxidized in mitochondria proving that mitochondria originated from sulfide-oxidizing bacteria. H_2S is oxidized by sulfide:quinone oxidoreductase (SQR) [270], which transfers electrons to coenzyme Q from which they are further transported to cytochrome c by ubiquinol:cytochrome c oxidase (complex III) and

finally to molecular O_2 by cytochrome c oxidase (complex IV) [271]. SQR represents the third source of electrons for mitochondrial respiratory chain in addition to NADH dehydrogenase (complex I) and succinate dehydrogenase (complex II) involved in oxidation of organic substrates. During SQR-catalyzed reaction, H_2S is oxidized to sulfur atom. Sulfur is then transferred to reduced glutathione to form glutathione persulfide (GSSH) and then may be either oxidized to sulfite by sulfur dioxygenase (persulfide dioxygenase, protein deficient in ethylmalonic encephalopathy, ETHE1) or transferred to sulfite by thiosulfate:cyanide sulfurtransferase (TST, rhodanese) to form thiosulfate [272]. The rate of mitochondrial H_2S oxidation is determined by O_2 level. The results of many studies strongly suggest that steady-state level of H_2S in tissues is maintained very low by its efficient oxidation. Under conditions of reduced O_2 supply, H_2S metabolism is compromised and its concentration increases making this gasotransmitter an important oxygen sensor in various tissues including blood vessels [273].

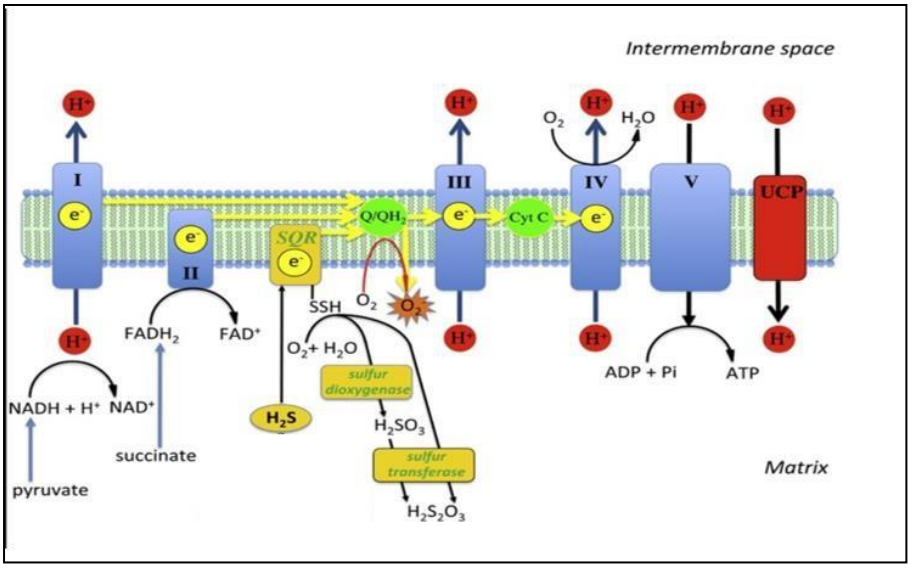

Figure 5.2: Mitochondrial oxidant production

Adapted from: Pharmacological Research Volume 113, Part A, November 2016, Pages 186-198 *The novel mitochondria-targeted hydrogen sulfide (H_2S) donors AP123 and AP39 protect against hyperglycemic injury in microvascular endothelial cells in vitro.*

5.1.6 Bell-shaped model for H_2S

The controversies regarding the different role of H_2S development have been harmonised by proposing the bell-shaped model [274]. The double role of H_2S can be resolved by considering a bell-shaped pharmacology of H_2S, whereby lower (endogenous) H_2S production tends to promote, while higher (generated from exogenously added H_2S donors) tends to inhibit cell proliferation [275]. In this cited study, a reasonable bell-shaped model to illustrate the effects of H_2S in cancer cells was provived; the bell-shaped curve is employed to describe the effects of H_2S on cell proliferation, since endogenous H_2S or a relatively low level of exogenous H_2S exhibited pro-cancer effect, while exposure to H_2S with high amounts contributed to cell death.

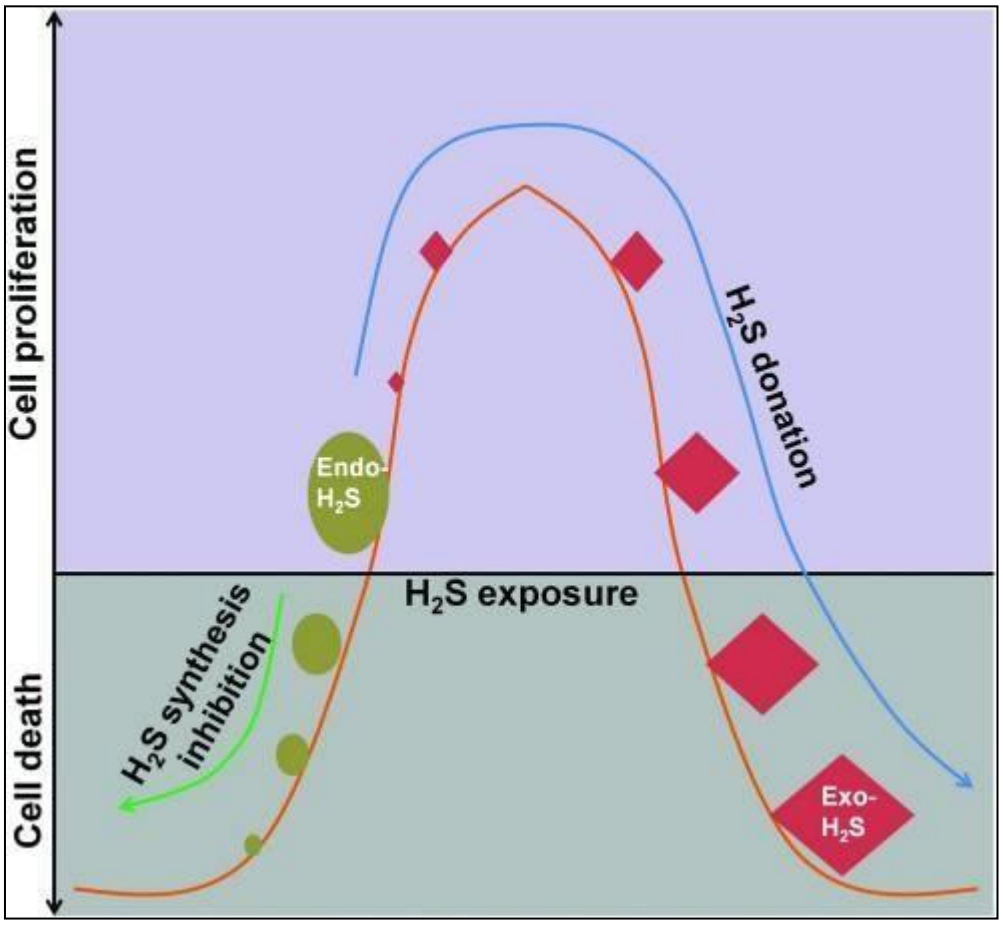

Figure 5.3: The bell-shaped model for the dual role of H_2S

Adapted from: Antioxid Redox Signal. 2019 Jul 1; 31(1): 1–38. A Review of Hydrogen Sulfide Synthesis, Metabolism, and Measurement: Is Modulation of Hydrogen Sulfide a Novel Therapeutic for Cancer?

5.2 H_2S signaling in oxidative stress

The ubiquitous distribution of H_2S-producing enzymes and the potent chemical reactivities of H_2S in biological system makes this molecule unique in regulating cellular and organ functions in both the mammalian and plants [276]. Pathophysiological abnormalities related to altered H_2S metabolism and function have been demonstrated in many cases, but H_2S possesses a great therapeutic potential in redox regulation of cellular functions [277]. However, the exact role of H_2S in redox regulation is controversial, since both anti- and pro-oxidant effects have been documented. Accumulating evidence suggests that H_2S exerts protective effects against various stimuli-triggered injuries in many organs including heart and nervous system [278] for instance by increasing glutathione (GSH) reduction [279], or by directly scavenging superoxide anions, H_2O_2 [280] and peroxynitrite to suppress oxidative stress [281]. H_2S displays a cytoprotective role against oxidative stress [282, 283], acting as antioxidant by direct scavenging peroxynitrite ($ONOOH/ONOO^-$) and hypochlorite ($HOCl/^-OCl$).

H_2S reaction with O_2, a process called autoxidation, generates polysulfanes, sulfite, thiolsulfate and sulfate as the intermediates and products, although the mechanisms remain undefined due to their complexity [284]. In mammalian cells, H_2S autoxidation is catalyzed by mitochondrial enzymes, generating hydrodisulfide, sulfite, thiolsulfate [270]. This rapid enzymatic process has been suggested to be the mechanism of H_2S-regulated oxygen sensing [285].

When H_2S reacts with H_2O_2 the pH of the reaction mixture oscillates between acid and base as the reaction proceeds due to a not yet defined mechanism [286].

Additionally, H_2S can be converted to sulfite by activated neutrophils via NADPH oxidase activity, a process that is inhibited by ascorbic acid [287].

5.2.1 Antioxidant roles of H_2S in the cardiovascular system

The robust antioxidant actions of H_2S are associated with direct scavenging of ROS and increased expression and functions of antioxidant enzymes. H_2S mediates cardiac protection

through the activation of Akt and MAPK (ERK1/2 and p38) pathways, upregulation and phosphorylation of vascular endothelial growth factor and opening the ATP-sensitive potassium channel [288]. More importantly, H_2S hinders ROS production and reduces oxidative stress, which greatly contributes to cardiac protection. In the vascular cells and tissues, H_2S has been reported to reduce oxidative stress by upregulating superoxide dismutase (SOD), increasing thiol levels and decreasing the production of ROS. Moreover, H_2S inhibits mitochondrial complex IV activity and increases the activities of Mn-SOD and CuZn-SOD, decreasing the levels of ROS in cardiomyocytes during ischemia–reperfusion [289].

Homocysteine, a sulfhydryl containing amino acid, is an independent and graded risk factor for atherosclerosis, but H_2S is able to attenuate homocysteine-mediated oxidative stress and cellular damage. H_2S also protects against vascular remodeling as a result of endothelial damage, through normalizing the levels of redox stress, matrix metalloproteinase and tissue inhibitor of metalloproteinase [290]. Furthermore, H_2S improves ischemic heart failure in mice by inhibiting oxidation, increasing mitochondrial biogenesis and reducing apoptosis [291].

5.2.2 Antioxidant roles of H_2S in nervous system

In the mammalian CNS, H_2S is predominantly produced by CBS and acts as a neuromodulator [292]. It is generally recognized that H_2S may protect the cells in CNS from apoptosis or degeneration following brain injury or as a result of chronic neurodegenerative diseases, through regulation of oxidative stress. H_2S inhibited hypochlorous acid-induced cytotoxicity, intracellular protein oxidation and lipid peroxidation in a human-derived dopaminergic neuroblastoma cell line [293]. H_2S also protects neuronal cells, against amyloid beta and 1-methyl4-phenylpyridinium ion (MPP+)-induced cytotoxicity by reducing the loss of mitochondrial membrane potential and attenuating the increase of intracellular ROS [294].

Zhao et al. reported that H_2S attenuated NLRP3 inflammasome-mediated neuroinflammation after intracerebral hemorrhage (ICH), showing that supplement with taurine could increase H_2S

content, enhanced CBS expression and effectively mitigated the severity of pathological inflammation after ICH [295].

The role of H_2S in the regulation of cardiovascular, gastrointestinal, nervous system function as well as in the regulation of inflammatory and immune response has been described in many excellent review articles [257, 260, 296]. Instead, the functions of H_2S in adipose tissue, until now, were much less studied, although some important data have been accumulated in this field.

5.3 Adipose tissue

Adipose tissue is the most consistent tissue in the human body; it is commonly found in subcutaneous loose connective tissue, generally surrounding internal organs. Mature adipocytes constitute the majority of cells in adipose tissue, but fat tissue contains several other cell types, including stromal-vascular cells (SVC) such as fibroblasts, smooth muscle cells, pericytes, endothelial cells and adipogenic progenitor cells. The degree of specialization of these cells is such that they are able to take up and accumulate large amounts of triglycerides during periods of energy excess, making them available under conditions of energy deficiency.

Adipose tissue is divided into two subtypes, white (WAT) and brown (BAT) fat [297]. WAT is widely distributed and it represents the primary site of fat metabolism and storage, whereas BAT is relatively scarce and its main role is to provide body heat [298]. The morphology of both adipocytes is reasonably different, because these lipids are organized in a unique droplet in white adipocytes (unilocular) and in many droplets in brown adipocytes (multilocular) [299]. White adipocytes contain a big lipid droplets consisting of triglycerides. Lipoprotein lipase (LPL), the enzyme attached to luminal surface of endothelial cells, hydrolyzes triglycerides contained in plasma lipoproteins and releases fatty acids which are then taken up and esterified inside the adipocyte. In this context, adipocytes accumulate fatty acids obtained from alimentary sources and synthesized in the liver which are transported in the blood by chylomicrons and very low density lipoproteins. In addition, fatty acids are synthesized *de novo*

inside the adipocytes from acetyl-coenzyme A, the product of glucose metabolism. Triglycerides stored in lipid droplets are substrates for lipolysis, the complex regulated process catalyzed by three consecutively acting enzymes, adipocyte triglyceride lipase, diglyceride lipase and monoglyceride lipase [300]. The final products of lipolysis are glycerol and non-esterified fatty acids (NEFA); glycerol is released to the extracellular space and then is metabolized by the liver whereas NEFA may be either released or esterified *de novo* in adipocytes to triglycerides with glycerol 3-phosphate provided by glycolysis as the co-substrate. NEFA released from the adipose tissue represent the energy substrate for other tissues such as the skeletal muscles and the heart as well as may be partially oxidized to ketone bodies in the liver.

Differently, BAT tissue is characterized by numerous large mitochondria which express uncoupling protein 1 (UCP1), the protein able to uncouple oxidative phosphorylation from ATP synthesis, resulting in the production of heat [301]. Interestingly, UCP1 immunoreactive brown adipocytes are present in all depots, also called “beige” or “brite” (brown in white). These brown/beige/brite cells in WAT are derived from precursor cells that could be different from classical brown adipocytes and are closer to the white adipocyte cell lineage [302].

Recently, another type of adipose tissue was showed, the marrow adipose tissue (MAT), described as a tissue formed by passive cells, occupying space not required for hematopoiesis or bone formation, but it has been finally documented the active role of MAT in the bone marrow microenvironment [303]. At birth, the bone marrow is mostly hematopoietic (the red marrow), but, throughout life, it is progressively transformed to fatty yellow marrow, expanding with the age in both genders [304]. This tissue accumulate in the appendicular skeleton until age of 20–25 and gradual MAT formation continues in the axial skeleton; in young subjects the content of marrow fat appears higher in men than women, while older female subjects have higher bone marrow adiposity [305]. This age-related increases in marrow fat content are

defined hypertrophy, if depends on increased size, or hyperplasia, if depends on increased number of adipocytes in the marrow. The critical role of MAT is to preserve energy. In fact, under pathological conditions, such as in state of calorie restriction and anorexia, there is an amount of MAT, that appears strongly increased [305].

The last fourth type of adipose tissue discovered was pink adipose tissue (PAT), characterized in mouse subcutaneous fat depots during pregnancy and lactation, when the adipose portion of the mammary gland gradually disappears, with the appearance of milk-secreting epithelial glands. These newly formed epithelial cells, called pink adipocytes, derive from a direct transdifferentiation of white adipocytes into milk-secreting epithelial cells (adipo-epithelial transdifferentiation) [306]. Interestingly, the formation of PAT is reversible, and following end of lactation, it can revert in WAT, restoring the adipose component of the mammary gland [307].

5.3.1 The anatomy of multi-deposit of adipose tissue

White and brown adipocytes have different morphology and functions, but in several locations, both cells cohabit together, forming the multi-depot adipose organ [308]. These depots are located in the subcutaneous space (subcutaneous depots) or close to organs located in the trunk (visceral depots). The anterior subcutaneous deposit is mainly located in the upper dorsal area at the level of the scapulae, while the posterior subcutaneous is located primarily in the lower ventral part of the body.- Furthermore, in females, it has been also described another anatomical form of fat called the abdominopelvic depot, which comprises perirenal, periovarian, parametrial, and perivesical fat [309]. All adipose deposits are associated with specific nerve-vascular peduncles, enabling the connection with the nervous system in order to respond to physiological and environmental stimuli. Most of the nerve fibers in contact with adipocytes express tyrosine hydroxylase, the enzyme marker of noradrenergic fibers [310]; when mammals are exposed to temperatures below thermoneutrality, the sympathetic nervous system is

activated because thermogenesis is required. This implies the action of norepinephrine on β_3 adrenoreceptors, which promotes the molecular pathway for thermogenesis in brown adipocytes [301]. Therefore, adipose tissues exposed to cold temperature appear browner and more innervated than those exposed to a warm environment. In contrast, aging seems to have an opposite effect on white and brown fat balance.

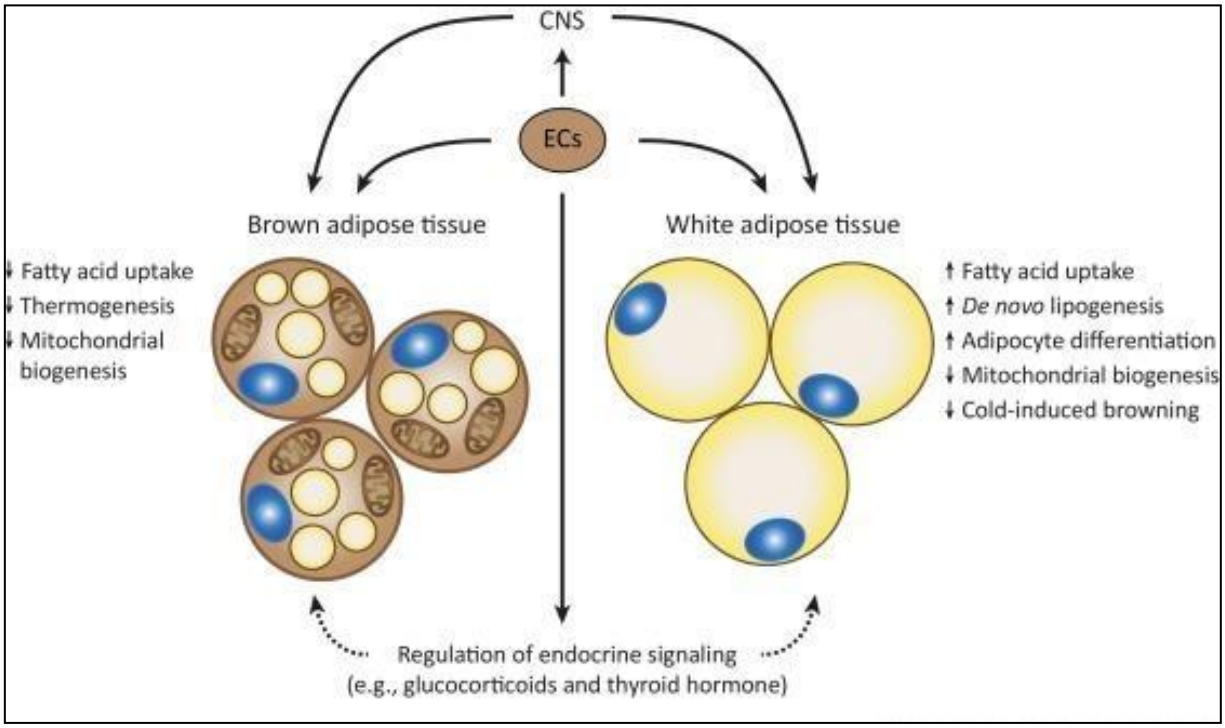

Figure 5.4: White and brown adipose tissue

Images by Trends Endocrinol Metab. 2018 *Regulation of Adipose Tissue Metabolism by the Endocannabinoid System.*
Regulation of endocrine signals for white and brown adipocytes formation.

5.3.2 Adipose cell differentiation

The formation of WAT begins shortly after birth, when mesenchymal stem cells become adipoblasts and differentiate into pre-adipocytes. The primary phase of adipogenesis is characterized by the proliferation of pre-adipocytes, which move forward into mitosis until they reach growth arrest. At this point, if pre-adipocytes exit the cell cycle, they change their morphology and accumulate cytoplasmic triglycerides, becoming mature adipocytes and loosing the ability to divide [311]. Both white and brown adipocytes originate from the

mesoderm, but they derive from different precursor cells. Mesenchymal stem cells can be committed to either a Myf5-negative adipogenic and osteoblastogenic lineage (white adipocytes) or to a Myf5-positive myogenic lineage (brown adipocytes) [312].

In white adipocytes, once differentiation is active, the cAMP response element binding protein becomes phosphorylated and then induces the expression of C/EBP-β [313]. The mitogen-activated protein kinase and GSK3β phosphorylate C/ EBP-β, which leads to dimerization of C/EBP-β, that binds to DNA allowing pre-adipocytes either to re-enter the cell cycle or to increase the levels of transcripton factors C/EBP-α and peroxisome proliferator-activated receptor-γ (PPAR-γ). PPAR-γ is crucial to promote lipid and glucose metabolism and insulin sensitivity in adipocytes [314].

Conversely, BAT develops before birth because it plays role in protecting newborn against cold. The differentiation of brown pre-adipocytes into mature brown adipocytes is positively and negatively controlled by bone morphogenetic protein (BMP)-7 [315]. C/EBP-β and PR domain containing 16 (PRDM16) have been shown to act as key transcriptional factors in the differentiation of brown adipocytes [316]. Thus, when PRDM16 was suppressed in brown precursor cells, the cells differentiated into skeletal muscle cells.

The fate of BAT from the myogenic lineage depends on transcriptional complex formed between PRDM16 and C/EBP-β [317] that induces the expression of peroxisome proliferator-activated receptor gamma coactivator-1 alpha (PGC-1α), which in turn regulates mitochondrial biogenesis and oxidative metabolism [318]. Furthermore, C/EBP-β is a key transcriptional activator that leads to UCP1 expression, inducing the thermogenesis process [317].

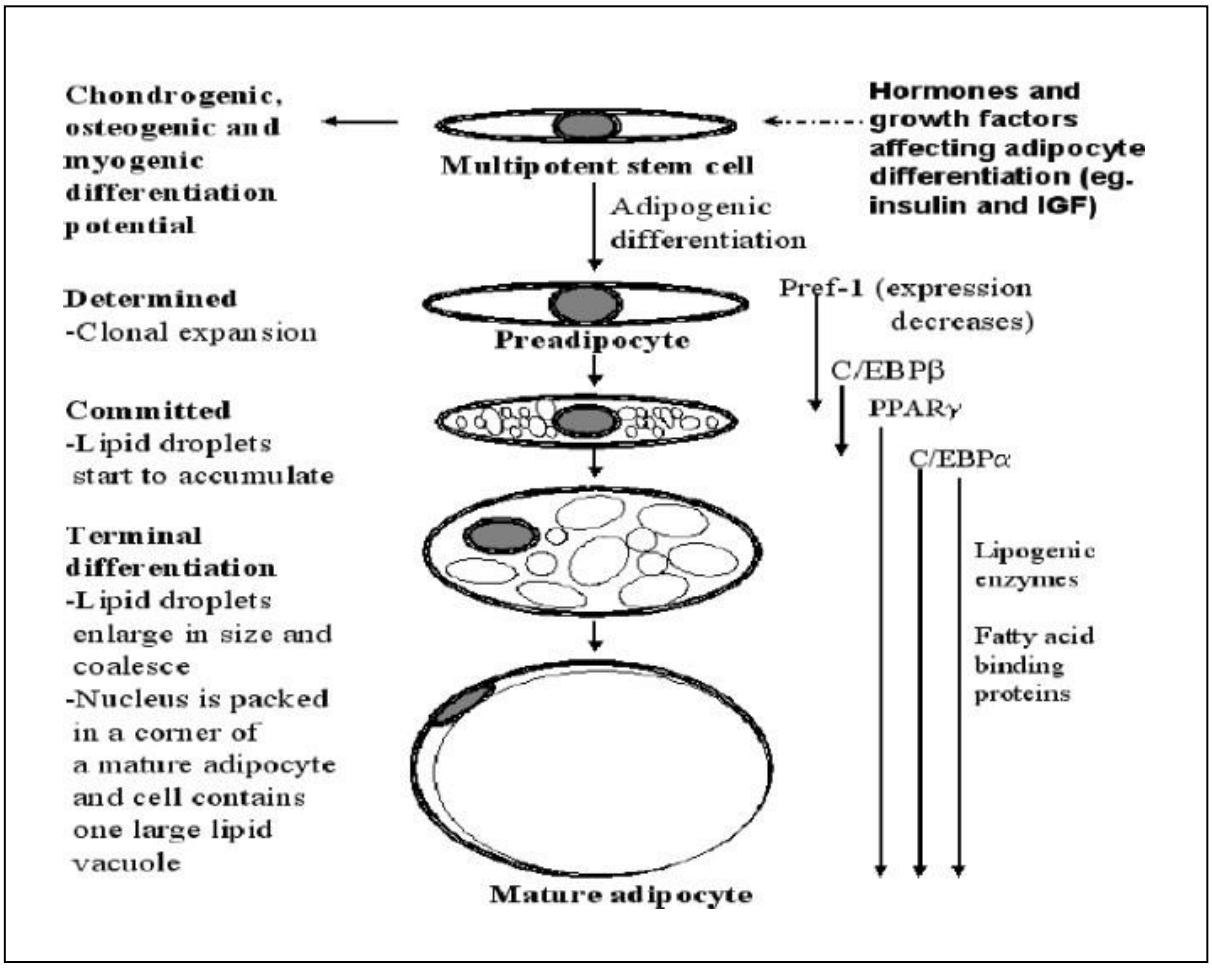

Figure 5.5 : Stages in adipocyte differentiation

Images by *Adipose Tissue and Adipocyte Differentiation: Molecular and Cellular Aspects and Tissue Engineering Applications* 2008

5.3.3 Transdifferentiation process

The white adipose deposits have the ability to switch between energy storage and energy expenditure. Thus, in specific physiologic conditions, white adipocytes transform into brown adipocytes to contribute to thermogenic needs [319]. Specifically, during the process called browning response, they can shift from a WAT phenotype to a BAT-like phenotype showing morphology, gene expression pattern and mitochondrial respiratory activity quite identical to those of classical BAT [320]. The strongest inducer of beige/brite cells activation is cold exposure via several molecular mechanisms. This conversion is principally mediated by the sympathetic nervous system. Transcription factors such as PPAR-γ, its coactivator PGC-1α,

C/EBP-β, and PRDM16 seem to play key roles in regulation of the browning program [321]; PGC-1α, originally described as a cofactor of PPARγ, is inducible by cold exposure in BAT [322], but also C/EBPβ and PRDM16 are powerful inducers of the brown phenotype of fat cells. They form a molecular complex that is essential for the brown differentiation of mesenchymal stem cells. Fibroblast growth factor 21 (FGF21) is a growth factor produced by the liver and BAT, acting in an autocrine/paracrine manner to increase expression of UCP1 and enhancing PGC-1α protein levels in adipose tissue. Conversely, transforming growth factor β (TGF-β) negatively affects the browning process [323].

The browning process can also be affected by other factors; interestingly, a recently discovered hormone called irisin, which is produced by skeletal muscles during physical exercise, has been proven to be efficient to convert WAT in BAT, both *in vitro* and *in vivo* [324].

The ability to transform itself according to the need of more energy consumption is defined as WAT plasticity. However, this extraordinary plasticity is not solely related to the browning response. As mentioned in paragraph 5.3, during pregnancy and lactation, all subcutaneous deposit of the adipose organ can turn into mammary glands; particularly, white adipocytes lose their lipid content, acquire epithelial features and form glandular structures able to produce and secrete milk, known as PAT. Following lactation, part of the epithelial component of the gland converts into adipocytes, allowing recovery of the adipose component in the subcutaneous deposit [325].

The adipose cell plasticity and ability to adapt to environmental stimuli, modifying their phenotype, satisfy important physiological needs of the organism.

5.3.4 Adipokines and Cytokines

Molecules secreted by adipose tissue play a key role in metabolic homeostasis and their deficiency, caused by massive adiposity or adipocyte dysfunction, leads to obesity or several obesity-related pathologies. Thus, adipose tissue is considered an endocrine organ whose action

on target tissues depends on the location of fat deposit and may differ according to its functional state.

Leptin is one of the most potent adipokines in metabolic regulation, that controls body weight by signaling sense of appetite or satiety to hypothalamus, which produces neurotransmitters that adapt food intake and energy expenditure. Leptin also regulates hepatic lipogenesis by suppressing fatty acid synthesis pathway [326] and improves muscle fatty acid oxidation [327]. Currently, researches for treatment of obesity-induced inflammation and insulin resistance are exploring strategies to increase adiponectin levels or adiponectin receptor activities [328]. Tumor necrosis factor alpha (TNF-α) was the first cytokine identified in the adipose tissue, involved in obesity-induced insulin resistance because it interferes with insulin signaling and blocks insulin actions [329].

The other pro-inflammatory cytokine is interleukin 6 (Il-6), whose expression level increases in the adipose tissue, but its role in glucose metabolism has not been fully determined. In addition, adipose tissue produces chemokines (interleukin-8, monocyte chemoattractant protein-1, MCP-1), hormones (angiotensin II, adrenomedullin, atrial natriuretic peptide), growth factors, enzymes and enzyme inhibitors (visfatin, vaspin, plasminogen activator inhibitor-1) and acute phase proteins. Also, non-protein biologically active mediators including gasotransmitters (NO, CO and H_2S) are producted by adipose tissue [330]. Fat tissue plays an important role in numerous processes through its secretory products and endocrine functions [331].

5.4 Obesity as adipose tissue disfunction

Obesity, the primary health burden of the 21st century, is a chronic disease that affects the quality of individual life physiologically, economically and psychologically [332], with an excess amount of body fat that reduces the quality of life but also increases both healthcare- associated costs and the risk of death [333].

The World Health Organization (WHO) defines overweight as a body mass index (BMI) of 25.0 to 29.9 kg/m2 and obesity as a BMI of ≥30 kg/m2, however, as a defining parameter, BMI has certain limitations as it cannot identify fat distribution [334]. Recent studies demonstrated that obesity-associated risk factors depend not only on excess body weight, but rather on the regional distribution of the excess body fat [335]. In light of this, it is now well recognized that abdominal fat is a significant risk factor for obesity-associated diseases.

Common specific causes of obesity include:

- poor diet of foods high in fats and calories
- sedentary (inactive) lifestyle
- high-calorie foods
- genetic factors, which can affect body processes food into energy and fat distribution
- polycystic ovary syndrome (PCOS): a condition that causes an imbalance of female reproductive hormones
- Prader-Willi syndrome: a rare condition that an individual is born with which causes excessive hunger
- Cushing syndrome: a condition caused by having an excessive amount of the hormone cortisol in system
- hypothyroidism (underactive thyroid): a condition in which the thyroid gland doesn't produce enough of certain important hormones
- osteoarthritis (and other conditions that cause pain that may lead to inactivity)

The ability of body to adapt to chronic changes in caloric intake largely depends on the ability of adipose tissue to accommodate a potential excess of calories. In obesity, the subcutaneous adipose tissue may fail to appropriately expand to store the energy surplus. This in turn may lead to ectopic fat deposition in other tissues involved in metabolic homeostasis (skeletal muscle, the liver, and visceral adipose tissue) and, consequently, insulin resistance [336].

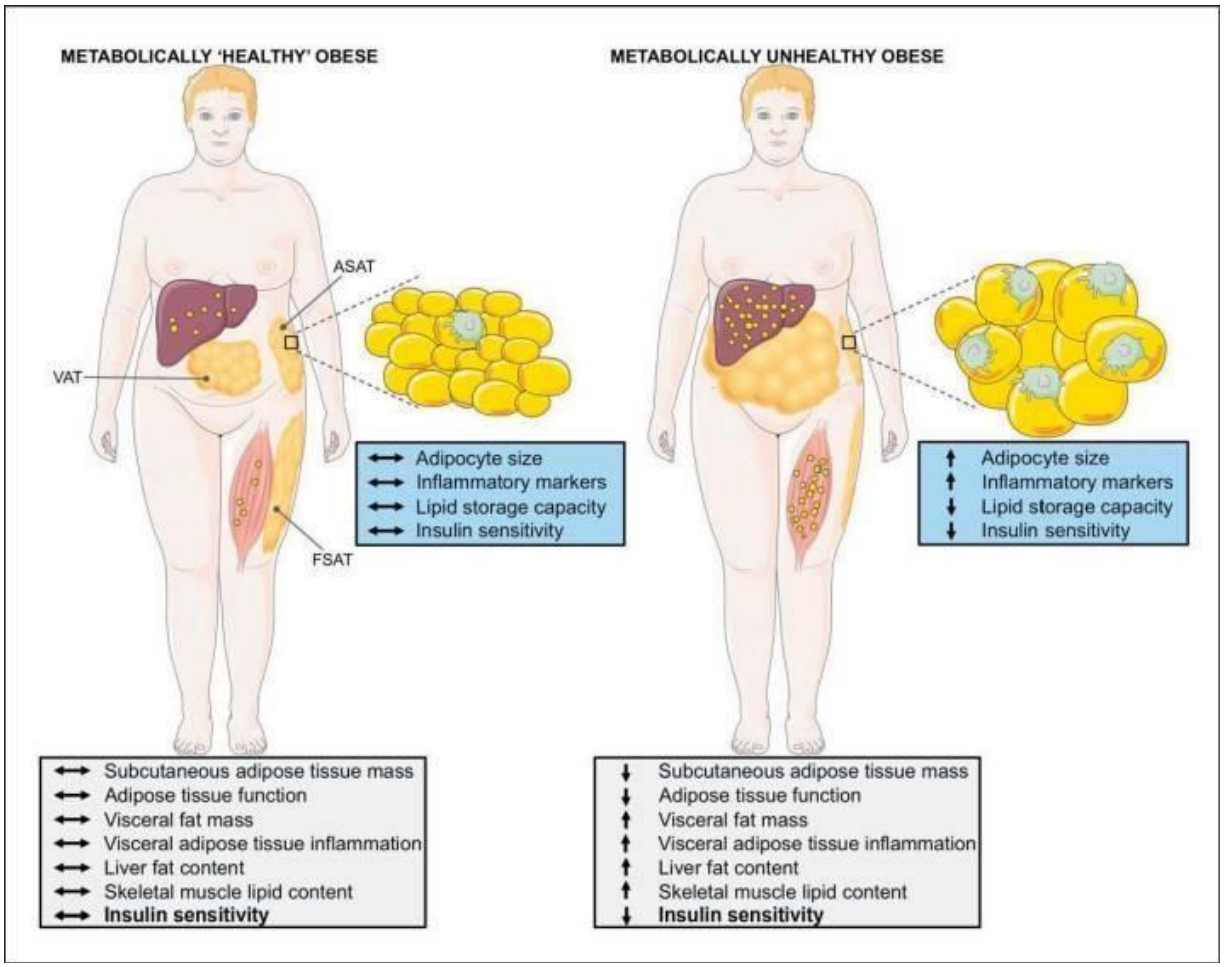

Figure 5.6 : Differences in adipose tissue function and body fat distribution between MHO and metabolically unhealthy obese individuals.

Image by Obes Facts. 2017 Jul; *The Metabolic Phenotype in Obesity: Fat Mass, Body Fat Distribution, and Adipose Tissue Function*

5.4.1 Obesity and oxidative stress

The role of oxidative stress in the pathogenesis of obesity and its associated risk factors are being studied [337]. Oxidative stress could trigger obesity by stimulating the deposition of WAT and altering food intake; it could cause an increase in preadipocyte proliferation, adipocyte differentiation and on the size of mature adipocytes [338]. Also ROS products have been found to be involved in the control of adipogenesis, by exerting different effects on hypothalamic neurons, which control satiety and hunger behavior [339]. Obesity can also induce oxidative stress through multiple biochemical mechanisms, such as superoxide generation from NADPH oxidases (NOX), oxidative phosphorylation, glyceraldehyde auto-

oxidation, protein kinase C (PKC) activation, and other pathways [340]. Other factors, such as hyperleptinemia, tissue dysfunction, chronic inflammation and postprandial ROS generation, could be associated to obesity development [341].

5.5 Regulation of H_2S in adipose tissue

Adipose tissue can synthesize and secrete the gasotransmitter H_2S, which acts as an autocrine factor and inhibits basal or insulin-stimulated glucose metabolism, affecting the pathogenesis of insulin resistance. H_2S is produced by epididymal, perirenal and brown adipose tissue. Both CBS and CSE were identified at the mRNA level in these adipose tissue depots, however, CSE inhibitors propargylglycine (PAG) or β-cyano-l-alanine (BCA) reduced H_2S production by adipose tissue by more than 80% suggesting that CSE is the main H_2S synthase [342].

Adipogenesis process, that is the formation of new adipocytes from their precursors, is a highly regulated process which contributes markedly to the amount and properties of adipose tissue. Tsai et al. [343] examined the role of H_2S in the regulation of adipogenesis using a fibroblast-like mouse preadipocyte cell line, 3T3L1. Stimulation of adipogenesis with the mixture of insulin, dexamethasone and the phosphodiesterase (PDE) inhibitor isobutylmethylxanthine (IBMX) was associated with the increase in CBS, CSE and 3-MST expression in these cells as well as increase in H_2S concentration in the culture medium. Numerous results suggested that H_2S production is up-regulated during adipogenesis and both endogenous and exogenous H_2S stimulates this process whereas inhibiting H_2S suppresses adipogenesis. Similarly, Cai et al. [344] have demonstrated that H_2S-saturated buffer, added during differentiation of 3T3L1 pre-adipocytes to the mature adipocytes, increased lipid accumulation, perilipin 1 expression and glycerol 3-phosphate dehydrogenase activity in these cells. The same was observed in cells overexpressing CSE. In contrast, other studies showed that organic sulfides, which may release H_2S in biological systems, suppressed adipogenesis in cultured 3T3L1 cells [345].

5.5.1 Role of H_2S in the regulation of lipolysis

The role of H_2S in the regulation of adipose tissue lipolysis is controversial. Geng et al. suggested that H_2S inhibits lipolysis [346]. These preliminary results suggest that H_2S stimulates adipose tissue lipolysis in cAMP-PKA dependent manner. Moreover, up-regulation of CSE-H_2S pathway in the adipose tissue may contribute to enhancedlipolysis in high fat diet fed obese animals.

5.5.2 Effect of H_2S on adipose tissue insulin sensitivity and glucose uptake

H_2S reduced basal and insulin-stimulated glucose uptake, while CSE inhibitors increased basal and insulin-stimulated glucose uptake by 40%, indicating that H_2S produced under baseline conditions inhibits glucose uptake. The effect of H_2S on glucose uptake is blocked by PI3Kinhibitor, LYY294002, but not by ATP-sensitive potassium channel inhibitor, suggesting that K-ATP channels, one of the main targets for H_2S in the vascular system, are not involved in the effect of H_2S on adipocytes [342].

Furthermore, a common model of insulin resistance and hyperlipidemia, increased CSE expression and H_2S production in the adipose tissue, showing a correlation with impaired insulin-induced glucose uptake. Together, these findings suggest that hyperactivity of the CSE-H_2S system is involved in adipose tissue insulin resistance in the metabolic syndrome.

TNF-α is overproduced in the adipose tissue of obese animals and humans and contributes to the insulin resistance by targeting several components of the insulin signaling pathway; its effect is accompanied by the increase in CSE expression and activity as well as H_2S accumulation. Thus, TNF-α induced H_2S overproduction may contribute to detrimental effect of this cytokine on adipose tissue insulin sensitivity [347].

Manna et al. [53] examined the effect of H_2S on insulin sensitivity in 3T3L1 adipocytes treated with high glucose concentration. Hyperglycemia reduced insulin-induced glucose uptake by these cells which was associated with reduced PI3K activity and higher activity of lipid

phosphates PTEN ultimately leading to lower phosphoinositide 3′,4′,5′-triphosphate. In addition, hyperglycemia decreased tyrosine phosphorylation of the insulin receptor substrate-1 as well as phosphorylation of protein kinase Akt and the expression of insulin-sensitive glucose transporter GLUT4. All these effects of hyperglycemia were blocked by H_2S. Moreover, the demonstration that hyperglycemia decreased CSE expression and H_2S production indicated that hyperglycemia-induced insulin resistance could be mediated by the downregulation of CSE-H_2S pathway [348].

Vitamin D intake and blood concentrations of vitamin D metabolites are inversely correlated with insulin sensitivity and vitamin D supplementation at low doses is suggested as the potential therapeutic approach in type 2 diabetes mellitus. Interestingly, an increase on CSE expression and H_2S production, was observed following administration of vitamin D3, suggesting that H_2S may be involved in beneficial effect of vitamin D on insulin sensitivity [348].

Besides, H_2S increased several components of the insulin signaling cascade that is phosphorylation of the insulin receptor β-subunit, PI3K activity and Akt phosphorylation [349]. Nevertheless, it is not yet clear how much of the effect on insulin sensitivity is mediated by the adipose tissue [346].

5.5.3 Role of H_2S in obesity

Treatment of high fat diet fed mice with H_2S solution or the H_2S donor GYY4137 increased body weight, epididymal, perirenal and subcutaneous adipose tissue depots. In contrast, treatment of these mice with CSE inhibitors had the opposite effect [346] . This effect of H_2S on adipose tissue could result from stimulation of adipogenesis, anabolic effect of insulin and triglyceride storage. Indeed, H_2S and GYY4137 increased whereas CSE inhibitor reduced total DNA content in the adipose tissue, indicating that H_2S stimulates both adipogenesis and adipocyte hypertrophy. The effect of H_2S/GYY4137 in high fat diet fed mice looks like that of PPAR-γ agonists, thiazolidinediones, which increase insulin sensitivity by stimulating

adipogenesis and increasing formation of small more insulin-sensitive adipocytes. Consistent data demonstrated that obesity is associated with a decreased expression of H_2S-synthesizing enzymes in fat tissues, with 3-MST downregulated in both brown and white fat and CBS and CSE affected in db/db mice, suggesting that loss of H_2S in fat tissue, may contribute to the altered metabolic responses associated with obesity [350].

5.6 The Nrf2 regulation on lipid metabolism

The role of Nrf2 in adipose biology and differentiation was investigated in several studies using a multitude of cell models. Adipocyte differentiation of 3T3L1 cells was enhanced by activation of Nrf2 through knockdown of its negative regulator Keap1. Deficiency of Nrf2 also resulted in a decrease in expression of key adipogenesis genes, including PPARγ, C/EBPα and downstream targets of mature adipocyte differentiation and this effect is exerted through direct regulation of PPARγ and Cebpβ by Nrf2 [351]. However, conflicting results have been reported showing that the loss of Nrf2 is associated with increased differentiation capacity. In these experiments, $Nrf2^{-/-}$ immortalized mouse embryonic fibroblast cells had markedly accelerated adipogenic differentiation compared with wild-type cell lines [352]. The inhibitory effect on differentiation caused by Nrf2 activation was less pronounced in cells differentiated at the early stages of adipogenesis. Similar to NQO1, there appears to be a temporal nature to the role of Nrf2 in adipogenesis and alteration of Nrf2 levels during the early stages of adipogenesis can have dramatic consequences for normal cell differentiation. Although it is not possible to rule out effects of Nrf2, these cell-based experiments underscore a role for Nrf2 and adipogenesis [353].

Nrf2 serves as a powerful tool for understanding this interaction between ROS and adipose tissue, because it sits at the crossroads of multiple interconnected pathways regulating the ability of the cell to react to a variety of endogenous and exogenous sources of stress. It is likely that the role of Nrf2 and oxidative stress in adipose tissue development and function is

complicated and depends on many factors. These factors can include the multitude of gene targets affected both directly and indirectly by Nrf2, the various sources of oxidative stress, the temporal aspects of Nrf2 expression in adipose differentiation, and even the age and genetic background of the mice used. It should also be noted that a large amount of work is being done looking into many of the other metabolic aspects of Nrf2. There are several informative reviews presenting other aspects of the ever-increasing role of Nrf2 in a variety of systems, including insulin signaling and lipid metabolism as well as mitochondrial biogenesis and the role of diet composition in Nrf2 pathway activity [354]. Future research will undoubtedly lead to a greater understanding of the critical role that Nrf2 and oxidative stress play in obesity and its related disorders.

5.7 Aim of the thesis PART II

On the basis of one mentioned above, H_2S plays an important role in the regulation of adipogenesis, adipocyte lipid uptake and lipid metabolism. Therefore, in this part of thesis:

- an inhibition of endogenous H_2S-synthesis, 3-MST-mediated, has been refuted for a possible contribution to an impairment of lipid homeostasis during various obesity/metabolic syndromes.
- the molecular mechanisms through which H_2S modulates the process of adipogenesis has been investigated in relation to a possible Nrf2 involvement.

6.0 CHAPTER SIX. The 3-mercaptopyruvate sulfurtransferase (3-MST)/ hydrogen sulfide (H_2S) system modulates adipogenesis in 3T3L1 cells

6.1 Introduction

Adipose tissue contributes to the maintenance of energy homeostasis and is considered to be an endocrine organ that contributes to the pathogenesis of obesity and obesity-related metabolic complications [355]. Excessive accumulation of adipose tissue in the body may cause the development of obesity and obesity-related diseases. Obesity, a major health issue in developed countries, is regarded as a chronic inflammatory state which contributes to numerous pathologies including dyslipidemia, coronary heart disease, non-alcoholic fatty liver, insulin resistance and type II diabetes [356]. Obesity is associated with accumulation of excess triacylglyceride (TG) in adipocytes either due to innate hyperadipogenesis or to lipid overloading in adipose tissue [357]. Lipid accumulation in adipose tissue is tightly controlled by a range of adipogenesis-related molecules including fatty acids binding protein 4 (FABP4/aP2), PPARγ, CCAAT/enhancer binding protein α (CEBPα), sterol regulatory element binding protein-1 (SREBP1), carbohydrate responsive element binding protein (ChREBP), fatty acid synthase (FAS), hormone-sensitive lipase (HSL) and perilipin A [358]. Among these, PPARγ and CEBPα are particularly important in the early stages of adipogenesis since they stimulate FABP4/aP2 thereby activating FABP4/aP2 to trigger downstream FAS, ChREPB and SREBP1 mRNA activation and thus promote adipocyte maturation [359]. Instead, HSL and perilipin A, enzymes which bind intracellular lipid droplets, serve to regulate TG breakdown and glycerol release from mature adipocytes [360].

In addition to these transcription factors, recent studies have shown that Nrf2 play important roles in adipogenic differentiation [361]. Nrf2 induces the expression of genes including those related to antioxidant enzymes, harming lipid accumulation in adipose tissue and inhibiting adipocyte differentiation [198, 352]. Deficiency of Nrf2 also resulted in a decrease in expression of key adipogenesis genes, including PPARγ, C/EBPα and downstream targets of

mature adipocyte differentiation, and this effect is exerted through direct regulation of PPARγ and Cebpβ by Nrf2 [351].

H_2S is generated from L-cysteine by CSE, CBS and from 3-mercaptopyruvate by 3-MST [362]. These enzymes occur in mammalian cells and tissues and produce H_2S which plays multiple roles in regulating cardiovascular function, inflammation, insulin resistance and glucose metabolism [348]. H_2S is also involved in fat tissues production and it can impair insulin signaling and glucose uptake into adipocytes [346].

Particularly, 3-MST, a Zn-dependent enzyme, shows both cytosolic and mitochondrial localizations. 3-MST appears to be present in all mammalian tissues, although its expression levels are tissue-dependent. Recent findings demonstrate that oxidative stress inhibited 3-MST activity and interferes with the positive bioenergetic role of the 3-MST/H_2S pathway, suggesting a potential role on pathophysiology of various conditions associated with increased oxidative stress, such as various forms of critical illness, cardiovascular diseases and diabetes [363].

Together, these studies suggest a role for 3-MST/H_2S pathway in adipogenesis. However, the precise biological effect of either endogenous or exogenous H_2S on adipocytes and the contribution which this gas makes on adipogenesis are not clear. With this in mind, in this thesis, 3T3L1 differentiated pre-adipocytes cells were treated with the slow-releasing H_2S donor GYY4137 and for comparison with the 3-MST inhibitor HMPSNE to assess the effect of H_2S on adipocyte biology *in vitro*.

6.2 Material and methods

6.2.1 Reagents

Dulbecco's modified Eagle's medium (DMEM+Glutamax) was purchased from Gibco (31966-021). GYY4137 and the HMPSNE were purchase from Sigma. GYY4137 was dissolved in DMEM, while HMPSNE was dissolved in DMSO (Sigma, D4540). A DMSO control was added to each experiment.

Oil Red O was purchased from Sigma (O-0625) and dissolved in Propan-2-ol (Fischer chemical, P/7490/15).

MTT (*3-(4,5-dimethylthiazol-2-yl)-2,5-diphenyltetrazoliumbromide* (Sigma, M5655) was dissolved in PBS.

LDH kit was purchased from Roche (04744926001).

The H_2S sensing probe AzMC (7-Azido-4-methylcoumarin) was purchased from Sigma (802409).

Transcription factors (TFs) Activation Profiling Arrays were purchased from Signosis (FA001, FA005).

6.2.2 Cell Culture and treatments

Murine 3T3L1 pre-adipocytes were cultured in high-glucose DMEM (Dulbecco's modified Eagle's medium) supplemented with 10% fetal bovine serum (FBS, Gibco, US), penicillin (100 µg/ml), and streptomycin (100 µg/ml) in a humidified atmosphere of 5% CO2 at 37°C. To induce differentiation in adipocytes, normal growth medium was substituted with *differerntiation medium* (DMEM supplemented with 1 µg/ml insulin, 1 µM dexamethasone and 10% FBS),. After 2 days, *differentiation medium* was replaced with *maintaing medium* (DMEM, supplemented with 10% FBS and 1 µg/ml insulin) and changed every 2 days up to one week. Cell treatments were performed during the differentiation process, by adding different concentrations GYY4137 (1, 3 and 6 mM) or HMPSNE (30, 100 and 200 µM) to both differentiation and maintaining media. For HMPSNE experiment, DMSO treatment was

included and used as control. Non treated pre-adipocytes and adipocytes samples were included in each experiment allowing direct comparison with the treatment effects.

6.2.3 Cell viability and toxicity assays

The 3T3L1 pre-adipocytes were seeded at a density of 5×10^3 cells per well in 96-well plates and subjected to cell differentiation and treatments. For cell viability measurements, adipocyte were incubated with 0.5 µg/ml MTT for 3 h at 37°C in the dark. After removing the supernatants,, DMSO was added to each well, and the plates were shaken to dissolve the formazan crystals . Absorbance was measured at 590 nm using a multiwell plate reader (TECAN Plate reader Infinite 200 PRO). The percentage of viable cells was calculated by defining the cell viability in control samples as 100%, as previously described [364].

pre-adipocytes, Cell cytotoxicity was assessed by measuring the amount of lactate dehydrogenase (LDH) release in the supernatants. Absorbance was then measured at 360-490 nm using a multiwell plate reader (TECAN Plate reader Infinite 200 PRO). The percentage of viable cells was calculated by defining the cell viability without treatment as 100%, as previously described [364].

6.2.4 Oil Red O Staining

Pre-adipocytes were seeded at a density of 3×10^4 cells per well in 12-well plates. After differentiation and cells treatments, adipocytes were fixed with 10% formalin in PBS for 1 h and washed with 60% isopropyl alcohol. After drying at room temperature, cells were stained with Oil Red O solution for 30 min. Stained cells were washed four times with distilled water. The phenotypic changes of adipogenic differentiation were observed using an inverted phase-contrast microscope (Olympus LX81, Japan). To quantify the amount of Oil Red O stained lipids, cells were eluted with 100% isopropyl alcohol for 10 min and the absorbance of the extracts was measured at 500 nm using a multiwell plate reader (TECAN Plate reader Infinite 200 PRO).

6.2.5 Detection of H_2S with AzMC probe

3T3L1 pre-adipocytes were seeded at a density of 5×10^3 cells per well in 96-well plates. After differentiation and treatments, cells were incubated with the H_2S sensing probe AzMC (10 nM, Sigma-Aldrich, St. Louis, MO) at 37 °C for 1 h [365], to measure both endogenous and released H_2S. AzMc fluorescence was detected and quantified measuring the fluorescent intensity with a plate reader (TECAN Plate reader Infinite 200 PRO).

6.2.6 Western Blot analysis

Pre-adipocytes were seeded at a density of 6×10^4 cells per well in 6-well plates. Following differentiation and treatments,, cells were washed twice with PBS and lysed with lysis buffer (ELISA lysis buffer, Thermo) containing proteinase and phosphatase inhibitors. Proteins were separated by SDS-PAGE, transferred to a PVDF membrane (Millipore, USA) and incubated with specific primary antibodies. The antibodies used in this study were directed against: ACTIN (Cell Signaling 8H10D10, 1:2000), CBS (Cell Signaling D8F2P, 1:500), CSE(Abcam Ab151769, 1:1000), 3-MST (Abcam Ab85377, 1:500), ETHE-1 (Abcam Ab174302, 1:1000), RHODANESE (Abcam Ab231248, 1:1000) and SBP-1 (Abcam Ab90135, 1:500). Detection of each protein was performed using ECL (Immobilon™ Western Chemiluminescent HRP Substrate, Millipore) according to the manufacturer's instructions.

6.2.7 Generation of stable 3-MST knockdown

Expression vectors encoding short hairpin RNA (shRNA) sequences targeting mouse 3-MST in a pLKO.1-puro plasmid were purchased from Sigma-Aldrich (sh3-MST: order number m-3-MST-25). Control cells (shCTR) were transfected with a non-targeting control shRNA in a pKLO.1 puromycin resistance vector (Sigma-Aldrich). Viral particles were produced in HEK293T cells by co-transfection of the respective transfer vector (3 μg) with the packaging plasmids pLP1 (4.2 μg), pLP2 (2 μg) and pVSV-G (2.8 μg, all from Invitrogen) using FuGene

(Promega) following the manufacturer instruction. 3T3L1 cells were infected with lentiviral-pseudotyped particles following puromycin selection.

6.2.8 Transcription factors (TFs) Activation Profiling Array

TF Activation Profiling Arrays (Signosis) were used to monitor the activities of multiple TFs simultaneously on adipocytes nuclear extracts. Nuclear extracts from adipocytes were mixed with a

6.2.9 Statistical analysis

All values in the figures and text are expressed as mean ± standard error of the mean (SEM) Statistical analysis was performed with GraphPad Prism 7 (GraphPad Software; USA). Differences were analyzed by t-test or by one-way analysis of variance (ANOVA) followed by Bonferroni post-hoc test for multiple comparisons. Values obtained were analyzed with TWO-way ANOVA Multiples comparison and Bonferroni post-hoc. A p-value of less than 0.05 was considered significant ($p<0.05$). Each P value was adjusted to account for multiple comparisons.

6.3 Results

6.3.1 Adipogenesis process in 3T3L1 cells

Standard protocols for 3T3L1 differentiation into adipocyte-like cells require a mixture of insulin, dexamethasone and IBMX . To avoid the use of the PDE inhibitor IBMX that would have masked the effect of H_2S on PDE itself, an optimized protocol was designed (Figure 1A). Cells were treated with differentiation medium twice per week (Day 1 and 5). Oil red O staining was quantified by reading the absorbance at 500 nm with a plate reader, confirming the time-dependent accumulation of lipids along with the differentiation (Figure 1B). The efficiency of the differentiation was assessed by Oil Red O, an oil-soluble dye that stains lipids in red (Figure 1C and 1D). Moreover, the expression of the adipocyte marker SBP-1 (Selenium binding

protein-1) was assessed by Western blot in both pre-adipocytes and adipocytes (Figure 1E), confirming complete adipocyte differentiation.

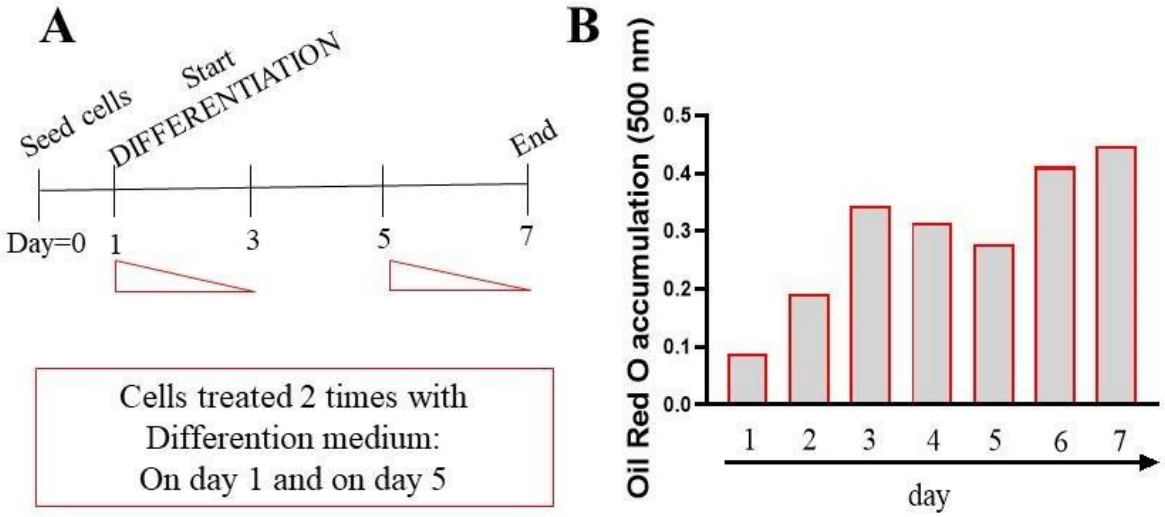
A
Seed cells
Start
DIFFERENTIATION
End
Day=0
1
3
5
7
Cells treated 2 times with
Differention medium:
On day 1 and on day 5
B
Oil Red O accumulation (500 nm)
0.5
0.4
0.3
0.2
0.1
0.0
1
2
3
4
5
6
7
day

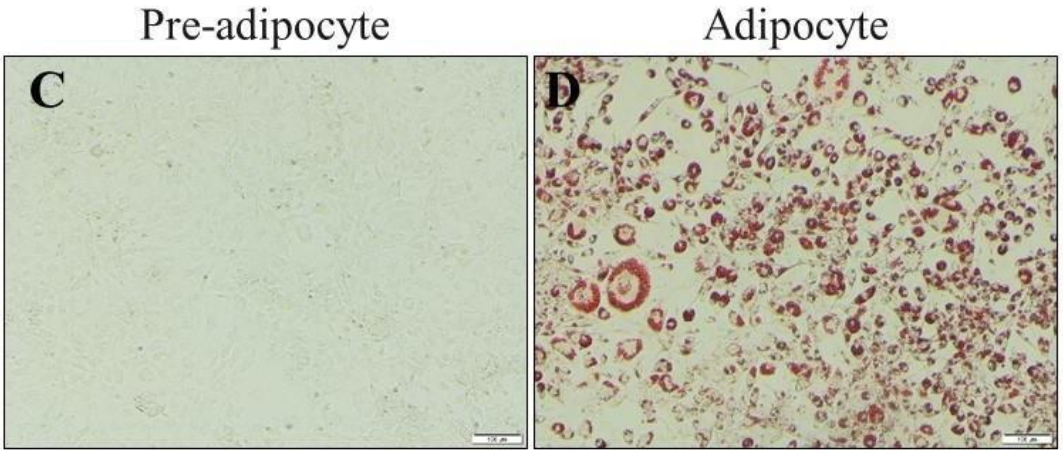
Pre-adipocyte
Adipocyte
C
D

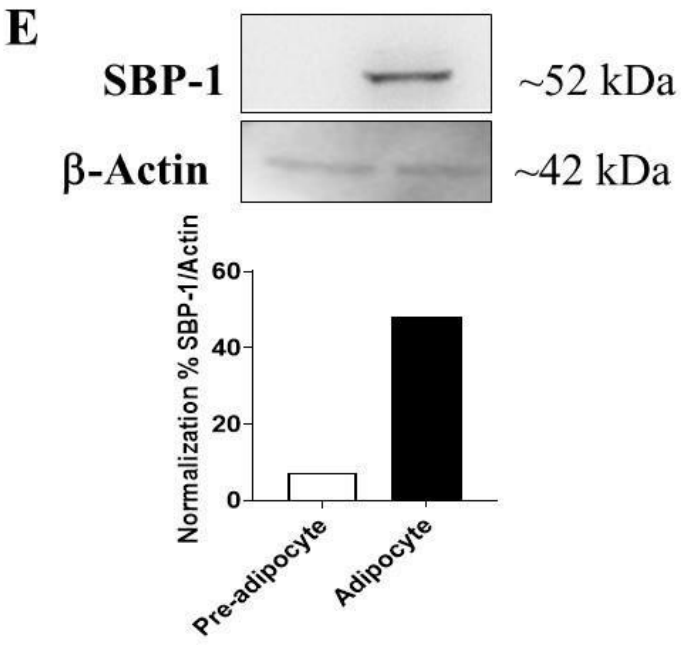
E
SBP-1
~52 kDa
β-Actin
~42 kDa
Normalization % SBP-1/Actin
60
40
20
0
Pre-adipocyte
Adipocyte

Figure 6.1: Adipogenesis process in 3T3L1 cells

Schematic overview of the differentiation process in 3T3L1 cells (A).The efficiency of adipocyte differentiation was assessed by Oil Red O staining (B) and expression of the adipocyte marker SBP-1 by Western blot (E). Representative picture showing non-differentiated 3T3L1 cells and adipocytes stained with Oil Red O (× 10) (C and D)

6.3.2 Effects of H_2S donor and 3-MST inhibitor on adipocyte differentiation

To investigate H_2S and 3-MST activity on adipogenesis, 3T3L1 cells were differentiated in presence or absence of the H_2S donor GYY4137 or the 3-MST inhibitor HMPSNE. Oil Red O staining showed a pronounced accumulation of lipid in HMPSNE-treated cells (30 and 100 µM) compared to control adipocytes (Figure 2D).

Conversely, GYY4137 treatment significantly inhibited adipocytes differentiation,as shown by Oil Red O staining and its relative quantification (Figure 2C).

In accordance to these results, SBP-1 expression was suppressed in GYY4137 treated samples, whereas HMPSNE treatment promoted its upregulation, as assessed by Western blot (Figure 2B).

Collectively, these data suggest that inhibition of 3-MST-mediated H_2S production during differentiation stimulated 3T3L1 pre-adipocytes differentiation into mature adipocytes, while H_2S donor abolished the differentiation process.

A

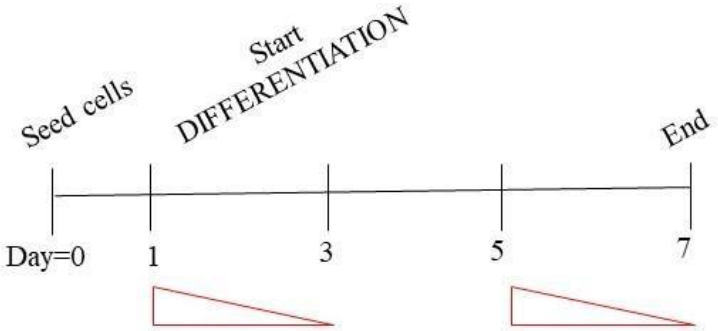

Cells treated two times with GYY4137 or HMPSNE:
On day 1 and on day 5

B

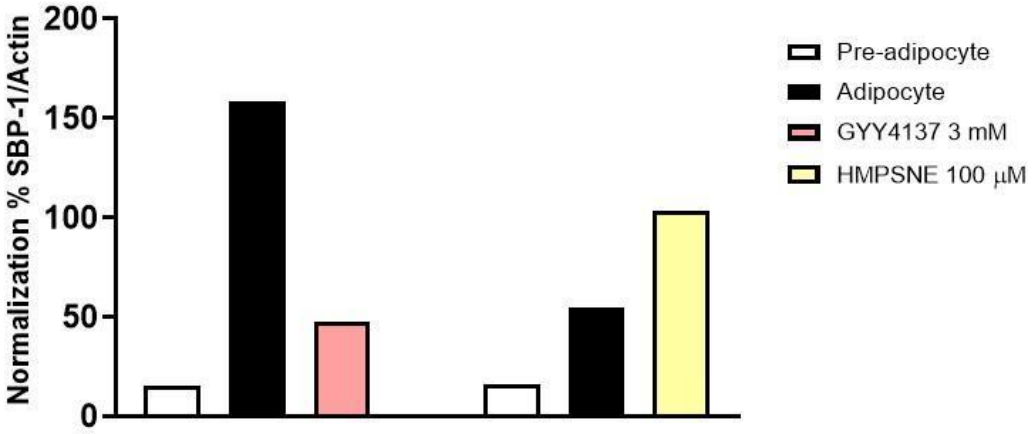

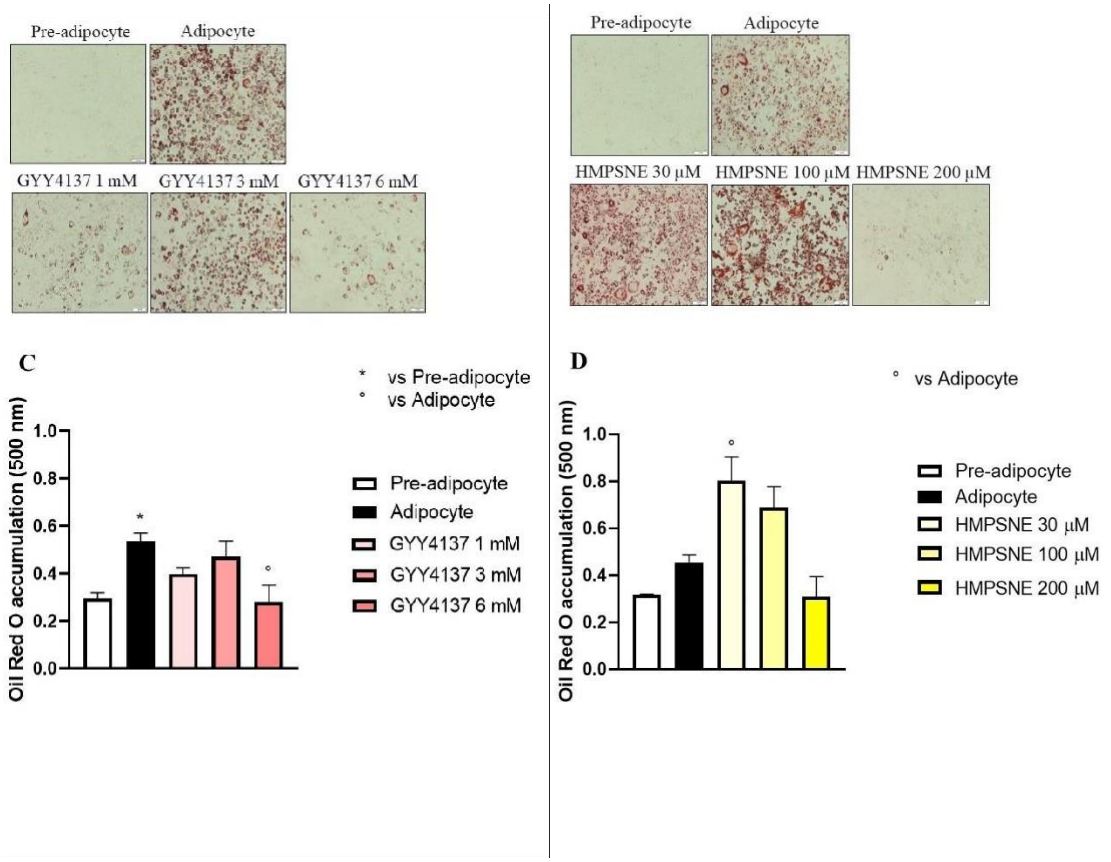

Figure 6.2: Effects of GYY4137 and HMPSNE on adipogenesis.

3T3L1 pre-adipocytes were cultured with differentiation medium in the absence or presence of GYY4137 (1, 3 and 6 mM) and HMPSNE (30, 100 and 200 µM) up to 7 days. Representative picture showing cell monolayers stained with Oil Red O (× 10). At day 7, intracellular lipid accumulation was quantified by Oil Red O staining (C and D). SBP-1 protein expression on adipocytes treated with GYY4137 3 mM or HMPSNE 100 µM was performed (B). Data are presented as mean ± SEM (n=3); *p<0.05 vs. Pre-adipocyte and °p<0.05 vs Adipocyte.

6.3.3 Effects of H_2S on adipocyte viability and toxicity

The reduction of tetrazolium dye MTT to its insoluble formazan was measured to assess cell viability. Tetrazolium dye reduction is generally assumed to be dependent on NAD(P)H-dependent oxidoreductase enzymes largely in the cytosolic compartment of the cell; also, spontaneous MTT reduction is involved in lipidic cellular compartments/structures, without enzymatic catalysis [366] .

Cells treated with 6 mM GYY4137 and 200 µM HMPSNE, showed a significant mortality (Figure 3A and 3B).

Furthermore, in adipocyte, pyruvate plays a versatile role in energy production, biosynthesis and redox balance. Pyruvate is mainly formed from glucose through glycolysis. While pyruvate can be converted into alanine by alanine aminotransferase, its metabolic fate is largely determined by the efflux from the cell via reduction to lactate by lactate dehydrogenase (LDH) [367]. LDH production was mainly detected on adipocytes treated with GYY4137 3 mM (Figure 3C) and HMPSNE 100 µM (Figure 3D).

MTT

A

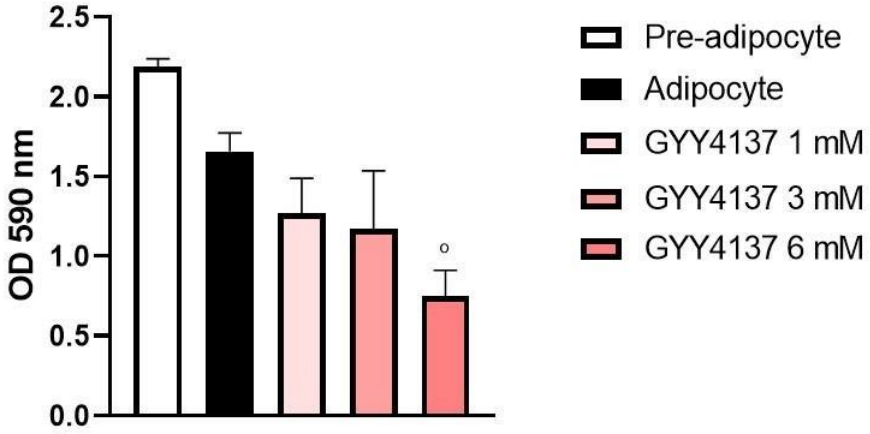
° vs Adipocyte
Pre-adipocyte
Adipocyte
GYY4137 1 mM
GYY4137 3 mM
GYY4137 6 mM
OD 590 nm
2.5
2.0
1.5
1.0
0.5
0.0
°

B

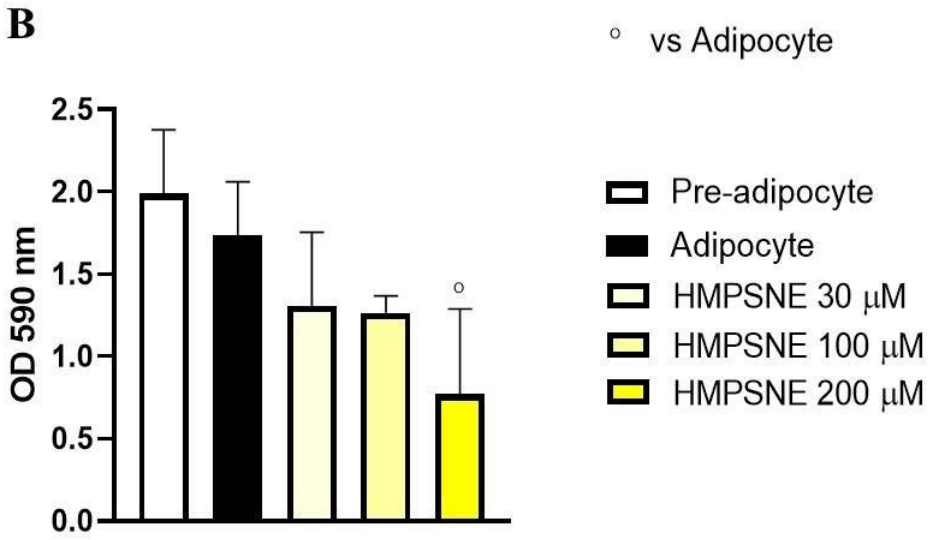
° vs Adipocyte
Pre-adipocyte
Adipocyte
HMPSNE 30 μM
HMPSNE 100 μM
HMPSNE 200 μM
OD 590 nm
2.5
2.0
1.5
1.0
0.5
0.0
°

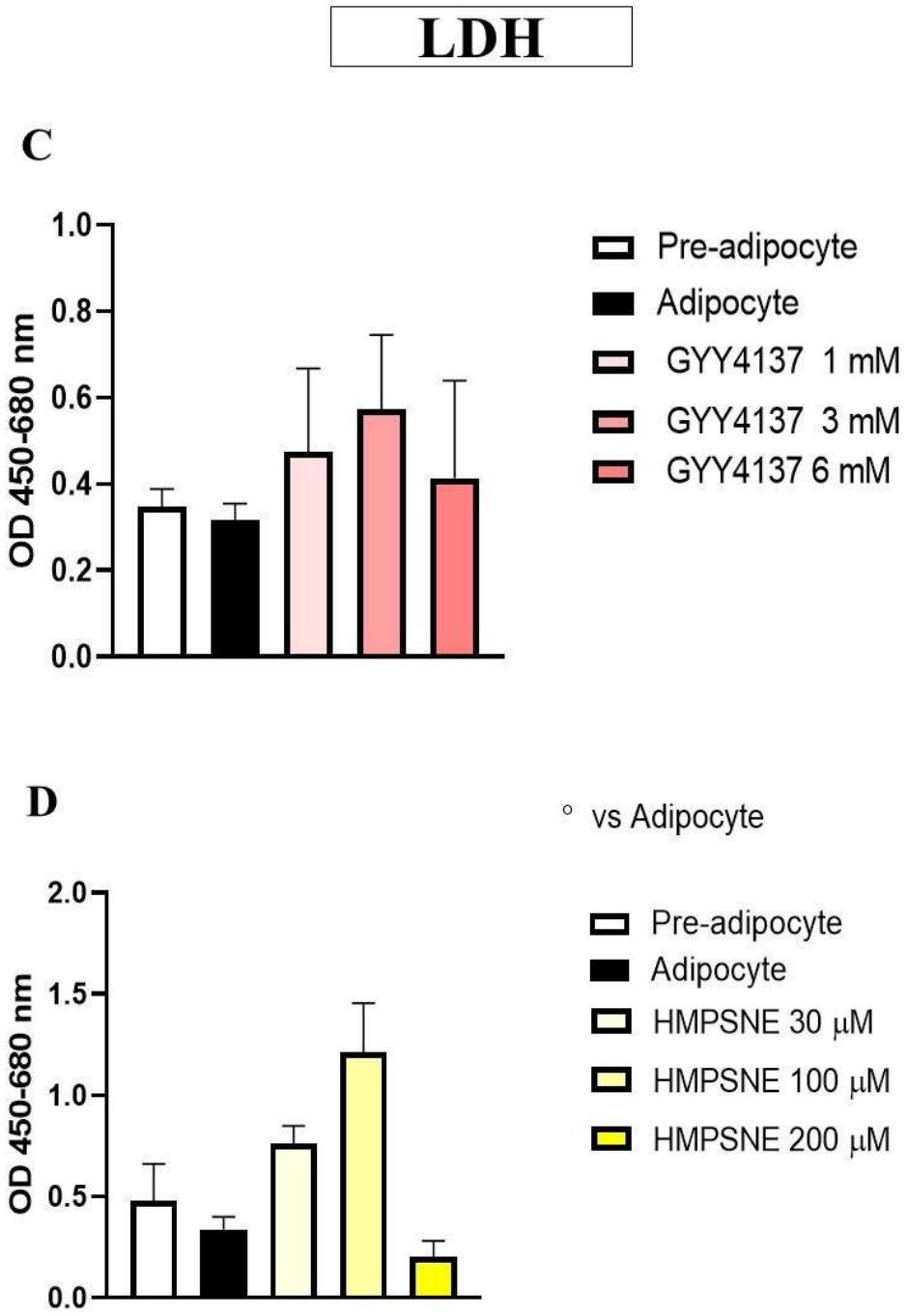

Figure 6.3: Effect of GYY4137 and HMPSNE on cell viability and cytotoxicity

MTT assay on GYY4137 (A) and HMPSNE (B) treated- cells. Citotoxicity assay (LDH) on GYY4137 (C) and HMPSNE (D) treated 3T3L1 adipocytes. Data are presented as mean ± SEM (n=3); °$p<0.05$ vs Adipocyte.

6.3.4 Effects of GYY4137 and HMPSNE treatment on H_2S release

The detection of intracellular H_2S in adipocytes treated with GYY4137 or HMPSNE, was performed using AzMC, a fluorogenic probe in which the aromatic azide moiety is selectively reduced in the presence of H_2S, producing the fluorescent 7-amino-4-methylcoumarin (AMC) with a concomitant increase in fluorescence with extitation-emission at 365-450 nm, respectively [368]. Enzymatic production of H_2S was reduced in adipocytes treated with GYY4137 (Figure 4A), while treatment with HMPSNE at 30 and 100 µM, showed an accumulation of H_2S (Figure 4B). AzMC signal was significantly reduced also at 200 µM HMPSNE, correlating to the low viability and Oil red O staining previously observed.

AzMC

A

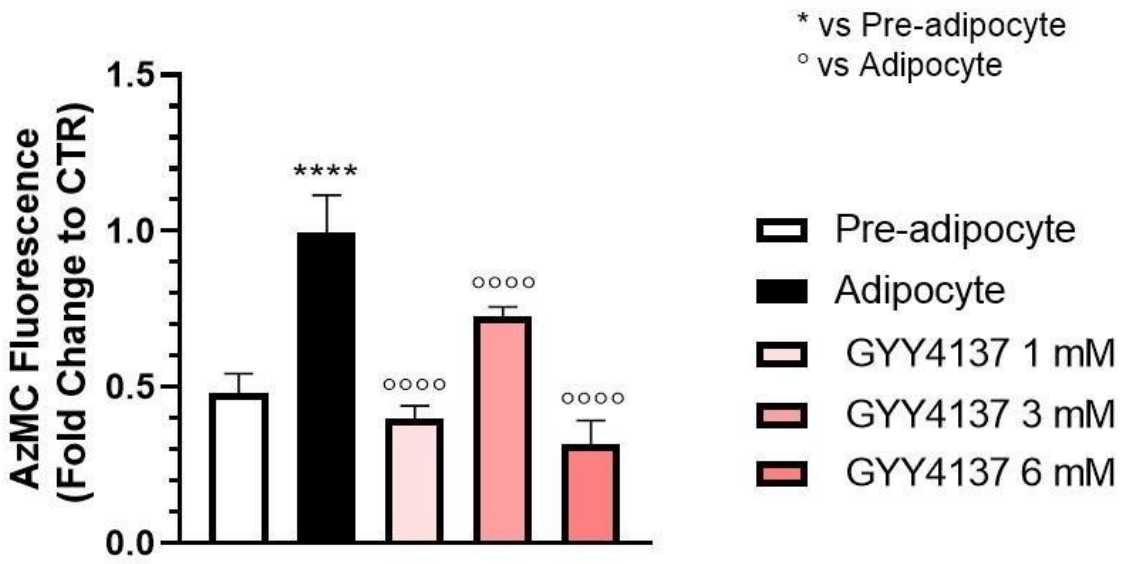
* vs Pre-adipocyte
° vs Adipocyte
AzMC Fluorescence (Fold Change to CTR)
1.5
1.0
0.5
0.0
****
°°°°
°°°°
°°°°
Pre-adipocyte
Adipocyte
GYY4137 1 mM
GYY4137 3 mM
GYY4137 6 mM

B

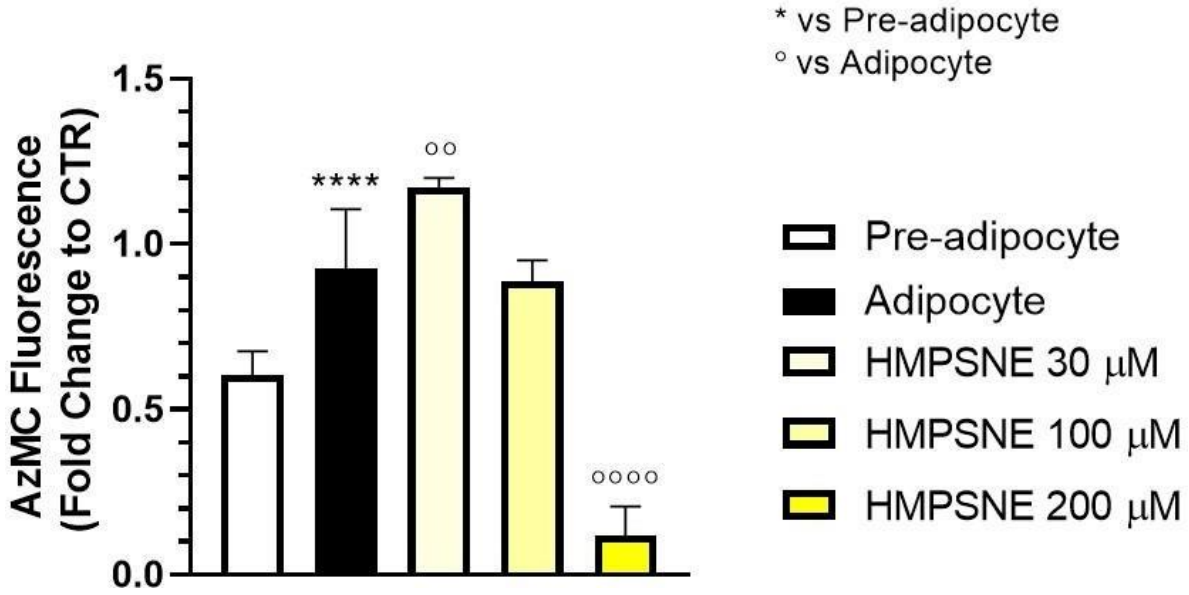
* vs Pre-adipocyte
° vs Adipocyte
AzMC Fluorescence (Fold Change to CTR)
1.5
1.0
0.5
0.0
****
°°
°°°°
Pre-adipocyte
Adipocyte
HMPSNE 30 μM
HMPSNE 100 μM
HMPSNE 200 μM

Figure 6.4: Detection of H_2S released by adipocytes using AzMC probe

AzMC fluorescence emitted by adipocytes treated with GYY4137 (A) or HMPSNE (B). Data are presented as mean ± SEM (n=3); *p<0.05, **p<0.01, ***p<0.001, ****p<0.0001 vs Pre-adipocytes; °°p<0.01 and °°°°p<0.0001 vs Adipocyte.

6.3.5 Effects of GYY4137 treatment on H_2S synthesis and degradation

In mammals, H_2S is synthetized by CBS, CSE and 3-MST, whereas it is catabolized by ETHE1 and TST/Rhodanese. To investigate whether GYY4137 treatment was associated with alterations in H_2S producing or catabolizing enzymes, the expression of CBS, 3-MST, CSE, ETHE1 and TST was assessed by Western blot. The H_2S producing enzymes 3-MST, CBS and CSE were all downregulated in GYY4137-treated samples, particularly at the highest concentrations (Figures 5A, 5B and 5C). Similarly, TST expression was reduced in GYY4137-treated adipocytes compared to non-treated cells (Figure 5D), while ETHE-1 levels were downregulated only at the highest concentration (6 mM) (Figure 5E). These results showed that high concentrations of GYY4137 impaired H_2S producing and degrading pathways in adipocytes.

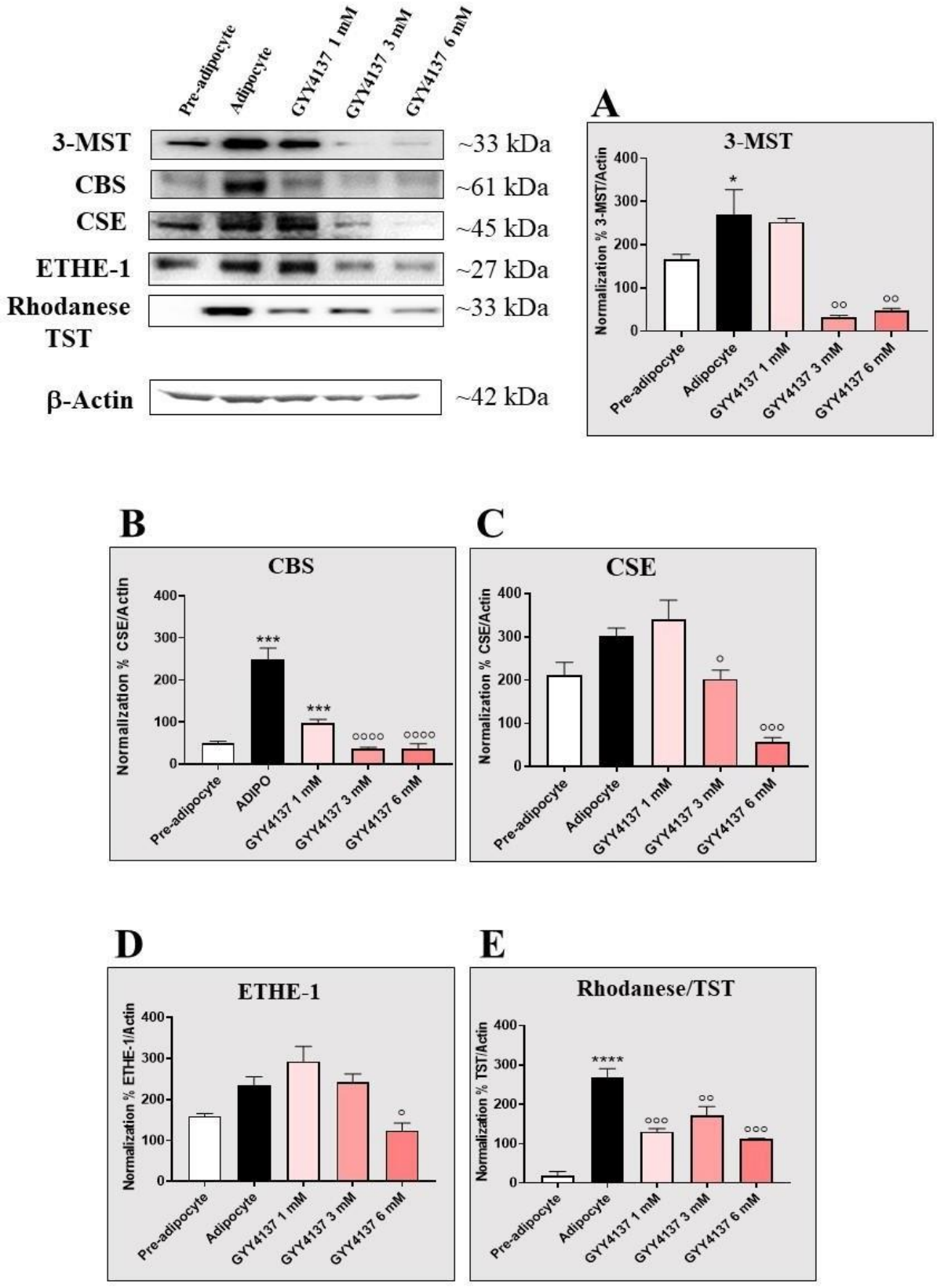

* vs Pre-adipocyte

° vs Adipocyte

Figure 6.5: GYY4137 treatment on H_2S synthesis and catabolism

Effect of GYY4137 treatment (1, 3 and 6 mM) on 3-MST (A), CBS (B), CSE (C), ETHE-1 (D) and Rhodanese/TST (E) protein expression. A representative blot of lysates obtained from each group is shown and densitometry analysis is reported (n = 3). One-Way ANOVA followed by Bonferroni post- test. *p<0.05, and ***p<0.001 vs Pre-adipocytes; °p<0.05, °°p<0.01, °°°p<0.001 and °°°°p<0.001 vs Adipocyte.

6.3.6 Effects of HMPSNE treatment on H_2S synthesis and degradation

Treatment with the 3-MST inhibitor HMPSNE, reduced 3-MST protein expression at the concentrations of 30 and 300 µM (Figure 6A), while CBS/CSE protein expression was reduced only at the highest concentrations of 200 and 300 µM (Figures 6B and 6C). 100, 200 and 300 µM HMPSNE significantly increased ETHE-1 protein expression (Figure 6D), while Rhodanese expression was pronouncedly decreased only at the highest concetrations of 200 and 300 µM (Figure 6E).

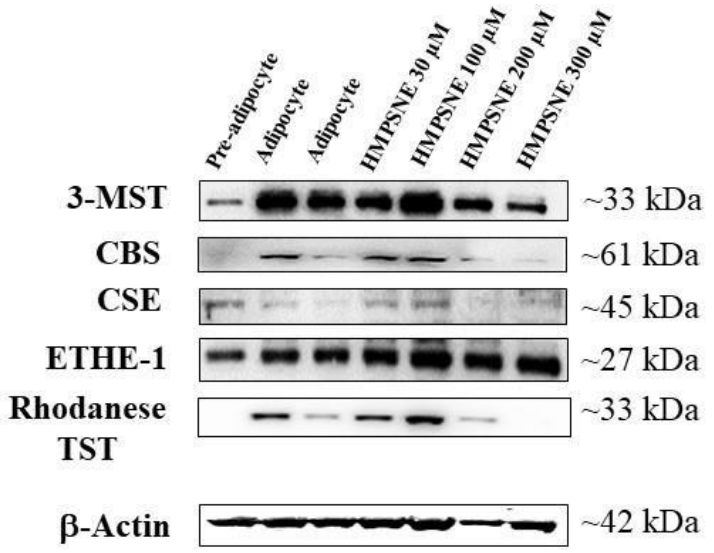

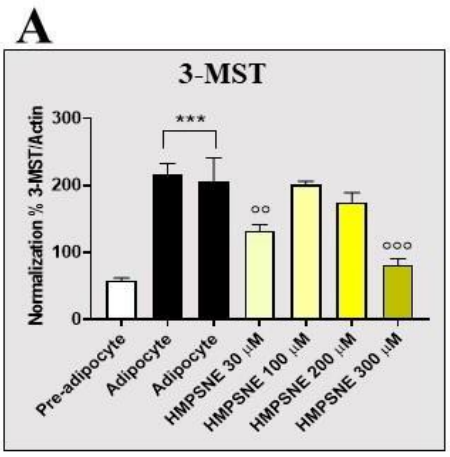

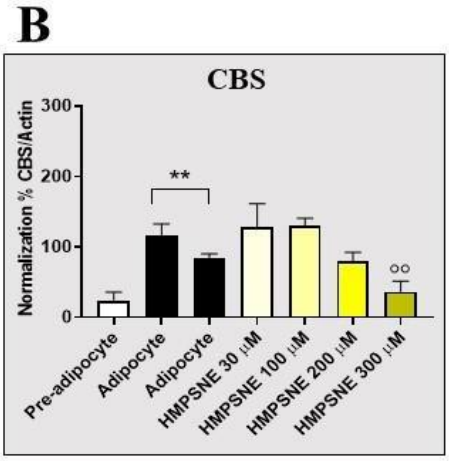

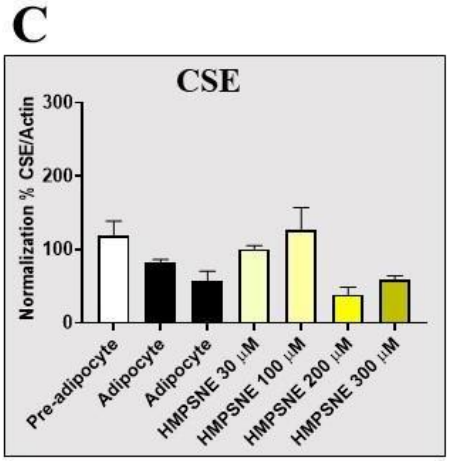

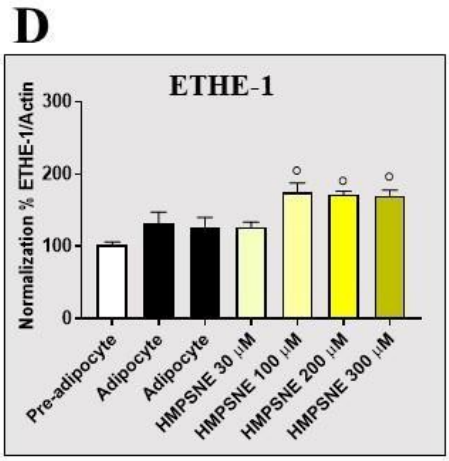

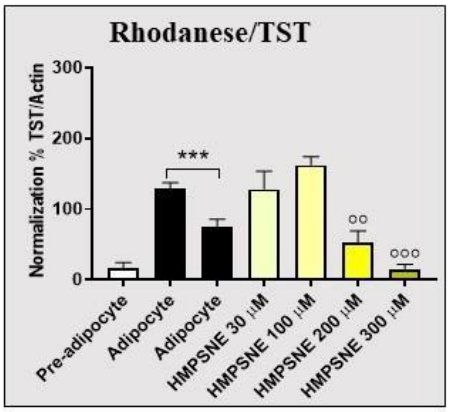

* vs Pre-adipocyte
° vs Adipocyte

Figure 6.6: HMPSNE treatment on H_2S synthesis and catabolism

Effect of HMPSNE treatment (30, 100, 200 and 300 µM) on 3-MST (A), CBS (B), CSE (C), ETHE-1 (D) and Rhodanese (E) protein expression. A representative blot of lysates obtained from each group is shown and densitometry analysis is reported (n = 3). One-Way ANOVA followed by Bonferroni post- test. **p<0.01 and ***p<0.001 vs Pre-adipocytes; °p<0.05, °°p<0.01 and °°°p<0.001 vs Adipocyte.

6.3.7 Effects of GYY4137 or HMPSNE treatments on 3-MST knockdown adipocytes

To investigate the specific contribution of 3-MST on adipogenesis, 3T3L1 cells were stably transfected with shRNA against 3-MST, generating a 3-MST knock-down cell line (sh3-MST). Sh3-MST and control cells (shCTR) were differentiated into adipocyte, and the efficiency of 3-MST knock-down was confirmed by Western blot (Figure 7A). To assess the effect of 3-MST knock-down on adipocyte differentiation, the expression of SBP-1 was assessed in shCTR, sh3-MST cells before and after differentiation by Western blot (Figure 7B). SBP-1 expression was reduced in differentiated sh3-MST, compared to differentiated shCTR, suggesting a correlation between 3-MST expression and adipocyte differentiation.

The effect of GYY4137 and HMPSNE treatments on shCTR and sh3-MST cells was investigated by measuring lipid accumulation by Oil Red O staining (Figures 7C and 7E). GYY4173 reduced the expression of SBP-1 (Figure 7D) and the accumulation of lipids (Figure 7C) in shCTR, confirming the previous results obtained in 3T3L1 cells. Sh3-MST cells displayed overall a decrease in SBP-1 expression (and Oil Red O staining), similar to the pre-adipocyte condition (Figures 7C and 7D).

GYY4137 treatment was associated with a decrease in lipid droplets in both control and 3-MST knock-down cells. Sh3-MST cells displayed an overall increase in Oil Red O staining, in contrast with HMPSNE treatment in 3T3L1 cells. HMPSNE treatment in shCTR cells led to a decrease in Oil Red O but an increase in SBP-1 expression (Figures 7E and 7F).

If treatment with HMPSNE on shCTR cells recapitulated the same effect as in WT cells, showing an upregulation of SBP-1, on sh3-MST it further inhibited adipogenesis, as shown by downregulation of SPB-1 protein expression (Figure 7F).

A

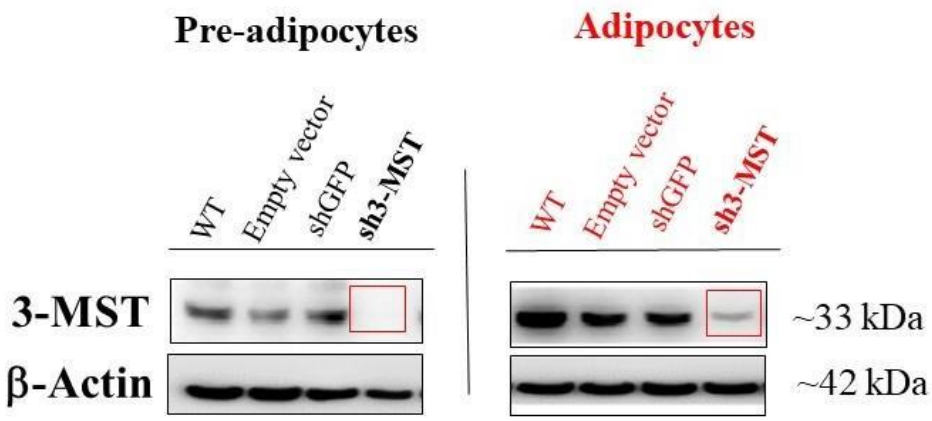
Pre-adipocytes
Adipocytes
WT
Empty vector
shGFP
sh3-MST
WT
Empty vector
shGFP
sh3-MST
3-MST
β-Actin
~33 kDa
~42 kDa

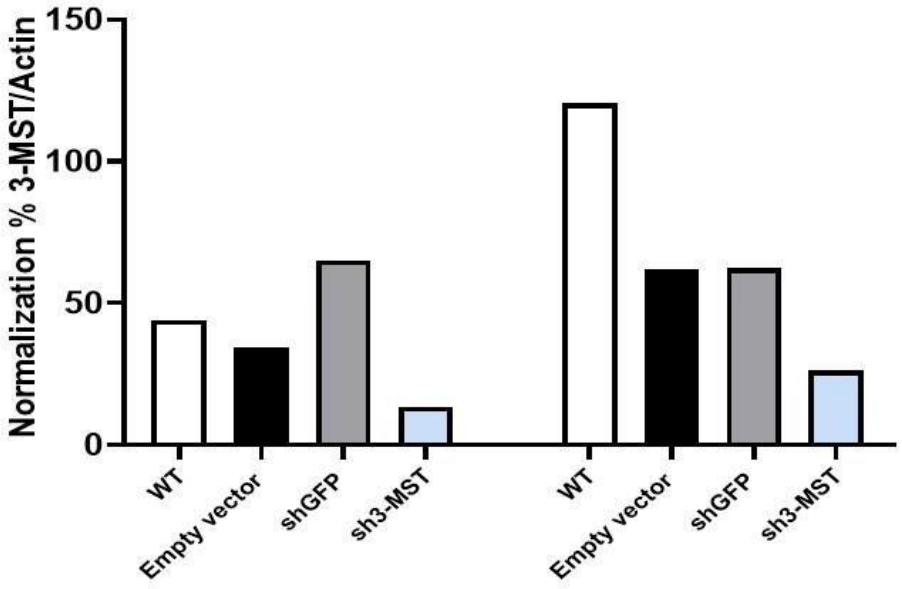
Normalization % 3-MST/Actin
150
100
50
0
WT
Empty vector
shGFP
sh3-MST
WT
Empty vector
shGFP
sh3-MST

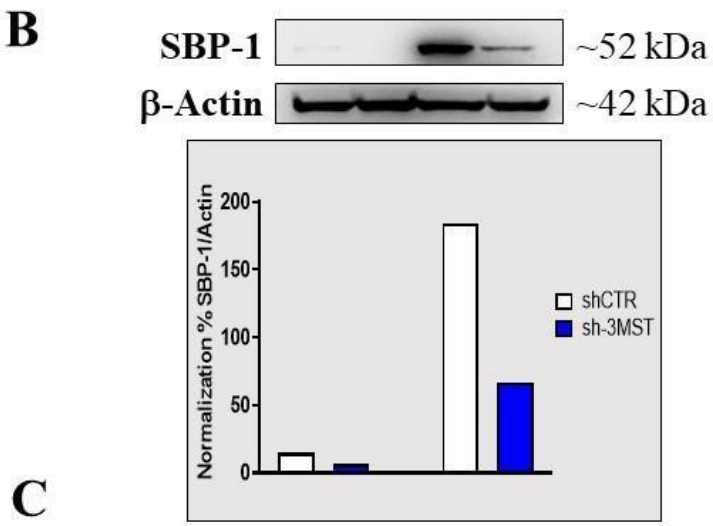
B
SBP-1
~52 kDa
β-Actin
~42 kDa
Normalization % SBP-1/Actin
200
150
100
50
0
shCTR
sh-3MST

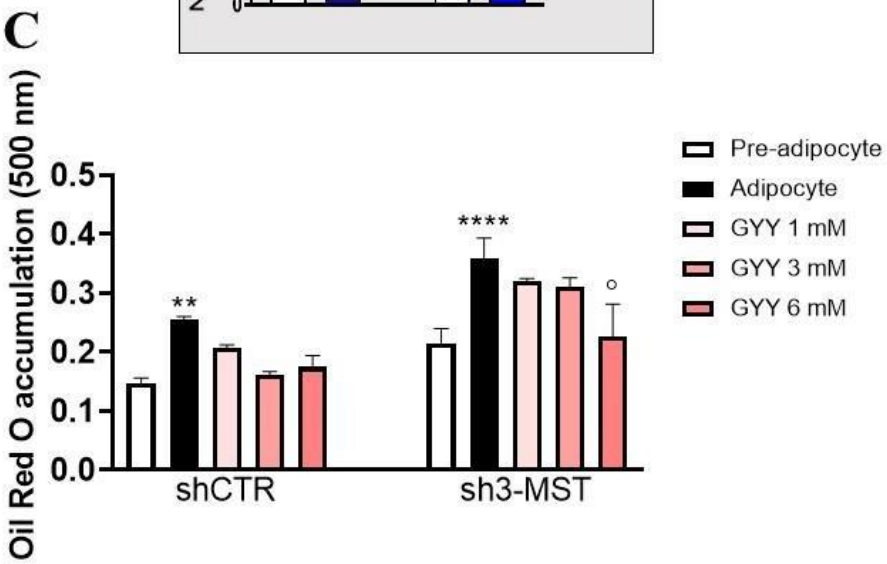
C
Oil Red O accumulation (500 nm)
0.5
0.4
0.3
0.2
0.1
0.0
**
****
°
shCTR
sh3-MST
Pre-adipocyte
Adipocyte
GYY 1 mM
GYY 3 mM
GYY 6 mM

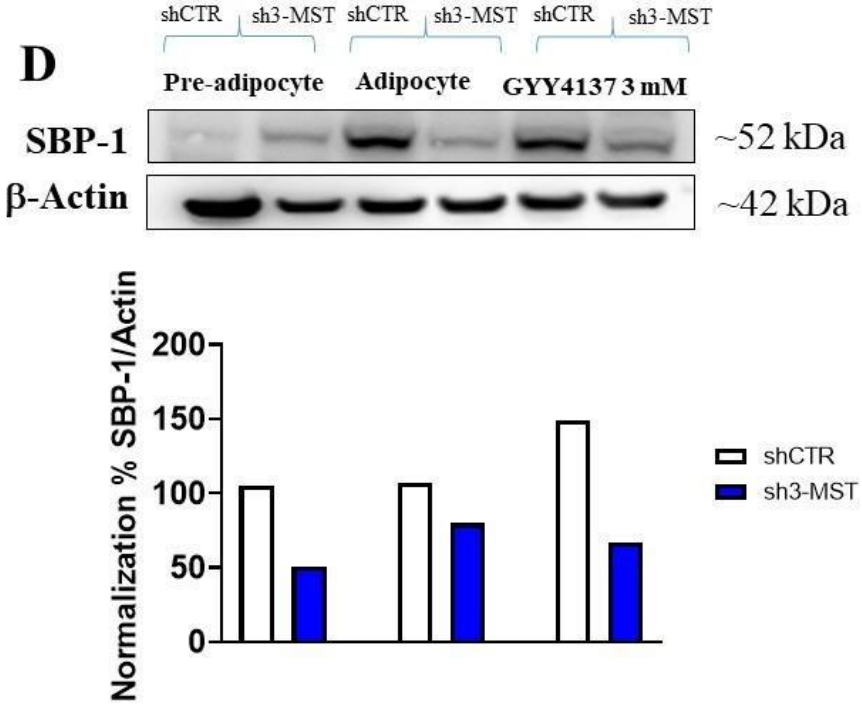
D
shCTR
sh3-MST
shCTR
sh3-MST
shCTR
sh3-MST
Pre-adipocyte
Adipocyte
GYY4137 3 mM
SBP-1
~52 kDa
β-Actin
~42 kDa
Normalization % SBP-1/Actin
200
150
100
50
0
shCTR
sh3-MST

E

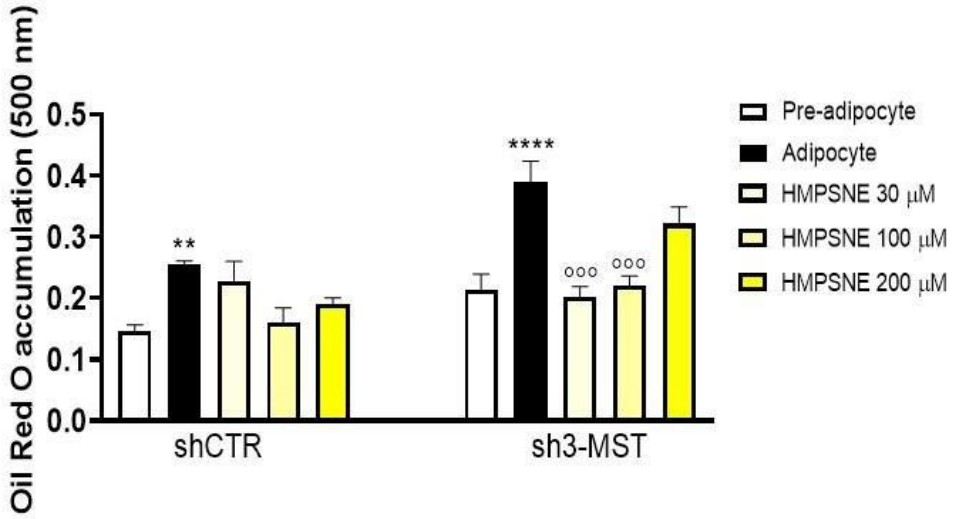
Oil Red O accumulation (500 nm)
0.5
0.4
0.3
0.2
0.1
0.0
**
****
°°°
°°°
shCTR
sh3-MST
Pre-adipocyte
Adipocyte
HMPSNE 30 μM
HMPSNE 100 μM
HMPSNE 200 μM

F

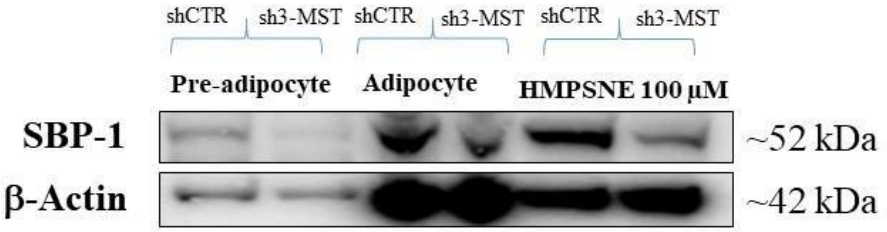
shCTR
sh3-MST
shCTR
sh3-MST
shCTR
sh3-MST
Pre-adipocyte
Adipocyte
HMPSNE 100 μM
SBP-1
β-Actin
~52 kDa
~42 kDa

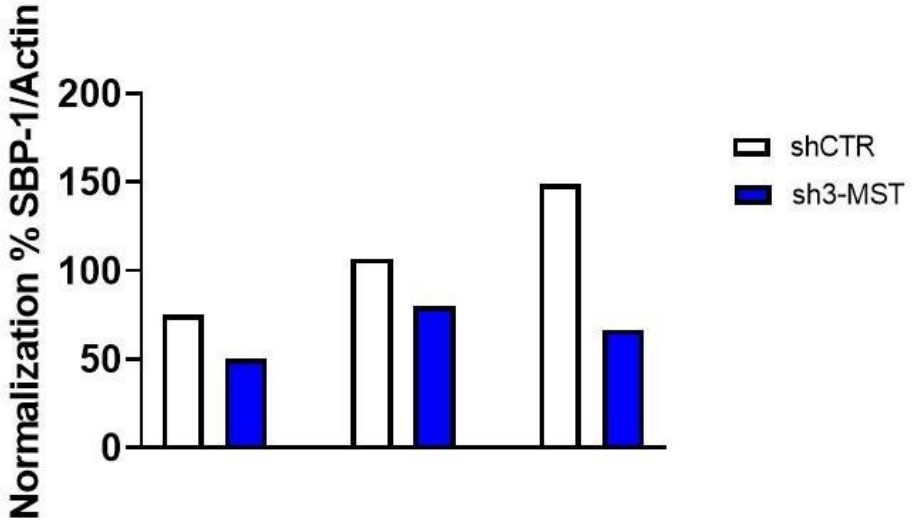
Normalization % SBP-1/Actin
200
150
100
50
0
shCTR
sh3-MST

Figure 6.7: GYY4137 and HMPSNE treatments on 3-MST knockdown adipocytes

Oil Red O staining on 3-MST knockdown adipocytes treated with GYY4137 (1, 3 and 6 mM) (C) or HMPSNE (30 µM, 100 µM and 200 µM) (E) for 7 days. Western Blot analysis of SBP-1 on shCTR/sh3-MST undifferentiated and adipocytes cells (B), treated with GYY4137 (3 mM) (D) or HMPSNE (100 µM) (F) for 7 days. A representative blot of lysates obtained from each group is shown and densitometry analysis is reported (n = 3). One-Way ANOVA followed by Bonferroni post- test. **p<0.01 and ****p<0.0001 vs Pre-adipocytes; °p<0.05 and °°°°p<0.0001 vs Adipocyte.

6.3.8 Nrf2 involvement on adipogenesis

To better elucidate the possible pathways involved in 3-MST-mediated adipogenesis, a transcription factor array was performed, comparing at the same time pre-adipocytes, adipocytes, HMPSNE-treated, shCTR and sh3-MST cells. The transcription factors that were showing more than 2-fold difference between shCTR and sh3-MST and more than 2-fold difference between pre-adipocytes and adipocytes were considered in this study. Among these, Nrf2 was showing a reduction in pre-adipocytes, HMPSNE-treated and sh3-MST cells, consistent with the pre-adipocyte-like pattern observed before (Figures 8A and 8B). It is known that Nrf2 plays a pivotal role in adipose biology, both directly and indirectly, influencing adipose cell differentiation; particularly, a loss of Nrf2 lead to impaired adipogenesis, while adipocyte differentiation of 3T3L1 cells is enhanced by activation of Nrf2 through knockdown of its negative regulator Keap1 [351], supporting our finding.

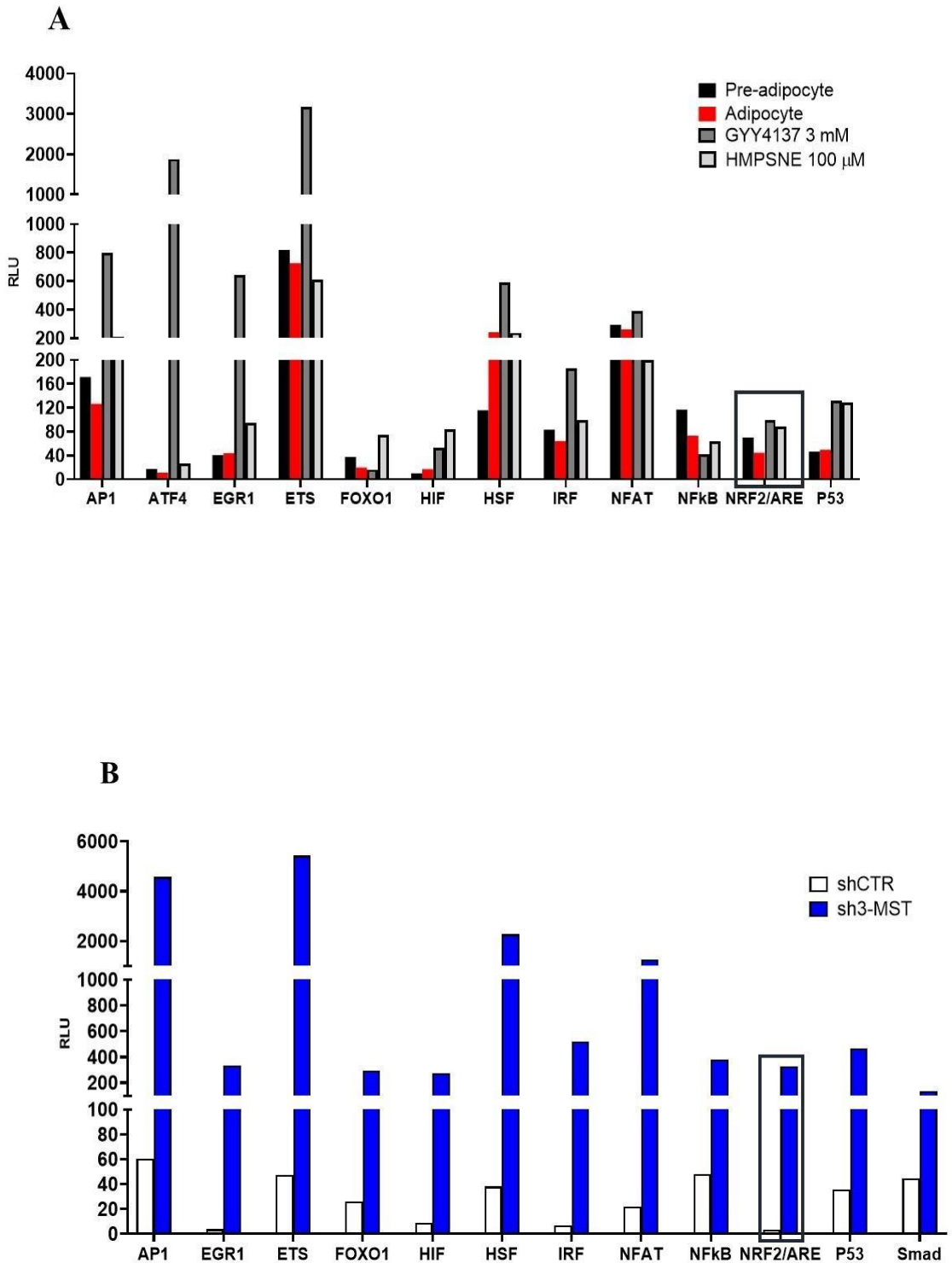

Figure 6.8: Role of Nrf2 transcriptional expression on adipogenesis

Signal transcriptional antibody Array on adipocytes treated with GYY4137 (3 mM) and HMPSNE (100 µM) (A) and on 3-MST knockdown adipocytes (B).

6.4 Discussion

Dysregulation of adipocyte proliferation, differentiation as well as altered adipocyte lipolysis contribute to obesity. The role of H_2S in this process and the underneath mechanism are still not well characterized [369].

In this study, 3T3L1 cells, a well-established mouse preadipocyte cell-line, were used as a cellular model to investigate H_2S-dependent adipogenesis. H_2S is naturally produced during 3T3L1 differentiation and the expression of all three H_2S-synthesisizing enzymes (CBS, CSE and 3-MST) was shown to be upregulated upon differentiation. To investigate the effect of H_2S modulation during adipocyte differentiation, 3T3L1 cells have been treated with the H2S donor GYY4137 as well as with the 3-MST inhibitor HMPSNE. GYY4137 has been already tested for activity in a range of pharmacological models both in vitro and in vivo, becoming increasingly employed as a pharmacological "tool" to explore the biological functions of H_2S. Initial work on the solution chemistry of GYY4137 indicated that it released low quantities of H_2S over a sustained period (hours to days) in aqueous solution (pH 7.4, 37 °C). Whilst most reports in the literature have focused on the effect of GYY4137 in the cardiovascular system and in inflammation, it is worth noting that a potential use of this drug in the treatment of cancer has also recently begun to be addressed; moreover, GYY4137 has been shown to influence cell cycle progression in a range of different cell types [370].

3-MST produces H_2S from 3-mercaptopyruvate (3MP), which is generated from l-cysteine and α-ketoglutarate (α-KG) by cysteine aminotransferase (CAT) in the presence of the cofactors thioredoxin and dihydrolipoic acid; numerous selective 3-MST inhibitors have been discovered and valuable for *in vitro* researches [371], but the abilities of HMPSNE, as 3-MST inhibitor, have excelled [372].

Nevertheless, the effect of HMPSNE has never been investigated in any biological process. In this study, HMPSNE was tested for the first time during adipocyte differentiation. The effect

of GYY4137 and HMPSNE on cell viability was concentration-dependent, showing minimum values at 6 mM and 200 μM, respectively (40% viability). On the other hand, the peak of citotoxicity was reached already at 3 mM for GYY4137 and 100 μM for HMPSNE, whereas at the highest concentrations the cytotoxcity was improved. This result can be explained by the "bell-shaped" effect of H_2S.

Lipid droplets are storage organelles that exert a key role in lipid and energy homeostasis. They have a unique architecture consisting of a hydrophobic core of neutral lipids, which is enclosed by a phospholipid monolayer that is decorated by a specific set of proteins. Originating from the endoplasmic reticulum, lipid droplets can associate with most other cellular organelles through membrane contact sites. It is becoming apparent that these contacts between lipid droplets and other organelles are highly dynamic and coupled to the cycles of lipid droplet expansion and shrinkage. Importantly, lipid droplet biogenesis and degradation, as well as their interactions with other organelles, are tightly coupled to cellular metabolism [373]. Tsai et al, demonstrated that a CSE inhibitor prevented lipid accumulation in lipid droplet suggesting a role for CSE in lipid droplets formation [343]. In this study, treatment with GYY4137 decreased lipid accumulation in a concentration-dependent manner, while HMPSNE treatment significantly enhanced lipid droplets formation, mainly at 30 and 100 μM.

Considering that dysregulation of lipid accumulation promotes an alteration on lipid synthesis and noting that H_2S plays a regulatory role in lipid droplet formation, H_2S synthesis and catabolism pathways have been investigated on adipocytes differentiation.

The expression of H_2S producing and catabolizing enzymes in GYY4137 and HMPSNE treated cells displayed different results. Whilst CBS, 3-MST and TST/Rhodanese are downregulated by GYY4137, CSE and ETHE-1 displayed a bell-shaped pattern. Similarly, HMPSNE-treated cells showed a concentration-dependent expression of all the enzymes, with a stable upregulation of ETHE-1.

The central role of 3-MST on adipogenesis was investigating by silencing 3-MST expression. Interestingly, in contrast with the transient 3-MST inhibition by HMPSNE, the stable 3-MST knockdown was associated with a different phenotype, leading to a decrease in adipocyte differentiation as highlighted by SBP-1 expression and suggesting as a downregulation of 3-MST could increase lipid droplets formation.

Finally, on the basis of Nrf2 role on adipogenesis, as previous discussed and showed, a possible correlation might emerge between 3-MST/Nrf2 pathway, providing a new approach to the study and pathological application of this pathway in lipid metabolism.

References

1. Sies, H., *Oxidative stress: a concept in redox biology and medicine.* Redox Biol, 2015. **4**: p. 180-3.
2. Tu, W., et al., *The Anti-Inflammatory and Anti-Oxidant Mechanisms of the Keap1/Nrf2/ARE Signaling Pathway in Chronic Diseases.* Aging Dis, 2019. **10**(3): p. 637-651.
3. Birben, E., et al., *Oxidative stress and antioxidant defense.* World Allergy Organ J, 2012. **5**(1): p. 9-19.
4. Bodega, G., et al., *Microvesicles: ROS scavengers and ROS producers.* J Extracell Vesicles, 2019. **8**(1): p. 1626654.
5. Chen, Q., et al., *Production of reactive oxygen species by mitochondria: central role of complex III.* J Biol Chem, 2003. **278**(38): p. 36027-31.
6. Powers, S.K., et al., *Reactive Oxygen Species: Impact on Skeletal Muscle.* Comprehensive Physiology, 2011. **1**(2): p. 941-969.
7. Salisbury, D. and U. Bronas, *Reactive Oxygen and Nitrogen Species Impact on Endothelial Dysfunction.* Nursing Research, 2015. **64**(1): p. 53-66.
8. Genestra, M., *Oxyl radicals, redox-sensitive signalling cascades and antioxidants.* Cellular Signalling, 2007. **19**(9): p. 1807-1819.
9. Phaniendra, A., D.B. Jestadi, and L. Periyasamy, *Free Radicals: Properties, Sources, Targets, and Their Implication in Various Diseases.* Indian Journal of Clinical Biochemistry, 2015. **30**(1): p. 11-26.
10. Schieber, M. and N.S. Chandel, *ROS function in redox signaling and oxidative stress.* Curr Biol, 2014. **24**(10): p. R453-62.
11. Poli, G., et al., *Oxidative stress and cell signalling.* Curr Med Chem, 2004. **11**(9): p. 1163-82.
12. Bottje, W., *Oxidative stress and efficiency: The tightrope act of mitochondria in health and disease.* Journal of Animal Science, 2018. **96**: p. 128-128.
13. Li, A.L., et al., *Novel diterpenoid-type activators of the Keap1/Nrf2/ARE signaling pathway and their regulation of redox homeostasis.* Free Radic Biol Med, 2019. **141**: p. 21-33.
14. Zolnourian, A., I. Galea, and D. Bulters, *Neuroprotective Role of the Nrf2 Pathway in Subarachnoid Haemorrhage and Its Therapeutic Potential.* Oxid Med Cell Longev, 2019. **2019**: p. 6218239.
15. Suzuki, T. and M. Yamamoto, *Molecular basis of the Keap1-Nrf2 system.* Free Radic Biol Med, 2015. **88**(Pt B): p. 93-100.
16. Tong, K.I., et al., *Two-site substrate recognition model for the Keap1-Nrf2 system: a hinge and latch mechanism.* Biol Chem, 2006. **387**(10-11): p. 1311-20.
17. Kobayashi, A., et al., *Oxidative stress sensor Keap1 functions as an adaptor for Cul3-based E3 ligase to regulate proteasomal degradation of Nrf2.* Mol Cell Biol, 2004. **24**(16): p. 7130-9.
18. Tong, K.I., et al., *Different electrostatic potentials define ETGE and DLG motifs as hinge and latch in oxidative stress response.* Mol Cell Biol, 2007. **27**(21): p. 7511-21.
19. Furukawa, M. and Y. Xiong, *BTB protein Keap1 targets antioxidant transcription factor Nrf2 for ubiquitination by the Cullin 3-Roc1 ligase.* Mol Cell Biol, 2005. **25**(1): p. 162-71.
20. Sparaneo, A., et al., *Effects of KEAP1 Silencing on the Regulation of NRF2 Activity in Neuroendocrine Lung Tumors.* Int J Mol Sci, 2019. **20**(10).
21. Sykiotis, G.P. and D. Bohmann, *Stress-activated cap'n'collar transcription factors in aging and human disease.* Sci Signal, 2010. **3**(112): p. re3.
22. Heightman, T.D., et al., *Structure-Activity and Structure-Conformation Relationships of Aryl Propionic Acid Inhibitors of the Kelch-like ECH-Associated Protein 1/Nuclear Factor Erythroid 2-Related Factor 2 (KEAP1/NRF2) Protein-Protein Interaction.* J Med Chem, 2019. **62**(9): p. 4683-4702.
23. Canning, P., F.J. Sorrell, and A.N. Bullock, *Structural basis of Keap1 interactions with Nrf2.* Free Radic Biol Med, 2015. **88**(Pt B): p. 101-107.

24. Tong, K.I., et al., *Keap1 recruits Neh2 through binding to ETGE and DLG motifs: characterization of the two-site molecular recognition model.* Mol Cell Biol, 2006. **26**(8): p. 2887-900.
25. Taguchi, K., H. Motohashi, and M. Yamamoto, *Molecular mechanisms of the Keap1-Nrf2 pathway in stress response and cancer evolution.* Genes Cells, 2011. **16**(2): p. 123-40.
26. McMahon, M., et al., *Redox-regulated turnover of Nrf2 is determined by at least two separate protein domains, the redox-sensitive Neh2 degron and the redox-insensitive Neh6 degron.* J Biol Chem, 2004. **279**(30): p. 31556-67.
27. Wu, J., H. Wang, and X. Tang, *Rexinoid inhibits Nrf2-mediated transcription through retinoid X receptor alpha.* Biochem Biophys Res Commun, 2014. **452**(3): p. 554-9.
28. Jain, A.K., D.A. Bloom, and A.K. Jaiswal, *Nuclear import and export signals in control of Nrf2.* J Biol Chem, 2005. **280**(32): p. 29158-68.
29. Uruno, A. and H. Motohashi, *The Keap1-Nrf2 system as an in vivo sensor for electrophiles.* Nitric Oxide, 2011. **25**(2): p. 153-60.
30. Friling, R.S., et al., *Xenobiotic-inducible expression of murine glutathione S-transferase Ya subunit gene is controlled by an electrophile-responsive element.* Proc Natl Acad Sci U S A, 1990. **87**(16): p. 6258-62.
31. Rushmore, T.H., M.R. Morton, and C.B. Pickett, *The antioxidant responsive element. Activation by oxidative stress and identification of the DNA consensus sequence required for functional activity.* J Biol Chem, 1991. **266**(18): p. 11632-9.
32. Wasserman, W.W. and W.E. Fahl, *Functional antioxidant responsive elements.* Proc Natl Acad Sci U S A, 1997. **94**(10): p. 5361-6.
33. Bryan, H.K., et al., *The Nrf2 cell defence pathway: Keap1-dependent and -independent mechanisms of regulation.* Biochem Pharmacol, 2013. **85**(6): p. 705-17.
34. Itoh, K., et al., *Keap1 represses nuclear activation of antioxidant responsive elements by Nrf2 through binding to the amino-terminal Neh2 domain.* Genes Dev, 1999. **13**(1): p. 76-86.
35. Dhakshinamoorthy, S. and A.K. Jaiswal, *Functional characterization and role of INrf2 in antioxidant response element-mediated expression and antioxidant induction of NAD(P)H:quinone oxidoreductase1 gene.* Oncogene, 2001. **20**(29): p. 3906-17.
36. Zipper, L.M. and R.T. Mulcahy, *The Keap1 BTB/POZ dimerization function is required to sequester Nrf2 in cytoplasm.* J Biol Chem, 2002. **277**(39): p. 36544-52.
37. Itoh, K., J. Mimura, and M. Yamamoto, *Discovery of the negative regulator of Nrf2, Keap1: a historical overview.* Antioxid Redox Signal, 2010. **13**(11): p. 1665-78.
38. Wakabayashi, N., et al., *Keap1-null mutation leads to postnatal lethality due to constitutive Nrf2 activation.* Nat Genet, 2003. **35**(3): p. 238-45.
39. Itoh, K., et al., *Keap1 regulates both cytoplasmic-nuclear shuttling and degradation of Nrf2 in response to electrophiles.* Genes Cells, 2003. **8**(4): p. 379-91.
40. Kwak, M.K., et al., *Enhanced expression of the transcription factor Nrf2 by cancer chemopreventive agents: role of antioxidant response element-like sequences in the nrf2 promoter.* Mol Cell Biol, 2002. **22**(9): p. 2883-92.
41. Levonen, A.L., et al., *Cellular mechanisms of redox cell signalling: role of cysteine modification in controlling antioxidant defences in response to electrophilic lipid oxidation products.* Biochem J, 2004. **378**(Pt 2): p. 373-82.
42. Rachakonda, G., et al., *Covalent modification at Cys151 dissociates the electrophile sensor Keap1 from the ubiquitin ligase CUL3.* Chem Res Toxicol, 2008. **21**(3): p. 705-10.
43. Nguyen, T., et al., *Nrf2 controls constitutive and inducible expression of ARE-driven genes through a dynamic pathway involving nucleocytoplasmic shuttling by Keap1.* J Biol Chem, 2005. **280**(37): p. 32485-92.
44. Watai, Y., et al., *Subcellular localization and cytoplasmic complex status of endogenous Keap1.* Genes Cells, 2007. **12**(10): p. 1163-78.
45. Sun, Z., et al., *Keap1 controls postinduction repression of the Nrf2-mediated antioxidant response by escorting nuclear export of Nrf2.* Mol Cell Biol, 2007. **27**(18): p. 6334-49.

46. Niture, S.K., R. Khatri, and A.K. Jaiswal, *Regulation of Nrf2-an update.* Free Radic Biol Med, 2014. **66**: p. 36-44.
47. Eggler, A.L., et al., *Cul3-mediated Nrf2 ubiquitination and antioxidant response element (ARE) activation are dependent on the partial molar volume at position 151 of Keap1.* Biochem J, 2009. **422**(1): p. 171-80.
48. Holland, R., et al., *Prospective type 1 and type 2 disulfides of Keap1 protein.* Chem Res Toxicol, 2008. **21**(10): p. 2051-60.
49. Lo, S.C., et al., *Structure of the Keap1:Nrf2 interface provides mechanistic insight into Nrf2 signaling.* EMBO J, 2006. **25**(15): p. 3605-17.
50. Kobayashi, M., et al., *The antioxidant defense system Keap1-Nrf2 comprises a multiple sensing mechanism for responding to a wide range of chemical compounds.* Mol Cell Biol, 2009. **29**(2): p. 493-502.
51. Dinkova-Kostova, A.T., R.V. Kostov, and P. Canning, *Keap1, the cysteine-based mammalian intracellular sensor for electrophiles and oxidants.* Arch Biochem Biophys, 2017. **617**: p. 84-93.
52. Hu, C., et al., *Modification of keap1 cysteine residues by sulforaphane.* Chem Res Toxicol, 2011. **24**(4): p. 515-21.
53. Kansanen, E., et al., *The Keap1-Nrf2 pathway: Mechanisms of activation and dysregulation in cancer.* Redox Biol, 2013. **1**: p. 45-9.
54. McMahon, M., et al., *Dimerization of substrate adaptors can facilitate cullin-mediated ubiquitylation of proteins by a "tethering" mechanism: a two-site interaction model for the Nrf2-Keap1 complex.* J Biol Chem, 2006. **281**(34): p. 24756-68.
55. Padmanabhan, B., et al., *Structural basis for defects of Keap1 activity provoked by its point mutations in lung cancer.* Mol Cell, 2006. **21**(5): p. 689-700.
56. Kaniuk, N.A., et al., *Ubiquitinated-protein aggregates form in pancreatic beta-cells during diabetes-induced oxidative stress and are regulated by autophagy.* Diabetes, 2007. **56**(4): p. 930-9.
57. Kim, P.K., et al., *Ubiquitin signals autophagic degradation of cytosolic proteins and peroxisomes.* Proc Natl Acad Sci U S A, 2008. **105**(52): p. 20567-74.
58. Copple, I.M., et al., *The Nrf2-Keap1 defence pathway: role in protection against drug-induced toxicity.* Toxicology, 2008. **246**(1): p. 24-33.
59. Fan, W., et al., *Keap1 facilitates p62-mediated ubiquitin aggregate clearance via autophagy.* Autophagy, 2010. **6**(5): p. 614-21.
60. Komatsu, M., et al., *The selective autophagy substrate p62 activates the stress responsive transcription factor Nrf2 through inactivation of Keap1.* Nat Cell Biol, 2010. **12**(3): p. 213-23.
61. Li, Y., J.D. Paonessa, and Y. Zhang, *Mechanism of chemical activation of Nrf2.* PLoS One, 2012. **7**(4): p. e35122.
62. Miao, W., et al., *Transcriptional regulation of NF-E2 p45-related factor (NRF2) expression by the aryl hydrocarbon receptor-xenobiotic response element signaling pathway: direct cross-talk between phase I and II drug-metabolizing enzymes.* J Biol Chem, 2005. **280**(21): p. 20340-8.
63. Rushmore, T.H., et al., *Regulation of glutathione S-transferase Ya subunit gene expression: identification of a unique xenobiotic-responsive element controlling inducible expression by planar aromatic compounds.* Proc Natl Acad Sci U S A, 1990. **87**(10): p. 3826-30.
64. Yamamoto, T., et al., *Identification of polymorphisms in the promoter region of the human NRF2 gene.* Biochem Biophys Res Commun, 2004. **321**(1): p. 72-9.
65. Guan, C.P., et al., *The susceptibility to vitiligo is associated with NF-E2-related factor2 (Nrf2) gene polymorphisms: a study on Chinese Han population.* Exp Dermatol, 2008. **17**(12): p. 1059-62.
66. Yang, M., et al., *MiR-28 regulates Nrf2 expression through a Keap1-independent mechanism.* Breast Cancer Res Treat, 2011. **129**(3): p. 983-91.

67. Kurinna, S. and S. Werner, *NRF2 and microRNAs: new but awaited relations.* Biochem Soc Trans, 2015. **43**(4): p. 595-601.
68. Sangokoya, C., M.J. Telen, and J.T. Chi, *microRNA miR-144 modulates oxidative stress tolerance and associates with anemia severity in sickle cell disease.* Blood, 2010. **116**(20): p. 4338-48.
69. Zhang, X., et al., *Proximal, Distal, and Combined Fixation Within the Tibial Tunnel in Transtibial Posterior Cruciate Ligament Reconstruction: A Time-Zero Biomechanical Study In Vitro.* Arthroscopy, 2019. **35**(6): p. 1667-1673.
70. Zhao, X., et al., *MicroRNA-128-3p aggravates doxorubicin-induced liver injury by promoting oxidative stress via targeting Sirtuin-1.* Pharmacol Res, 2019. **146**: p. 104276.
71. Rojo, A.I., et al., *Signaling pathways activated by the phytochemical nordihydroguaiaretic acid contribute to a Keap1-independent regulation of Nrf2 stability: Role of glycogen synthase kinase-3.* Free Radic Biol Med, 2012. **52**(2): p. 473-87.
72. Yuan, X., et al., *Butylated hydroxyanisole regulates ARE-mediated gene expression via Nrf2 coupled with ERK and JNK signaling pathway in HepG2 cells.* Mol Carcinog, 2006. **45**(11): p. 841-50.
73. He, X. and Q. Ma, *NRF2 cysteine residues are critical for oxidant/electrophile-sensing, Kelch-like ECH-associated protein-1-dependent ubiquitination-proteasomal degradation, and transcription activation.* Mol Pharmacol, 2009. **76**(6): p. 1265-78.
74. Kobayashi, A., et al., *Oxidative and electrophilic stresses activate Nrf2 through inhibition of ubiquitination activity of Keap1.* Mol Cell Biol, 2006. **26**(1): p. 221-9.
75. Li, W., et al., *Caveolin-1 inhibits expression of antioxidant enzymes through direct interaction with nuclear erythroid 2 p45-related factor-2 (Nrf2).* J Biol Chem, 2012. **287**(25):p. 20922-30.
76. Mishra, P., et al., *Possible activation of NRF2 by Vitamin E/Curcumin against altered thyroid hormone induced oxidative stress via NFkB/AKT/mTOR/KEAP1 signalling in rat heart.* Sci Rep, 2019. **9**(1): p. 7408.
77. Hybertson, B.M., et al., *Oxidative stress in health and disease: the therapeutic potential of Nrf2 activation.* Mol Aspects Med, 2011. **32**(4-6): p. 234-46.
78. Kavian, N., et al., *The Nrf2-Antioxidant Response Element Signaling Pathway Controls Fibrosis and Autoimmunity in Scleroderma.* Front Immunol, 2018. **9**: p. 1896.
79. Taniyama, Y. and K.K. Griendling, *Reactive oxygen species in the vasculature: molecular and cellular mechanisms.* Hypertension, 2003. **42**(6): p. 1075-81.
80. Holmstrom, K.M., et al., *Nrf2 impacts cellular bioenergetics by controlling substrate availability for mitochondrial respiration.* Biol Open, 2013. **2**(8): p. 761-70.
81. Cominacini, L., et al., *Endoplasmic reticulum stress and Nrf2 signaling in cardiovascular diseases.* Free Radic Biol Med, 2015. **88**(Pt B): p. 233-242.
82. Yan, S.H., et al., *Modulations of Keap1-Nrf2 signaling axis by TIIA ameliorated the oxidative stress-induced myocardial apoptosis.* Free Radic Biol Med, 2018. **115**: p. 191-201.
83. Enomoto, A., et al., *High sensitivity of Nrf2 knockout mice to acetaminophen hepatotoxicity associated with decreased expression of ARE-regulated drug metabolizing enzymes and antioxidant genes.* Toxicol Sci, 2001. **59**(1): p. 169-77.
84. Copple, I.M., et al., *The hepatotoxic metabolite of acetaminophen directly activates the Keap1-Nrf2 cell defense system.* Hepatology, 2008. **48**(4): p. 1292-301.
85. Klaassen, C.D. and S.A. Reisman, *Nrf2 the rescue: effects of the antioxidative/electrophilic response on the liver.* Toxicol Appl Pharmacol, 2010. **244**(1): p. 57-65.
86. Wu, K.C., J. Liu, and C.D. Klaassen, *Role of Nrf2 in preventing ethanol-induced oxidative stress and lipid accumulation.* Toxicol Appl Pharmacol, 2012. **262**(3): p. 321-9.
87. Schmidlin, C.J., M.B. Dodson, and D.D. Zhang, *Filtering through the role of NRF2 in kidney disease.* Arch Pharm Res, 2019.
88. Yoh, K., et al., *Hyperglycemia induces oxidative and nitrosative stress and increases renal functional impairment in Nrf2-deficient mice.* Genes Cells, 2008. **13**(11): p. 1159-70.

89. Aleksunes, L.M., et al., *Transcriptional regulation of renal cytoprotective genes by Nrf2 and its potential use as a therapeutic target to mitigate cisplatin-induced nephrotoxicity.* J Pharmacol Exp Ther, 2010. **335**(1): p. 2-12.
90. Yagishita, Y., et al., *Nrf2 represses the onset of type 1 diabetes in non-obese diabetic mice.* J Endocrinol, 2019.
91. Uruno, A., Y. Yagishita, and M. Yamamoto, *The Keap1-Nrf2 system and diabetes mellitus.* Arch Biochem Biophys, 2015. **566**: p. 76-84.
92. Qin, Q., et al., *Ginsenoside Rg1 ameliorates cardiac oxidative stress and inflammation in streptozotocin-induced diabetic rats.* Diabetes Metab Syndr Obes, 2019. **12**: p.1091-1103.
93. Taguchi, K. and M. Yamamoto, *The KEAP1-NRF2 System in Cancer.* Front Oncol, 2017. **7**: p. 85.
94. Milkovic, L., N. Zarkovic, and L. Saso, *Controversy about pharmacological modulation of Nrf2 for cancer therapy.* Redox Biol, 2017. **12**: p. 727-732.
95. Jeong, Y., et al., *Role of KEAP1/NRF2 and TP53 Mutations in Lung Squamous Cell Carcinoma Development and Radiation Resistance.* Cancer Discov, 2017. **7**(1): p. 86-101.
96. Yamazaki, H., et al., *Role of the Keap1/Nrf2 pathway in neurodegenerative diseases.* Pathol Int, 2015. **65**(5): p. 210-9.
97. Deshmukh, P., et al., *The Keap1-Nrf2 pathway: promising therapeutic target to counteract ROS-mediated damage in cancers and neurodegenerative diseases.* Biophys Rev, 2017. **9**(1): p. 41-56.
98. Branca, C., et al., *Genetic reduction of Nrf2 exacerbates cognitive deficits in a mouse model of Alzheimer's disease.* Hum Mol Genet, 2017. **26**(24): p. 4823-4835.
99. Kanninen, K., et al., *Targeting Glycogen Synthase Kinase-3beta for Therapeutic Benefit against Oxidative Stress in Alzheimer's Disease: Involvement of the Nrf2-ARE Pathway.* Int J Alzheimers Dis, 2011. **2011**: p. 985085.
100. Cuadrado, A., S. Kugler, and I. Lastres-Becker, *Pharmacological targeting of GSK-3 and NRF2 provides neuroprotection in a preclinical model of tauopathy.* Redox Biol, 2018. **14**: p. 522-534.
101. Ramsey, C.P., et al., *Expression of Nrf2 in neurodegenerative diseases.* J Neuropathol Exp Neurol, 2007. **66**(1): p. 75-85.
102. Smith, D., *Fumaric acid esters for psoriasis: a systematic review.* Ir J Med Sci, 2017. **186**(1): p. 161-177.
103. Mrowietz, U. and K. Asadullah, *Dimethylfumarate for psoriasis: more than a dietary curiosity.* Trends Mol Med, 2005. **11**(1): p. 43-8.
104. Meissner, M., et al., *Dimethyl fumarate - only an anti-psoriatic medication?* J Dtsch Dermatol Ges, 2012. **10**(11): p. 793-801.
105. Breuer, K., et al., *Therapy of noninfectious granulomatous skin diseases with fumaric acid esters.* Br J Dermatol, 2005. **152**(6): p. 1290-5.
106. Gold, R., et al., *Placebo-controlled phase 3 study of oral BG-12 for relapsing multiple sclerosis.* N Engl J Med, 2012. **367**(12): p. 1098-107.
107. Lehmann, J.C., et al., *Dimethylfumarate induces immunosuppression via glutathione depletion and subsequent induction of heme oxygenase 1.* J Invest Dermatol, 2007. **127**(4): p. 835-45.
108. Fox, R.J., et al., *Placebo-controlled phase 3 study of oral BG-12 or glatiramer in multiple sclerosis.* N Engl J Med, 2012. **367**(12): p. 1087-97.
109. Stoof, T.J., et al., *The antipsoriatic drug dimethylfumarate strongly suppresses chemokine production in human keratinocytes and peripheral blood mononuclear cells.* Br J Dermatol, 2001. **144**(6): p. 1114-20.
110. Rubant, S.A., et al., *Dimethylfumarate reduces leukocyte rolling in vivo through modulation of adhesion molecule expression.* J Invest Dermatol, 2008. **128**(2): p. 326-31.
111. Sebok, B., et al., *Antiproliferative and cytotoxic profiles of antipsoriatic fumaric acid derivatives in keratinocyte cultures.* Eur J Pharmacol, 1994. **270**(1): p. 79-87.

112. Linker, R.A. and A. Haghikia, *Dimethyl fumarate in multiple sclerosis: latest developments, evidence and place in therapy.* Ther Adv Chronic Dis, 2016. **7**(4): p. 198-207.
113. Sheikh, S.I., et al., *Tolerability and pharmacokinetics of delayed-release dimethyl fumarate administered with and without aspirin in healthy volunteers.* Clin Ther, 2013. **35**(10): p. 1582-1594 e9.
114. Kappos, L., et al., *Efficacy and safety of oral fumarate in patients with relapsing-remitting multiple sclerosis: a multicentre, randomised, double-blind, placebo-controlled phase IIb study.* Lancet, 2008. **372**(9648): p. 1463-72.
115. Gross, C.C., et al., *Dimethyl fumarate treatment alters circulating T helper cell subsets in multiple sclerosis.* Neurol Neuroimmunol Neuroinflamm, 2016. **3**(1): p. e183.
116. Mrowietz, U., et al., *Efficacy and safety of LAS41008 (dimethyl fumarate) in adults with moderate-to-severe chronic plaque psoriasis: a randomized, double-blind, Fumaderm((R)) - and placebo-controlled trial (BRIDGE).* Br J Dermatol, 2017. **176**(3): p. 615-623.
117. Treumer, F., et al., *Dimethylfumarate is a potent inducer of apoptosis in human T cells.* J Invest Dermatol, 2003. **121**(6): p. 1383-8.
118. Ghoreschi, K., et al., *Fumarates improve psoriasis and multiple sclerosis by inducing type II dendritic cells.* J Exp Med, 2011. **208**(11): p. 2291-303.
119. Albrecht, P., et al., *Effects of dimethyl fumarate on neuroprotection and immunomodulation.* J Neuroinflammation, 2012. **9**: p. 163.
120. Offermanns, S. and M. Schwaninger, *Nutritional or pharmacological activation of HCA(2) ameliorates neuroinflammation.* Trends Mol Med, 2015. **21**(4): p. 245-55.
121. Chen, H., et al., *Hydroxycarboxylic acid receptor 2 mediates dimethyl fumarate's protective effect in EAE.* J Clin Invest, 2014. **124**(5): p. 2188-92.
122. Corrigan, J.D., A.W. Selassie, and J.A. Orman, *The epidemiology of traumatic brain injury.* J Head Trauma Rehabil, 2010. **25**(2): p. 72-80.
123. Peeters, W., et al., *Epidemiology of traumatic brain injury in Europe.* Acta Neurochir (Wien), 2015. **157**(10): p. 1683-96.
124. Cheng, G., et al., *Mitochondria in traumatic brain injury and mitochondrial-targeted multipotential therapeutic strategies.* Br J Pharmacol, 2012. **167**(4): p. 699-719.
125. Wang, L., et al., *The influence of subarachnoid hemorrhage on neurons: an animal model.* Ann Clin Lab Sci, 2005. **35**(1): p. 79-85.
126. Chesnut, R.M., et al., *The role of secondary brain injury in determining outcome from severe head injury.* J Trauma, 1993. **34**(2): p. 216-22.
127. Signoretti, S., et al., *The protective effect of cyclosporin A upon N-acetylaspartate and mitochondrial dysfunction following experimental diffuse traumatic brain injury.* J Neurotrauma, 2004. **21**(9): p. 1154-67.
128. Sahuquillo, J., M.A. Poca, and S. Amoros, *Current aspects of pathophysiology and cell dysfunction after severe head injury.* Curr Pharm Des, 2001. **7**(15): p. 1475-503.
129. Wada, K., et al., *Inducible nitric oxide synthase expression after traumatic brain injury and neuroprotection with aminoguanidine treatment in rats.* Neurosurgery, 1998. **43**(6): p. 1427-36.
130. Murphy, M.P., *How mitochondria produce reactive oxygen species.* Biochem J, 2009. **417**(1): p. 1-13.
131. Zhao, X., et al., *Transcription factor Nrf2 protects the brain from damage produced by intracerebral hemorrhage.* Stroke, 2007. **38**(12): p. 3280-6.
132. Jin, W., et al., *Transcription factor Nrf2 plays a pivotal role in protection against traumatic brain injury-induced acute intestinal mucosal injury in mice.* J Surg Res, 2009. **157**(2): p. 251-60.
133. DeLong, W.G., Jr. and C.T. Born, *Cytokines in patients with polytrauma.* Clin Orthop Relat Res, 2004(422): p. 57-65.
134. Barreto, G., et al., *Astrocytes: targets for neuroprotection in stroke.* Cent Nerv Syst Agents Med Chem, 2011. **11**(2): p. 164-73.

135. Liu, Y., et al., *Dimethylfumarate alleviates early brain injury and secondary cognitive deficits after experimental subarachnoid hemorrhage via activation of Keap1-Nrf2-ARE system.* J Neurosurg, 2015. **123**(4): p. 915-23.
136. Vandermeeren, M., et al., *Dimethylfumarate is an inhibitor of cytokine-induced nuclear translocation of NF-kappa B1, but not RelA in normal human dermal fibroblast cells.* J Invest Dermatol, 2001. **116**(1): p. 124-30.
137. Xiong, Y., A. Mahmood, and M. Chopp, *Emerging treatments for traumatic brain injury.* Expert Opin Emerg Drugs, 2009. **14**(1): p. 67-84.
138. Campolo, M., et al., *Hydrogen sulfide-releasing cyclooxygenase inhibitor ATB-346 enhances motor function and reduces cortical lesion volume following traumatic brain injury in mice.* J Neuroinflammation, 2014. **11**: p. 196.
139. Casili, G., et al., *Dimethyl Fumarate Reduces Inflammatory Responses in Experimental Colitis.* J Crohns Colitis, 2016. **10**(4): p. 472-83.
140. Cordaro, M., et al., *Fumaric Acid Esters Attenuate Secondary Degeneration after Spinal Cord Injury.* J Neurotrauma, 2017. **34**(21): p. 3027-3040.
141. Campolo, M., et al., *The Neuroprotective Effect of Dimethyl Fumarate in an MPTP-Mouse Model of Parkinson's Disease: Involvement of Reactive Oxygen Species/Nuclear Factor-kappaB/Nuclear Transcription Factor Related to NF-E2.* Antioxid Redox Signal, 2017. **27**(8): p. 453-471.
142. Sullivan, P.G., A.H. Sebastian, and E.D. Hall, *Therapeutic window analysis of the neuroprotective effects of cyclosporine A after traumatic brain injury.* J Neurotrauma, 2011. **28**(2): p. 311-8.
143. Meythaler, J.M., et al., *Current concepts: diffuse axonal injury-associated traumatic brain injury.* Arch Phys Med Rehabil, 2001. **82**(10): p. 1461-71.
144. Kawai, T. and S. Akira, *Signaling to NF-kappaB by Toll-like receptors.* Trends Mol Med, 2007. **13**(11): p. 460-9.
145. Loane, D.J., et al., *Progressive neurodegeneration after experimental brain trauma: association with chronic microglial activation.* J Neuropathol Exp Neurol, 2014. **73**(1): p. 14-29.
146. Cernak, I., et al., *A novel mouse model of penetrating brain injury.* Front Neurol, 2014. **5**: p. 209.
147. Pellow, S., et al., *Validation of open:closed arm entries in an elevated plus-maze as a measure of anxiety in the rat.* J Neurosci Methods, 1985. **14**(3): p. 149-67.
148. Ahmad, A., et al., *Administration of palmitoylethanolamide (PEA) protects the neurovascular unit and reduces secondary injury after traumatic brain injury in mice.* Brain Behav Immun, 2012. **26**(8): p. 1310-21.
149. Begum, G., et al., *Docosahexaenoic acid reduces ER stress and abnormal protein accumulation and improves neuronal function following traumatic brain injury.* J Neurosci, 2014. **34**(10): p. 3743-55.
150. Ahmad, A., et al., *Absence of TLR4 reduces neurovascular unit and secondary inflammatory process after traumatic brain injury in mice.* PLoS One, 2013. **8**(3): p. e57208.
151. Cryan, J.F., C. Mombereau, and A. Vassout, *The tail suspension test as a model for assessing antidepressant activity: review of pharmacological and genetic studies in mice.* Neurosci Biobehav Rev, 2005. **29**(4-5): p. 571-625.
152. Esposito, E., et al., *Neuroprotective activities of palmitoylethanolamide in an animal model of Parkinson's disease.* PLoS One, 2012. **7**(8): p. e41880.
153. Bruschetta, G., et al., *FeTPPS Reduces Secondary Damage and Improves Neurobehavioral Functions after Traumatic Brain Injury.* Front Neurosci, 2017. **11**: p. 6.
154. Raghupathi, R., et al., *Temporal alterations in cellular Bax:Bcl-2 ratio following traumatic brain injury in the rat.* J Neurotrauma, 2003. **20**(5): p. 421-35.

155. Yu, G., et al., *Inhibition of myeloperoxidase oxidant production by N-acetyl lysyltyrosylcysteine amide reduces brain damage in a murine model of stroke.* J Neuroinflammation, 2016. **13**(1): p. 119.
156. Narayan, R.K., et al., *Clinical trials in head injury.* J Neurotrauma, 2002. **19**(5): p. 503-57.
157. Sandberg, M., et al., *NRF2-regulation in brain health and disease: implication of cerebral inflammation.* Neuropharmacology, 2014. **79**: p. 298-306.
158. Mestas, J. and C.C. Hughes, *Of mice and not men: differences between mouse and human immunology.* J Immunol, 2004. **172**(5): p. 2731-8.
159. Bomprezzi, R., *Dimethyl fumarate in the treatment of relapsing-remitting multiple sclerosis: an overview.* Ther Adv Neurol Disord, 2015. **8**(1): p. 20-30.
160. Esposito, E., M. Cordaro, and S. Cuzzocrea, *Roles of fatty acid ethanolamides (FAE) in traumatic and ischemic brain injury.* Pharmacol Res, 2014. **86**: p. 26-31.
161. Xiong, Y., A. Mahmood, and M. Chopp, *Animal models of traumatic brain injury.* Nat Rev Neurosci, 2013. **14**(2): p. 128-42.
162. Mendez-David, I., et al., *Nrf2-signaling and BDNF: A new target for the antidepressant-like activity of chronic fluoxetine treatment in a mouse model of anxiety/depression.* Neurosci Lett, 2015. **597**: p. 121-6.
163. Wieloch, T. and K. Nikolich, *Mechanisms of neural plasticity following brain injury.* Curr Opin Neurobiol, 2006. **16**(3): p. 258-64.
164. Nakamura, M., et al., *Overexpression of Bcl-2 is neuroprotective after experimental brain injury in transgenic mice.* J Comp Neurol, 1999. **412**(4): p. 681-92.
165. Cornelius, C., et al., *Traumatic brain injury: oxidative stress and neuroprotection.* Antioxid Redox Signal, 2013. **19**(8): p. 836-53.
166. Zhao, X., et al., *Dimethyl Fumarate Protects Brain From Damage Produced by Intracerebral Hemorrhage by Mechanism Involving Nrf2.* Stroke, 2015. **46**(7): p. 1923-8.
167. Cheng, Z.G., et al., *Expression and antioxidation of Nrf2/ARE pathway in traumatic brain injury.* Asian Pac J Trop Med, 2013. **6**(4): p. 305-10.
168. Mendes Arent, A., et al., *Perspectives on molecular biomarkers of oxidative stress and antioxidant strategies in traumatic brain injury.* Biomed Res Int, 2014. **2014**: p. 723060.
169. Morganti-Kossmann, M.C., et al., *Inflammatory response in acute traumatic brain injury: a double-edged sword.* Curr Opin Crit Care, 2002. **8**(2): p. 101-5.
170. Campolo, M., et al., *A hydrogen sulfide-releasing cyclooxygenase inhibitor markedly accelerates recovery from experimental spinal cord injury.* FASEB J, 2013. **27**(11):p. 4489-99.
171. Viatour, P., et al., *Phosphorylation of NF-kappaB and IkappaB proteins: implications in cancer and inflammation.* Trends Biochem Sci, 2005. **30**(1): p. 43-52.
172. Molina-Holgado, E., et al., *Induction of COX-2 and PGE(2) biosynthesis by IL-1beta is mediated by PKC and mitogen-activated protein kinases in murine astrocytes.* Br J Pharmacol, 2000. **131**(1): p. 152-9.
173. Hickey, R.W., et al., *Cyclooxygenase-2 activity following traumatic brain injury in the developing rat.* Pediatr Res, 2007. **62**(3): p. 271-6.
174. Yokoyama, H., et al., *Targeting reactive oxygen species, reactive nitrogen species and inflammation in MPTP neurotoxicity and Parkinson's disease.* Neurol Sci, 2008. **29**(5): p. 293-301.
175. Cherian, L., R. Hlatky, and C.S. Robertson, *Nitric oxide in traumatic brain injury.* Brain Pathol, 2004. **14**(2): p. 195-201.
176. Garry, P.S., et al., *The role of the nitric oxide pathway in brain injury and its treatment--from bench to bedside.* Exp Neurol, 2015. **263**: p. 235-43.
177. Khan, M., et al., *Administration of S-nitrosoglutathione after traumatic brain injury protects the neurovascular unit and reduces secondary injury in a rat model of controlled cortical impact.* J Neuroinflammation, 2009. **6**: p. 32.

178. Bao, F., et al., *A CD11d monoclonal antibody treatment reduces tissue injury and improves neurological outcome after fluid percussion brain injury in rats.* J Neurotrauma, 2012. **29**(14): p. 2375-92.
179. Ryu, S., et al., *Amelioration of Cerebral Ischemic Injury by a Synthetic Seco-nucleoside LMT497.* Exp Neurobiol, 2015. **24**(1): p. 31-40.
180. Bellanti, F., et al., *Sex hormones modulate circulating antioxidant enzymes: impact of estrogen therapy.* Redox Biol, 2013. **1**: p. 340-6.
181. De la Fuente, M. and J. Miquel, *An update of the oxidation-inflammation theory of aging: the involvement of the immune system in oxi-inflamm-aging.* Curr Pharm Des, 2009. **15**(26): p. 3003-26.
182. Longbrake, E.E., et al., *Dimethyl fumarate-associated lymphopenia: Risk factors and clinical significance.* Mult Scler J Exp Transl Clin, 2015. **1**.
183. Zhang, X., et al., *Identifying module biomarker in type 2 diabetes mellitus by discriminative area of functional activity.* BMC Bioinformatics, 2015. **16**: p. 92.
184. Agosti, R., *Migraine Burden of Disease: From the Patient's Experience to a Socio-Economic View.* Headache, 2018. **58 Suppl 1**: p. 17-32.
185. Mulder, E.J., et al., *Genetic and environmental influences on migraine: a twin study across six countries.* Twin Res, 2003. **6**(5): p. 422-31.
186. Reddy, D.S., *The pathophysiological and pharmacological basis of current drug treatment of migraine headache.* Expert Rev Clin Pharmacol, 2013. **6**(3): p. 271-88.
187. Lupi, C., et al., *Pharmacokinetics and pharmacodynamics of new acute treatments for migraine.* Expert Opin Drug Metab Toxicol, 2019. **15**(3): p. 189-198.
188. Rujan, R.M. and C.A. Reynolds, *Calcitonin Gene-Related Peptide Antagonists and Therapeutic Antibodies.* Handb Exp Pharmacol, 2019.
189. Hay, D.L. and C.S. Walker, *CGRP and its receptors.* Headache, 2017. **57**(4): p. 625-636.
190. Edvinsson, L., *CGRP receptor antagonists and antibodies against CGRP and its receptor in migraine treatment.* Br J Clin Pharmacol, 2015. **80**(2): p. 193-9.
191. Deen, M., et al., *Blocking CGRP in migraine patients - a review of pros and cons.* J Headache Pain, 2017. **18**(1): p. 96.
192. Borkum, J.M., *Migraine Triggers and Oxidative Stress: A Narrative Review and Synthesis.* Headache, 2016. **56**(1): p. 12-35.
193. de Vries, B., et al., *Molecular genetics of migraine.* Hum Genet, 2009. **126**(1): p. 115-32.
194. Kowalska, M., et al., *Molecular factors in migraine.* Oncotarget, 2016. **7**(31): p. 50708-50718.
195. Geyik, S., et al., *Oxidative stress and DNA damage in patients with migraine.* J Headache Pain, 2016. **17**: p. 10.
196. Belcher, J.D., et al., *Control of Oxidative Stress and Inflammation in Sickle Cell Disease with the Nrf2 Activator Dimethyl Fumarate.* Antioxid Redox Signal, 2017. **26**(14): p. 748-762.
197. Kappos, L., et al., *Efficacy and safety of oral fumarate in patients with relapsing-remitting multiple sclerosis: a multicentre, randomised, double-blind, placebo-controlled phase IIb study.* Lancet, 2008. **372**(9648): p. 1463-72.
198. Nguyen, T., P. Nioi, and C.B. Pickett, *The Nrf2-antioxidant response element signaling pathway and its activation by oxidative stress.* J Biol Chem, 2009. **284**(20): p. 13291-5.
199. Di, W., et al., *Activation of the nuclear factor E2-related factor 2/anitioxidant response element alleviates the nitroglycerin-induced hyperalgesia in rats.* J Headache Pain, 2016. **17**(1): p. 99.
200. Di Clemente, L., et al., *Nitroglycerin sensitises in healthy subjects CNS structures involved in migraine pathophysiology: evidence from a study of nociceptive blink reflexes and visual evoked potentials.* Pain, 2009. **144**(1-2): p. 156-61.
201. Pini, L.A., et al., *Tolerability and efficacy of a combination of paracetamol and caffeine in the treatment of tension-type headache: a randomised, double-blind, double-dummy, cross-over study versus placebo and naproxen sodium.* J Headache Pain, 2008. **9**(6): p. 367-73.

202. Sandrini, M., et al., *The effect of paracetamol on nociception and dynorphin A levels in the rat brain.* Neuropeptides, 2001. **35**(2): p. 110-6.
203. Lipton, R.B., et al., *Caffeine in the management of patients with headache.* J Headache Pain, 2017. **18**(1): p. 107.
204. Diener, H.C., et al., *The fixed combination of acetylsalicylic acid, paracetamol and caffeine is more effective than single substances and dual combination for the treatment of headache: a multicentre, randomized, double-blind, single-dose, placebo-controlled parallel group study.* Cephalalgia, 2005. **25**(10): p. 776-87.
205. Pini, L.A., et al., *Comparison of tolerability and efficacy of a combination of paracetamol + caffeine and sumatriptan in the treatment of migraine attack: a randomized, double-blind, double-dummy, cross-over study.* J Headache Pain, 2012. **13**(8): p. 669-75.
206. Wang, Z.Q., et al., *A newly identified role for superoxide in inflammatory pain.* J Pharmacol Exp Ther, 2004. **309**(3): p. 869-78.
207. Tjolsen, A., et al., *The formalin test: an evaluation of the method.* Pain, 1992. **51**(1): p. 5-17.
208. Tassorelli, C. and S.A. Joseph, *Systemic nitroglycerin induces Fos immunoreactivity in brainstem and forebrain structures of the rat.* Brain Res, 1995. **682**(1-2): p. 167-81.
209. Yamamoto, T., N. Nozaki-Taguchi, and T. Chiba, *Analgesic effect of intrathecally administered orexin-A in the rat formalin test and in the rat hot plate test.* Br J Pharmacol, 2002. **137**(2): p. 170-6.
210. Sufka, K.J., et al., *Clinically relevant behavioral endpoints in a recurrent nitroglycerin migraine model in rats.* J Headache Pain, 2016. **17**: p. 40.
211. Tureyen, K., et al., *Infarct volume quantification in mouse focal cerebral ischemia: a comparison of triphenyltetrazolium chloride and cresyl violet staining techniques.* J Neurosci Methods, 2004. **139**(2): p. 203-7.
212. Casili, G., et al., *Dimethyl Fumarate Attenuates Neuroinflammation and Neurobehavioral Deficits Induced by Experimental Traumatic Brain Injury.* J Neurotrauma, 2018. **35**(13): p. 1437-1451.
213. Campolo, M., et al., *Combination therapy with melatonin and dexamethasone in a mouse model of traumatic brain injury.* J Endocrinol, 2013. **217**(3): p. 291-301.
214. Abdallah, K., et al., *Bilateral descending hypothalamic projections to the spinal trigeminal nucleus caudalis in rats.* PLoS One, 2013. **8**(8): p. e73022.
215. Noseda, R. and R. Burstein, *Migraine pathophysiology: anatomy of the trigeminovascular pathway and associated neurological symptoms, CSD, sensitization and modulation of pain.* Pain, 2013. **154 Suppl 1**.
216. Pradhan, A.A., et al., *Characterization of a novel model of chronic migraine.* Pain, 2014. **155**(2): p. 269-74.
217. Furman, J.M., et al., *Migraine-anxiety related dizziness (MARD): a new disorder?* J Neurol Neurosurg Psychiatry, 2005. **76**(1): p. 1-8.
218. Minen, M.T., et al., *Migraine and its psychiatric comorbidities.* J Neurol Neurosurg Psychiatry, 2016. **87**(7): p. 741-9.
219. Wu, Y. and M. Hallett, *Photophobia in neurologic disorders.* Transl Neurodegener, 2017. **6**: p. 26.
220. Alp, R., et al., *Oxidative and antioxidative balance in patients of migraine.* Eur Rev Med Pharmacol Sci, 2010. **14**(10): p. 877-82.
221. Weatherall, M.W., *The diagnosis and treatment of chronic migraine.* Ther Adv Chronic Dis. **6**(3): p. 115-23.
222. Lee, I., et al., *The role of reactive oxygen species in capsaicin-induced mechanical hyperalgesia and in the activities of dorsal horn neurons.* Pain, 2007. **133**(1-3): p. 9-17.
223. Takano, T., et al., *Cortical spreading depression causes and coincides with tissue hypoxia.* Nat Neurosci, 2007. **10**(6): p. 754-62.
224. Viggiano, A., et al., *Cortical spreading depression affects reactive oxygen species production.* Brain Res, 2011. **1368**: p. 11-8.

225. Halliwell, B., *Reactive oxygen species and the central nervous system.* J Neurochem, 1992. **59**(5): p. 1609-23.
226. Tozzi-Ciancarelli, M.G., et al., *Oxidative stress and platelet responsiveness in migraine.* Cephalalgia, 1997. **17**(5): p. 580-4.
227. Bockowski, L., et al., *Serum and intraerythrocyte antioxidant enzymes and lipid peroxides in children with migraine.* Pharmacol Rep, 2008. **60**(4): p. 542-8.
228. Tuncel, D., et al., *Oxidative stress in migraine with and without aura.* Biol Trace Elem Res, 2008. **126**(1-3): p. 92-7.
229. Lee, J.M. and J.A. Johnson, *An important role of Nrf2-ARE pathway in the cellular defense mechanism.* J Biochem Mol Biol, 2004. **37**(2): p. 139-43.
230. Ellrichmann, G., et al., *Efficacy of fumaric acid esters in the R6/2 and YAC128 models of Huntington's disease.* PLoS One, 2011. **6**(1): p. e16172.
231. Yao, Y., et al., *Dimethyl Fumarate and Monomethyl Fumarate Promote Post-Ischemic Recovery in Mice.* Transl Stroke Res, 2016. **7**(6): p. 535-547.
232. Hiruma-Lima, C.A., et al., *The juice of fresh leaves of Boerhaavia diffusa L. (Nyctaginaceae) markedly reduces pain in mice.* J Ethnopharmacol, 2000. **71**(1-2): p. 267-74.
233. Oh, K., et al., *Erratum to: Combination of anxiety and depression is associated with an increased headache frequency in migraineurs: a population-based study.* BMC Neurol, 2016. **16**: p. 51.
234. Kawasaki, A. and V.A. Purvin, *Photophobia as the presenting visual symptom of chiasmal compression.* J Neuroophthalmol, 2002. **22**(1): p. 3-8.
235. Basbaum, A.I., et al., *Cellular and molecular mechanisms of pain.* Cell, 2009. **139**(2): p. 267-84.
236. Burstein, R., et al., *Thalamic sensitization transforms localized pain into widespread allodynia.* Ann Neurol, 2010. **68**(1): p. 81-91.
237. Burstein, R., et al., *Chemical stimulation of the intracranial dura induces enhanced responses to facial stimulation in brain stem trigeminal neurons.* J Neurophysiol, 1998. **79**(2): p. 964-82.
238. Pardutz, A., et al., *Effect of systemic nitroglycerin on CGRP and 5-HT afferents to rat caudal spinal trigeminal nucleus and its modulation by estrogen.* Eur J Neurosci, 2002. **15**(11): p. 1803-9.
239. Li, Y., et al., *Valproate ameliorates nitroglycerin-induced migraine in trigeminal nucleus caudalis in rats through inhibition of NF-small ka, CyrillicB.* J Headache Pain, 2016. **17**: p. 49.
240. Tassorelli, C., et al., *Parthenolide is the component of tanacetum parthenium that inhibits nitroglycerin-induced Fos activation: studies in an animal model of migraine.* Cephalalgia, 2005. **25**(8): p. 612-21.
241. Reuter, U., et al., *Nuclear factor-kappaB as a molecular target for migraine therapy.* Ann Neurol, 2002. **51**(4): p. 507-16.
242. Perry, C.J., et al., *Upregulation of inflammatory gene transcripts in periosteum of chronic migraineurs: Implications for extracranial origin of headache.* Ann Neurol, 2016. **79**(6): p. 1000-13.
243. Conti, P., et al., *Progression in migraine: Role of mast cells and pro-inflammatory and anti-inflammatory cytokines.* Eur J Pharmacol, 2019. **844**: p. 87-94.
244. Singh, N., et al., *Effect of dimethyl fumarate on neuroinflammation and apoptosis in pentylenetetrazol kindling model in rats.* Brain Res Bull, 2019. **144**: p. 233-245.
245. Kobayashi, E.H., et al., *Nrf2 suppresses macrophage inflammatory response by blocking proinflammatory cytokine transcription.* Nat Commun, 2016. **7**: p. 11624.
246. Kaspar, J.W., S.K. Niture, and A.K. Jaiswal, *Nrf2:INrf2 (Keap1) signaling in oxidative stress.* Free Radic Biol Med, 2009. **47**(9): p. 1304-9.
247. Hammer, A., et al., *The NRF2 pathway as potential biomarker for dimethyl fumarate treatment in multiple sclerosis.* Ann Clin Transl Neurol, 2018. **5**(6): p. 668-676.
248. Szabo, C., et al., *Regulation of mitochondrial bioenergetic function by hydrogen sulfide. Part I. Biochemical and physiological mechanisms.* Br J Pharmacol, 2014. **171**(8): p. 2099-122.

249. Abou-Hamdan, A., et al., *Oxidation of H2S in mammalian cells and mitochondria.* Methods Enzymol, 2015. **554**: p. 201-28.
250. Vandiver, M. and S.H. Snyder, *Hydrogen sulfide: a gasotransmitter of clinical relevance.* J Mol Med (Berl), 2012. **90**(3): p. 255-63.
251. Szabo, C., *Hydrogen sulphide and its therapeutic potential.* Nat Rev Drug Discov, 2007. **6**(11): p. 917-35.
252. Li, T., et al., *Regulatory effects of hydrogen sulfide on IL-6, IL-8 and IL-10 levels in the plasma and pulmonary tissue of rats with acute lung injury.* Exp Biol Med (Maywood), 2008. **233**(9): p. 1081-7.
253. Shrotriya, S., et al., *Diallyl trisulfide inhibits phorbol ester-induced tumor promotion, activation of AP-1, and expression of COX-2 in mouse skin by blocking JNK and Akt signaling.* Cancer Res, 2010. **70**(5): p. 1932-40.
254. Buckler, K.J., *Effects of exogenous hydrogen sulphide on calcium signalling, background (TASK) K channel activity and mitochondrial function in chemoreceptor cells.* Pflugers Arch, 2012. **463**(5): p. 743-54.
255. Lisjak, M., et al., *A novel hydrogen sulfide donor causes stomatal opening and reduces nitric oxide accumulation.* Plant Physiol Biochem, 2010. **48**(12): p. 931-5.
256. Osborne, N.N., et al., *Glutamate oxidative injury to RGC-5 cells in culture is necrostatin sensitive and blunted by a hydrogen sulfide (H2S)-releasing derivative of aspirin (ACS14).* Neurochem Int, 2012. **60**(4): p. 365-78.
257. Kashfi, K. and K.R. Olson, *Biology and therapeutic potential of hydrogen sulfide and hydrogen sulfide-releasing chimeras.* Biochem Pharmacol, 2013. **85**(5): p. 689-703.
258. Wagner, F., et al., *Bench-to-bedside review: Hydrogen sulfide--the third gaseous transmitter: applications for critical care.* Crit Care, 2009. **13**(3): p. 213.
259. Li, Q. and J.R. Lancaster, Jr., *Chemical foundations of hydrogen sulfide biology.* Nitric Oxide, 2013. **35**: p. 21-34.
260. Kimura, H., *Hydrogen sulfide and polysulfides as biological mediators.* Molecules, 2014. **19**(10): p. 16146-57.
261. Li, L. and P.K. Moore, *Putative biological roles of hydrogen sulfide in health and disease: a breath of not so fresh air?* Trends Pharmacol Sci, 2008. **29**(2): p. 84-90.
262. Chiku, T., et al., *H2S biogenesis by human cystathionine gamma-lyase leads to the novel sulfur metabolites lanthionine and homolanthionine and is responsive to the grade of hyperhomocysteinemia.* J Biol Chem, 2009. **284**(17): p. 11601-12.
263. Fan, J., et al., *Hydrogen sulfide lowers hyperhomocysteinemia dependent on cystathionine gamma lyase S-sulfhydration in ApoE-knockout atherosclerotic mice.* Br J Pharmacol, 2019. **176**(17): p. 3180-3192.
264. Mikami, Y., et al., *Hydrogen sulfide protects the retina from light-induced degeneration by the modulation of Ca2+ influx.* J Biol Chem, 2011. **286**(45): p. 39379-86.
265. Singh, S., et al., *Relative contributions of cystathionine beta-synthase and gamma-cystathionase to H2S biogenesis via alternative trans-sulfuration reactions.* J Biol Chem, 2009. **284**(33): p. 22457-66.
266. Zhao, Y., et al., *Controllable hydrogen sulfide donors and their activity against myocardial ischemia-reperfusion injury.* ACS Chem Biol, 2013. **8**(6): p. 1283-90.
267. Li, L., et al., *Characterization of a novel, water-soluble hydrogen sulfide-releasing molecule (GYY4137): new insights into the biology of hydrogen sulfide.* Circulation, 2008. **117**(18): p. 2351-60.
268. De Cicco, P., et al., *ATB-346, a novel hydrogen sulfide-releasing anti-inflammatory drug, induces apoptosis of human melanoma cells and inhibits melanoma development in vivo.* Pharmacol Res, 2016. **114**: p. 67-73.
269. Cenac, N., et al., *A novel orally administered trimebutine compound (GIC-1001) is anti-nociceptive and features peripheral opioid agonistic activity and Hydrogen Sulphide-releasing capacity in mice.* Eur J Pain, 2016. **20**(5): p. 723-30.

270. Hildebrandt, T.M. and M.K. Grieshaber, *Three enzymatic activities catalyze the oxidation of sulfide to thiosulfate in mammalian and invertebrate mitochondria.* FEBS J, 2008. **275**(13): p. 3352-61.
271. Jackson, M.R., S.L. Melideo, and M.S. Jorns, *Human sulfide:quinone oxidoreductase catalyzes the first step in hydrogen sulfide metabolism and produces a sulfane sulfur metabolite.* Biochemistry, 2012. **51**(34): p. 6804-15.
272. Libiad, M., et al., *Organization of the human mitochondrial hydrogen sulfide oxidation pathway.* J Biol Chem, 2014. **289**(45): p. 30901-10.
273. Olson, K.R., *Hydrogen sulfide is an oxygen sensor in the carotid body.* Respir Physiol Neurobiol, 2011. **179**(2-3): p. 103-10.
274. Cao, X., et al., *A Review of Hydrogen Sulfide Synthesis, Metabolism, and Measurement: Is Modulation of Hydrogen Sulfide a Novel Therapeutic for Cancer?* Antioxid Redox Signal, 2019. **31**(1): p. 1-38.
275. Hellmich, M.R. and C. Szabo, *Hydrogen Sulfide and Cancer.* Handb Exp Pharmacol, 2015. **230**: p. 233-41.
276. Wang, R., *Gasotransmitters: growing pains and joys.* Trends Biochem Sci, 2014. **39**(5): p. 227-32.
277. Ju, Y., et al., *H(2)S signaling in redox regulation of cellular functions.* Can J Physiol Pharmacol, 2013. **91**(1): p. 8-14.
278. Lan, A., et al., *Hydrogen sulfide protects against chemical hypoxia-induced injury by inhibiting ROS-activated ERK1/2 and p38MAPK signaling pathways in PC12 cells.* PLoS One, 2011. **6**(10): p. e25921.
279. Kimura, Y. and H. Kimura, *Hydrogen sulfide protects neurons from oxidative stress.* FASEB J, 2004. **18**(10): p. 1165-7.
280. Geng, B., et al., *Endogenous hydrogen sulfide regulation of myocardial injury induced by isoproterenol.* Biochem Biophys Res Commun, 2004. **318**(3): p. 756-63.
281. Whiteman, M., et al., *The novel neuromodulator hydrogen sulfide: an endogenous peroxynitrite 'scavenger'?* J Neurochem, 2004. **90**(3): p. 765-8.
282. Yonezawa, D., et al., *A protective role of hydrogen sulfide against oxidative stress in rat gastric mucosal epithelium.* Toxicology, 2007. **241**(1-2): p. 11-8.
283. Lu, M., et al., *Hydrogen sulfide protects astrocytes against H(2)O(2)-induced neural injury via enhancing glutamate uptake.* Free Radic Biol Med, 2008. **45**(12): p. 1705-13.
284. Luther, G.W., 3rd, et al., *Thermodynamics and kinetics of sulfide oxidation by oxygen: a look at inorganically controlled reactions and biologically mediated processes in the environment.* Front Microbiol, 2011. **2**: p. 62.
285. Olson, K.R., *A theoretical examination of hydrogen sulfide metabolism and its potential in autocrine/paracrine oxygen sensing.* Respir Physiol Neurobiol, 2013. **186**(2): p. 173-9.
286. Searcy, D.G., J.P. Whitehead, and M.J. Maroney, *Interaction of Cu,Zn superoxide dismutase with hydrogen sulfide.* Arch Biochem Biophys, 1995. **318**(2): p. 251-63.
287. Mitsuhashi, H., et al., *Oxidative stress-dependent conversion of hydrogen sulfide to sulfite by activated neutrophils.* Shock, 2005. **24**(6): p. 529-34.
288. Papapetropoulos, A., et al., *Hydrogen sulfide is an endogenous stimulator of angiogenesis.* Proc Natl Acad Sci U S A, 2009. **106**(51): p. 21972-7.
289. Sun, W.H., et al., *Hydrogen sulfide decreases the levels of ROS by inhibiting mitochondrial complex IV and increasing SOD activities in cardiomyocytes under ischemia/reperfusion.* Biochem Biophys Res Commun, 2012. **421**(2): p. 164-9.
290. Yan, S.K., et al., *Effects of hydrogen sulfide on homocysteine-induced oxidative stress in vascular smooth muscle cells.* Biochem Biophys Res Commun, 2006. **351**(2): p. 485-91.
291. Wu, T., et al., *Hydrogen Sulfide Reduces Recruitment of CD11b(+)Gr-1(+) Cells in Mice With Myocardial Infarction.* Cell Transplant, 2017. **26**(5): p. 753-764.
292. Qu, K., et al., *Hydrogen sulfide is a mediator of cerebral ischemic damage.* Stroke, 2006. **37**(3): p. 889-93.

293. Whiteman, M., et al., *Hydrogen sulphide: a novel inhibitor of hypochlorous acid-mediated oxidative damage in the brain?* Biochem Biophys Res Commun, 2005. **326**(4): p. 794-8.
294. Yin, W.L., et al., *Hydrogen sulfide inhibits MPP(+)-induced apoptosis in PC12 cells.* Life Sci, 2009. **85**(7-8): p. 269-75.
295. Zhao, H., et al., *Taurine supplementation reduces neuroinflammation and protects against white matter injury after intracerebral hemorrhage in rats.* Amino Acids, 2018. **50**(3-4): p. 439-451.
296. Popov, D., *An outlook on vascular hydrogen sulphide effects, signalling, and therapeutic potential.* Arch Physiol Biochem, 2013. **119**(5): p. 189-94.
297. Strissel, K.J., et al., *Adipocyte death, adipose tissue remodeling, and obesity complications.* Diabetes, 2007. **56**(12): p. 2910-8.
298. Lee, P., M.M. Swarbrick, and K.K. Ho, *Brown adipose tissue in adult humans: a metabolic renaissance.* Endocr Rev, 2013. **34**(3): p. 413-38.
299. Cinti, S., *The adipose organ: morphological perspectives of adipose tissues.* Proc Nutr Soc, 2001. **60**(3): p. 319-28.
300. Bolsoni-Lopes, A. and M.I. Alonso-Vale, *Lipolysis and lipases in white adipose tissue - An update.* Arch Endocrinol Metab, 2015. **59**(4): p. 335-42.
301. Cannon, B. and J. Nedergaard, *Brown adipose tissue: function and physiological significance.* Physiol Rev, 2004. **84**(1): p. 277-359.
302. Petrovic, N., et al., *Chronic peroxisome proliferator-activated receptor gamma (PPARgamma) activation of epididymally derived white adipocyte cultures reveals a population of thermogenically competent, UCP1-containing adipocytes molecularly distinct from classic brown adipocytes.* J Biol Chem, 2010. **285**(10): p. 7153-64.
303. Rosen, C.J. and M.L. Bouxsein, *Mechanisms of disease: is osteoporosis the obesity of bone?* Nat Clin Pract Rheumatol, 2006. **2**(1): p. 35-43.
304. Moore, S.G. and K.L. Dawson, *Red and yellow marrow in the femur: age-related changes in appearance at MR imaging.* Radiology, 1990. **175**(1): p. 219-23.
305. Griffith, J.F., et al., *Bone marrow fat content in the elderly: a reversal of sex difference seen in younger subjects.* J Magn Reson Imaging, 2012. **36**(1): p. 225-30.
306. Morroni, M., et al., *Reversible transdifferentiation of secretory epithelial cells into adipocytes in the mammary gland.* Proc Natl Acad Sci U S A, 2004. **101**(48): p. 16801-6.
307. De Matteis, R., et al., *In vivo physiological transdifferentiation of adult adipose cells.* Stem Cells, 2009. **27**(11): p. 2761-8.
308. Cinti, S., *The adipose organ.* Prostaglandins Leukot Essent Fatty Acids, 2005. **73**(1): p. 9-15.
309. Frontini, A. and S. Cinti, *Distribution and development of brown adipocytes in the murine and human adipose organ.* Cell Metab, 2010. **11**(4): p. 253-6.
310. Giordano, A., A. Frontini, and S. Cinti, *Adipose organ nerves revealed by immunohistochemistry.* Methods Mol Biol, 2008. **456**: p. 83-95.
311. Otto, T.C. and M.D. Lane, *Adipose development: from stem cell to adipocyte.* Crit Rev Biochem Mol Biol, 2005. **40**(4): p. 229-42.
312. Timmons, J.A., et al., *Myogenic gene expression signature establishes that brown and white adipocytes originate from distinct cell lineages.* Proc Natl Acad Sci U S A, 2007. **104**(11): p. 4401-6.
313. Zhang, J.W., et al., *Dominant-negative C/EBP disrupts mitotic clonal expansion and differentiation of 3T3-L1 preadipocytes.* Proc Natl Acad Sci U S A, 2004. **101**(1): p. 43-7.
314. Rosen, E.D. and O.A. MacDougald, *Adipocyte differentiation from the inside out.* Nat Rev Mol Cell Biol, 2006. **7**(12): p. 885-96.
315. Tseng, Y.H., et al., *New role of bone morphogenetic protein 7 in brown adipogenesis and energy expenditure.* Nature, 2008. **454**(7207): p. 1000-4.
316. Seale, P., et al., *PRDM16 controls a brown fat/skeletal muscle switch.* Nature, 2008. **454**(7207): p. 961-7.

317. Kajimura, S., et al., *Initiation of myoblast to brown fat switch by a PRDM16-C/EBP-beta transcriptional complex.* Nature, 2009. **460**(7259): p. 1154-8.
318. Stanford, K.I., et al., *Brown adipose tissue regulates glucose homeostasis and insulin sensitivity.* J Clin Invest, 2013. **123**(1): p. 215-23.
319. Cinti, S., *Transdifferentiation properties of adipocytes in the adipose organ.* Am J Physiol Endocrinol Metab, 2009. **297**(5): p. E977-86.
320. Wu, J., P. Cohen, and B.M. Spiegelman, *Adaptive thermogenesis in adipocytes: is beige the new brown?* Genes Dev, 2013. **27**(3): p. 234-50.
321. Kajimura, S., P. Seale, and B.M. Spiegelman, *Transcriptional control of brown fat development.* Cell Metab, 2010. **11**(4): p. 257-62.
322. Puigserver, P. and B.M. Spiegelman, *Peroxisome proliferator-activated receptor-gamma coactivator 1 alpha (PGC-1 alpha): transcriptional coactivator and metabolic regulator.* Endocr Rev, 2003. **24**(1): p. 78-90.
323. Tiraby, C., et al., *Acquirement of brown fat cell features by human white adipocytes.* J Biol Chem, 2003. **278**(35): p. 33370-6.
324. Bostrom, P., et al., *A PGC1-alpha-dependent myokine that drives brown-fat-like development of white fat and thermogenesis.* Nature, 2012. **481**(7382): p. 463-8.
325. Giordano, A., et al., *White, brown and pink adipocytes: the extraordinary plasticity of the adipose organ.* Eur J Endocrinol, 2014. **170**(5): p. R159-71.
326. Cohen, P., et al., *Role for stearoyl-CoA desaturase-1 in leptin-mediated weight loss.* Science, 2002. **297**(5579): p. 240-3.
327. Minokoshi, Y., et al., *Leptin stimulates fatty-acid oxidation by activating AMP-activated protein kinase.* Nature, 2002. **415**(6869): p. 339-43.
328. Yamauchi, T. and T. Kadowaki, *Physiological and pathophysiological roles of adiponectin and adiponectin receptors in the integrated regulation of metabolic and cardiovascular diseases.* Int J Obes (Lond), 2008. **32 Suppl 7**: p. S13-8.
329. Hotamisligil, G.S., et al., *Tumor necrosis factor alpha inhibits signaling from the insulin receptor.* Proc Natl Acad Sci U S A, 1994. **91**(11): p. 4854-8.
330. Luo, L. and M. Liu, *Adipose tissue in control of metabolism.* J Endocrinol, 2016. **231**(3): p. R77-R99.
331. Gregoire, F.M., C.M. Smas, and H.S. Sul, *Understanding adipocyte differentiation.* Physiol Rev, 1998. **78**(3): p. 783-809.
332. Zhang, Z.Y. and M.W. Wang, *Obesity, a health burden of a global nature.* Acta Pharmacol Sin, 2012. **33**(2): p. 145-7.
333. Pollin, I.S., et al., *High prevalence of cardiometabolic risk factors in women considered low risk by traditional risk assessment.* J Womens Health (Larchmt), 2008. **17**(6): p. 947-53.
334. Sikaris, K.A., *The clinical biochemistry of obesity.* Clin Biochem Rev, 2004. **25**(3): p. 165-81.
335. Despres, J.P., et al., *Regional distribution of body fat, plasma lipoproteins, and cardiovascular disease.* Arteriosclerosis, 1990. **10**(4): p. 497-511.
336. Stinkens, R., et al., *Targeting fatty acid metabolism to improve glucose metabolism.* Obes Rev, 2015. **16**(9): p. 715-57.
337. Savini, I., et al., *Obesity-associated oxidative stress: strategies finalized to improve redox state.* Int J Mol Sci, 2013. **14**(5): p. 10497-538.
338. Furukawa, S., et al., *Increased oxidative stress in obesity and its impact on metabolic syndrome.* J Clin Invest, 2004. **114**(12): p. 1752-61.
339. Horvath, T.L., Z.B. Andrews, and S. Diano, *Fuel utilization by hypothalamic neurons: roles for ROS.* Trends Endocrinol Metab, 2009. **20**(2): p. 78-87.
340. Serra, D., et al., *Mitochondrial fatty acid oxidation in obesity.* Antioxid Redox Signal, 2013. **19**(3): p. 269-84.
341. Patel, C., et al., *Prolonged reactive oxygen species generation and nuclear factor-kappaB activation after a high-fat, high-carbohydrate meal in the obese.* J Clin Endocrinol Metab, 2007. **92**(11): p. 4476-9.

342. Feng, X., et al., *Hydrogen sulfide from adipose tissue is a novel insulin resistance regulator.* Biochem Biophys Res Commun, 2009. **380**(1): p. 153-9.
343. Tsai, C.Y., et al., *Hydrogen sulfide promotes adipogenesis in 3T3L1 cells.* PLoS One, 2015. **10**(3): p. e0119511.
344. Cai, J., et al., *Cystathionine gamma lyase-hydrogen sulfide increases peroxisome proliferator-activated receptor gamma activity by sulfhydration at C139 site thereby promoting glucose uptake and lipid storage in adipocytes.* Biochim Biophys Acta, 2016. **1861**(5): p. 419-29.
345. Ambati, S., et al., *Ajoene exerts potent effects in 3T3-L1 adipocytes by inhibiting adipogenesis and inducing apoptosis.* Phytother Res, 2009. **23**(4): p. 513-8.
346. Geng, B., et al., *Increase or decrease hydrogen sulfide exert opposite lipolysis, but reduce global insulin resistance in high fatty diet induced obese mice.* PLoS One, 2013. **8**(9): p. e73892.
347. Huang, C.Y., et al., *Endogenous CSE/H2 S system mediates TNF-alpha-induced insulin resistance in 3T3-L1 adipocytes.* Cell Biochem Funct, 2013. **31**(6): p. 468-75.
348. Manna, P. and S.K. Jain, *Vitamin D up-regulates glucose transporter 4 (GLUT4) translocation and glucose utilization mediated by cystathionine-gamma-lyase (CSE) activation and H2S formation in 3T3L1 adipocytes.* J Biol Chem, 2012. **287**(50): p. 42324-32.
349. Xue, R., et al., *Hydrogen sulfide treatment promotes glucose uptake by increasing insulin receptor sensitivity and ameliorates kidney lesions in type 2 diabetes.* Antioxid Redox Signal, 2013. **19**(1): p. 5-23.
350. Katsouda, A., C. Szabo, and A. Papapetropoulos, *Reduced adipose tissue H2S in obesity.* Pharmacol Res, 2018. **128**: p. 190-199.
351. Pi, J., et al., *Deficiency in the nuclear factor E2-related factor-2 transcription factor results in impaired adipogenesis and protects against diet-induced obesity.* J Biol Chem, 2010. **285**(12): p. 9292-300.
352. Shin, S., et al., *NRF2 modulates aryl hydrocarbon receptor signaling: influence on adipogenesis.* Mol Cell Biol, 2007. **27**(20): p. 7188-97.
353. Chorley, B.N., et al., *Identification of novel NRF2-regulated genes by ChIP-Seq: influence on retinoid X receptor alpha.* Nucleic Acids Res, 2012. **40**(15): p. 7416-29.
354. Yu, Z.W., et al., *Role of nuclear factor (erythroid-derived 2)-like 2 in metabolic homeostasis and insulin action: A novel opportunity for diabetes treatment?* World J Diabetes, 2012. **3**(1): p. 19-28.
355. Wozniak, S.E., et al., *Adipose tissue: the new endocrine organ? A review article.* Dig Dis Sci, 2009. **54**(9): p. 1847-56.
356. Guilherme, A., et al., *Adipocyte dysfunctions linking obesity to insulin resistance and type 2 diabetes.* Nat Rev Mol Cell Biol, 2008. **9**(5): p. 367-77.
357. Lafontan, M. and D. Langin, *Lipolysis and lipid mobilization in human adipose tissue.* Prog Lipid Res, 2009. **48**(5): p. 275-97.
358. Shimano, H., *Sterol regulatory element-binding proteins (SREBPs): transcriptional regulators of lipid synthetic genes.* Prog Lipid Res, 2001. **40**(6): p. 439-52.
359. Shi, Y. and P. Burn, *Lipid metabolic enzymes: emerging drug targets for the treatment of obesity.* Nat Rev Drug Discov, 2004. **3**(8): p. 695-710.
360. Arner, P., *Human fat cell lipolysis: biochemistry, regulation and clinical role.* Best Pract Res Clin Endocrinol Metab, 2005. **19**(4): p. 471-82.
361. Xu, J., et al., *Enhanced Nrf2 activity worsens insulin resistance, impairs lipid accumulation in adipose tissue, and increases hepatic steatosis in leptin-deficient mice.* Diabetes, 2012. **61**(12): p. 3208-18.
362. Yu, B., et al., *Inhaled nitric oxide enables artificial blood transfusion without hypertension.* Circulation, 2008. **117**(15): p. 1982-90.
363. Modis, K., et al., *Oxidative stress suppresses the cellular bioenergetic effect of the 3-mercaptopyruvate sulfurtransferase/hydrogen sulfide pathway.* Biochem Biophys Res Commun, 2013. **433**(4): p. 401-7.

364. Park, Y.S., et al., *Specific down regulation of 3T3-L1 adipocyte differentiation by cell-permeable antisense HIF1alpha-oligonucleotide.* J Control Release, 2010. **144**(1): p. 82-90.
365. Gero, D., et al., *The novel mitochondria-targeted hydrogen sulfide (H2S) donors AP123 and AP39 protect against hyperglycemic injury in microvascular endothelial cells in vitro.* Pharmacol Res, 2016. **113**(Pt A): p. 186-198.
366. Kang, J.W., et al., *Effect of Gambisan on the Inhibition of Adipogenesis in 3T3-L1 Adipocytes.* Evid Based Complement Alternat Med, 2013. **2013**: p. 789067.
367. Si, Y., H. Shi, and K. Lee, *Impact of perturbed pyruvate metabolism on adipocyte triglyceride accumulation.* Metab Eng, 2009. **11**(6): p. 382-90.
368. DeLeon, E.R., et al., *Garlic oil polysulfides: H2S- and O2-independent prooxidants in buffer and antioxidants in cells.* Am J Physiol Regul Integr Comp Physiol, 2016. **310**(11): p. R1212-25.
369. Fajas, L., J.C. Fruchart, and J. Auwerx, *Transcriptional control of adipogenesis.* Curr Opin Cell Biol, 1998. **10**(2): p. 165-73.
370. Qabazard, B., et al., *Hydrogen sulfide is an endogenous regulator of aging in Caenorhabditis elegans.* Antioxid Redox Signal, 2014. **20**(16): p. 2621-30.
371. Hanaoka, K., et al., *Discovery and Mechanistic Characterization of Selective Inhibitors of H2S-producing Enzyme: 3-Mercaptopyruvate Sulfurtransferase (3MST) Targeting Active-site Cysteine Persulfide.* Sci Rep, 2017. **7**: p. 40227.
372. Olah, G., et al., *Role of endogenous and exogenous nitric oxide, carbon monoxide and hydrogen sulfide in HCT116 colon cancer cell proliferation.* Biochem Pharmacol, 2018. **149**: p. 186-204.
373. Olzmann, J.A. and P. Carvalho, *Dynamics and functions of lipid droplets.* Nat Rev Mol Cell Biol, 2019. **20**(3): p. 137-155.